



University of Aveiro
2014

Department of Materials Engineering and Ceramic

**Daniel Eduardo
Loureiro Vieira**

**Active protective treatments for galvanically
coupled AA2024 and CFRP**

Dissertation submitted to the University of Aveiro to fulfill the requirements for obtaining a Master's degree in materials engineering, held under the scientific guidance of Dra. Maria Serdechnova, post – doctoral researcher at the Department of Ceramic and Materials Engineering at the University of Aveiro and Dr. Mikhail Zhelukedvich invited associate professor in the Department of Ceramic and Materials Engineering at the University of Aveiro.

The jury

Doctor José Filipe Alves de Oliveira

Assistant researcher in Department of Ceramic and Materials Engineering at the University of Aveiro.

Doctor Sviatlana Valeriana Lamaka

Assistant researcher in Institute of Materials and Surfaces Science and Engineering at Technical University of Lisbon

Doctor Maria Vladimirovna Serdechnova

Post – doctoral researcher in the Department of Ceramic and Materials Engineering at the University of Aveiro

Acknowledgements

A big thank you to my family and girlfriend for all the moral support and patience throughout the course and in particular over the last year because without them everything would have been much more complicated.

A huge thank you to the University of Aveiro and the Airbus group for having given me this gigantic opportunity to intern at one of the world's largest companies, especially to Dr. Mikhail Zhelukedvich and Mr. Theo Hack for they have put their trust in me and gave me the possibility to perform the internship and work in PROAIR project.

Other huge thanks to my advisor Dra. Maria Serdechnova for everything you taught me, all the patience to explain and to correct errors, for all the fun times offered, once again thank you very much.

A thank you to all my colleagues at Airbus group for all the good times provided in the company, in particular to Sonja Nixon throughout the patience to explain and help when needed.

I am also grateful to my laboratory colleagues at the University of Aveiro, in particular, Pedro Moreira and MsC. André Oliveira, to Dr. Alexandre Bastos, Dr. Andrei Salak and Dr. Silvar Kallip by all teachings transmitted and all the help you have provided during this year because even with a lot of work they always had a little time to help when needed.

And last but not least, I thank all my colleagues and friends for all the great and happy moments we have during the academic career and a special thank you to Marco Oliveira and Alexandre Rocha for listening and sharing ideas in this final stage of master's thesis.

Resumo

No presente trabalho revestimentos "inteligentes" foram sintetizados com a finalidade de proteger contra a corrosão a liga de alumínio AA2024 acoplada galvanicamente com a fibra de carbono reforçada com plástico (CFRP). Os nanocontenedores LDH Mg/Al LDH e Zn/Al LDH foram carregados com os inibidores orgânicos 2-mercaptobenzotiazole e 1,2,3-benzotriazole, e com inibidores inorgânicos metavanadato, tungstato e molibdato. No caso dos nanocontenedores de bentonite o inibidor incorporado foi o $Ce(NO_3)_3$.

A análise por difração de raios-X (DRX) e microscopia eletrônica de varrimento (MEV) foram realizadas a fim de caracterizar os nanocontenedores obtidos.

Os nanocontenedores foram aplicados em revestimento epóxi na superfície do sistema modelo (AA2024 galvanicamente acoplado com CFRP), os LDH's preenchidos com inibidores em mistura com Ce^{3+} carregado na bentonite foram usados com o objetivo de aumentar as propriedades de proteção do revestimento contra a corrosão. As análises das propriedades anticorrosivas dos revestimentos foram realizadas utilizando o ZRA (Zero resistance ammeter), espectroscopia de impedância eletroquímica (EIS), microscopia ótica, teste de nevoeiro salino (SST) e SVET (scanning vibrating electrode technique).

O trabalho foi realizado em ambiente laboratorial e posteriormente em ambiente industrial (Airbus group).

Palavras - chave

Revestimentos inteligentes, inibidores, nanocontenedores, proteção contra corrosão.

Abstract

In the present work “smart” nanocontainers were synthesized in order to incorporate them into an organic coating and protect against corrosion of the aluminum alloy (AA2024) galvanically coupled with carbon fiber reinforced plastic (CFRP). The containers were loaded with organic (2-mercaptobenzothiazole and 1,2,3 – benzotriazole) and inorganic (metavanadate, tungstate and molybdate) inhibitors in the case of Mg/Al and Zn/Al LDH nanoreservoirs. In the case of the bentonite nanocontainers, the containers were loaded with $\text{Ce}(\text{NO}_3)_3$. X-ray diffraction (XRD) and scanning electron microscopy (SEM) analyses were performed in order to characterize the obtained nanocontainers.

The nanocontainers were embedded into epoxy coating on the surface of model multi-material system (AA2024 galvanically coupled with CFRP). The LDHs loaded with different inhibitors and combined with bentonite loaded with Ce^{3+} , increase the anticorrosion protection properties of the coating. The analyses of the anticorrosion properties of the coatings were performed using zero resistance ammetry (ZRA), electrochemical impedance spectroscopy (EIS), optical microscopy, salt spray test (SST) and scanning vibrating electrode technique (SVET) measurements.

The laboratory work was realized in University of Aveiro in collaboration with industrial environment of Airbus group.

Key-words

Smart self – healing coatings, inhibitors, nanocontainers, corrosion protection

Abstrakt

In der vorliegenden Arbeit wurden die “intelligenten” Nanocontainers zum Schutz gegen Korrosion der Aluminiumlegierung AA2024, galvanisch mit Kohlefaserstarkem Kunststoff (CFK) gekoppelt, synthetisiert. Die Containers wurden mit Bio-(2-Mercaptobenzothiazol und 1,2,3-Benzotriazol) und anorganischen (Metavanadat, Wolframat und Molybdat) Inhibitoren, wenn Mg/Al und Zn/Al-LDH nanoreservoirs wurden angewendet, und $\text{Ce}(\text{NO}_3)_3$, wenn Bentoniten Nanocontainers wurden angewendet, geladen. Röntgenbeugung (XRD) und Rasterelektronenmikroskopie (SEM)-Analysen wurden durchgeführt, um die erhaltenen Nanocontainers kennzeichnen. Die LDHs wurden in Epoxidüberzug auf der Oberfläche des Modells Multi-Material-System (AA2024 galvanisch mit CFK-gekoppelt) aufgetragen, mit Inhibitoren in Mischung mit Ce^{3+} in Bentonit geladen, erhöhen die Korrosionsschutzeigenschaften der Beschichtungen. Die Analysen der Korrosionsschutzeigenschaften der Beschichtungen wurden mittels Null-Widerstand Ampermeter (ZRA), elektrochemische Impedanzspektroskopie (EIS), optische Mikroskopie, Salzspruhtest (SST) und Raster vibrierenden Elektrodentechnik (SVET) - Messungen durchgeführt. Die Arbeit im Labor wurde in der Universität von Aveiro in Zusammenarbeit mit industriellen Umfeld in AirbusGruppe (Deutschland) leistet.

Schlüsselworte

“intelligenten” selbstheilende Beschichtungen, Inhibitoren, Nanocontainers, Korrosionsschutz

Content

List of abbreviations	XIII
Figure content.....	XV
Table content	XIX
1. Introduction	1
1.1. Basics of protection with coatings	2
1.1.1. Corrosion processes	2
1.1.2. Typical protection mechanisms	3
1.1.3. Barrier protection	3
1.1.4. Galvanic protection.....	4
1.1.5. Inhibitors	4
1.1.6. Multi-layer construction	7
1.2. Materials of the aeronautic industry.....	7
1.2.1. Aluminum	7
1.2.2. Role of pH for the aluminum corrosion.....	8
1.2.3. Role of chloride for aluminum corrosion	9
1.2.4. Carbon fiber reinforced plastic	9
1.3. Objective of the work.....	10
2. Experimental procedure and conditions used.....	12
2.1. Materials used	12
2.2. Type of coatings	12
2.3. Techniques	12
2.4. Samples and sample holder used.....	15
2.5. LDH synthesis	18

2.6. Inhibitors intercalation	19
2.7. Synergistic mixtures	20
3. Results	22
3.1. Research laboratory	22
3.1.1. Nanocontainer characterization	22
3.1.2. Results of the different types of coated formulations	24
3.2. Industrial results	41
3.2.1. X-ray diffraction (XRD)	41
3.2.2. Electrochemical tests	44
4. Discussion.....	72
4.1. Sample holder.....	72
4.2. Protection with inhibitors	72
4.3. Inhibition efficiency	76
4.4. EIS improvement.....	77
4.5. Synergistic effect.....	78
4.6. SVET.....	79
5. Conclusions	81
6. Bibliography	83

List of abbreviations

CFRP - Carbon fiber reinforced plastic;

AA2024 - Aluminum alloy 2024;

LDH - Layered double hydroxides;

SST - Salt spray test;

EIS - Electrochemical impedance spectroscopy;

ZRA - Zero resistance ammeter;

SEM - Scanning electron microscopy;

SVET - Scanning vibrating electrode technique;

XRD – X – Ray diffraction;

MBT – 2-mercaptobenzothiazole;

BTA – 1,2,3 – benzotriazole;

IE – Inhibitors efficiency.

Figure content

Figure 1 - Corrosion around: airplanes, cars and bridges.....	1
Figure 2 - Different mechanisms of corrosion protection	3
Figure 3 - Schematic presentation of 2-mercaptobenzothiazole and 1,2,3-benzotriazole molecules.....	5
Figure 4 - Multilayer construction.....	7
Figure 5 - Carbon fiber for CFRP.....	9
Figure 6 - Materials breakdown for Airbus A350 aircraft.....	11
Figure 7 - SVET equipment.....	14
Figure 8 - Sample used for electrochemical tests in Aveiro University	15
Figure 9 - Aluminum and CFRP Samples used in Airbus group	15
Figure 10 - Sample holder used in Airbus group	16
Figure 11 - Sample holder with the wires and the sealant already applied.	17
Figure 12 - LDH Synthesis.....	18
Figure 13 - Inhibitors intercalation.....	20
Figure 14 - SEM images for the different types of nanocontainers, used in this work	22
Figure 15 - The XRD patterns of Mg/Al LDH before and after intercalated with BTA and MBT	23
Figure 16 - XRD of Zn/Al LDH loaded with MBT	24
Figure 17 - Corrosion test for different types of coating.....	25
Figure 18 - EIS for reference sample without scratch and scratched.	27
Figure 19 - EIS for Reference sample and Tungstate loaded into Mg/Al LDH mixed with Ce ³⁺ loaded into bentonite.	27
Figure 20 - EIS analyses for MBT loaded into Mg/Al LDH mixed with Ce ³⁺ loaded into bentonite, MBT loaded into Mg/Al LDH.....	29
Figure 21 - EIS analyses for BTA loaded into Mg/Al LDH mixed with Ce ³⁺ loaded into bentonite, Ce ³⁺ loaded into bentonite.	29
Figure 22 - EIS analyses for Metavanadate loaded into Mg/Al LDH mixed with Ce ³⁺ loaded into bentonite, metavanadate loaded into Mg/Al LDH.	30
Figure 23 - EIS analyses for Tungstate loaded into Mg/Al LDH mixed with Ce ³⁺ loaded into bentonite, tungstate loaded into Mg/Al LDH.	30
Figure 24 - SVET general results	32

Figure 25 - SVET measurement from coating formulation molybdate loaded into Mg/Al LDH mixed with Ce ³⁺ loaded into bentonite.....	37
Figure 26 - Maximum and minimum peaks of corrosion.....	38
Figure 27 - Corrosion currents calculated through “Total current” for Tungstate loaded into Mg/Al LDH mixed with Ce ³⁺ loaded into bentonite, Tungstate loaded into Mg/Al LDH and Reference.....	39
Figure 28 - Corrosion currents calculated through “Total current” for MBT loaded into Mg/Al LDH mixed with Ce ³⁺ loaded into bentonite, MBT loaded into Mg/Al LDH and reference.....	40
Figure 29 - Total current during 24 hours between MBT loaded into Mg/Al LDH mixed with Ce ³⁺ loaded into bentonite and tungstate loaded into Mg/Al LDH mixed with Ce ³⁺ loaded into bentonite.....	40
Figure 30 - XRD pattern of BTA intercalated into Mg/Al LDH.....	41
Figure 31 - XRD pattern of MBT intercalated into Mg/Al LDH.....	42
Figure 32 - XRD pattern of vanadate intercalated into Mg/Al LDH.....	42
Figure 33 - XRD pattern of Mg/Al LDH intercalated with molybdate.....	43
Figure 34 - XRD pattern of Mg/Al LDH loaded with tungstate.....	43
Figure 35 - Old Reference.....	44
Figure 65 - Different types of coating application.....	45
Figure 36 - ZRA measurements of all samples.....	45
Figure 37 - ZRA analyses in percentage of efficiency for all samples.....	46
Figure 38 - Reference coating without any inhibitors.....	47
Figure 39 - Equivalent circuit used during the measurements.....	48
Figure 40 - Equivalent circuit after the formation of artificial scratch.....	48
Figure 41 - The EIS spectra obtained from galvanically coupled AA2024 and CFRP coated with epoxy coating containing mixture of MBT loaded into Mg/Al LDH and Ce ³⁺ loaded into bentonite.....	49
Figure 42 - The EIS spectra obtained from galvanically coupled AA2024 and CFRP coated with epoxy coating containing mixture of BTA loaded into Mg/Al LDH and Ce ³⁺ loaded into bentonite.....	50

Figure 43 - The EIS spectra obtained from galvanically coupled AA2024 and CFRP coated with epoxy coating containing mixture of metavanadate loaded into Mg/Al LDH and Ce ³⁺ loaded into bentonite	50
Figure 44 - The EIS spectra obtained from galvanically coupled AA2024 and CFRP coated with epoxy coating containing mixture of tungstate loaded into Mg/Al LDH and Ce ³⁺ loaded into bentonite	51
Figure 45 - The EIS spectra obtained from galvanically coupled AA2024 and CFRP coated with epoxy coating containing mixture of molybdate loaded into Mg/Al LDH and Ce ³⁺ loaded into bentonite	51
Figure 46 - Comparison of EIS results for a1) 1 hour without scratch, a2) 24 hours without scratch, b1) 1 hour with scratch and b2) 24 hours with scratch, for the different coating formulations.....	52
Figure 47 - Photos of the corroded reference sample during the immersion test.....	53
Figure 48 - Photos of the corrosion processes of the sample coating the mixture of inhibitors (MBT loaded into Mg/Al LDH together with the Ce ³⁺ loaded into bentonite)	54
Figure 49 - Photos of the corrosion processes of the sample containing the mixture of inhibitors (BTA loaded into Mg/Al LDH together with Ce ³⁺ loaded into bentonite)	55
Figure 50 - Photos of the corrosion processes of the sample containing the mixture of inhibitors (metavanadate loaded into Mg/Al LDH together with Ce ³⁺ loaded into bentonite).....	56
Figure 51 - Photos of the corrosion processes of the sample containing the mixture of inhibitors (Tungstate loaded into Mg/Al LDH together with Ce ³⁺ loaded into bentonite) .	57
Figure 52 - Photos of the corrosion processes of the sample containing the mixture of inhibitors (molybdate loaded into Mg/Al LDH together with Ce ³⁺ loaded into bentonite)	58
Figure 53 - 200x times magnification of the corroded zone of aluminum after 24h of immersion.....	58
Figure 54 - Photos of all samples with different mixtures of inhibitors into the coating formulation after 48 hours of immersion.....	59
Figure 55 - Photos of AA2024 aluminum alloy protected by coating containing mixture of inhibitors into the formulation after 24 hours of SST	61
Figure 56 - Photos of AA2024 aluminum alloy protected by coating containing mixture of inhibitors into the formulation after 48 hours of SST	62

Figure 57 - Photos of AA2024 aluminum alloy protected by coating containing mixture of inhibitors into the formulation after 72 hours of SST	62
Figure 58 - “Zone1” (near CFRP) and “Zone 2” (about 4 mm from CFRP)	63
Figure 59 - Photos of galvanically coupled AA2024 and CFRP after 4 hours in SST	64
Figure 60 - General view of the sample after 48 hours in SST	67
Figure 61 - EIS results for 24 hours of immersion test and after 72 hours of SST	70
Figure 62 - Results from SST after 24 hours with new scratch applied	71
Figure 63 - Anion exchange reaction occurred with LDHs during corrosion protection....	73
Figure 64 - The schematic presentation of the chemisorbed layer formed by BTA	73
Figure 66 – Corrosion progress on AA2024 through time	79

Table content

Table 1 - pH used for intercalation of different inhibitors into Mg/Al LDH	19
Table 2 - Synergistic mixtures produced in Aveiro University and Airbus Group	21
Table 3 - Times needed to corrosion starts for samples with different coatings	26
Table 4 - SVET map's for different types of coating formulation, using MBT as inhibitor protection	34
Table 5 - SVET map's for different types of coating formulation using tungstate as inhibitor protection	35
Table 6 - Maximum and minimum average of the corrosion peaks and average total currents	36
Table 7 - Photos of galvanically coupled AA2024 and CFRP after 24 hours of SST.....	65
Table 8 - Photos of galvanically coupled AA2024 and CFRP after 28 hours of SST.....	66
Table 9 - Photos of galvanically coupled AA2024 and CFRP after 48 hours of SST.....	67
Table 10 - Photos of galvanically coupled AA2024 and CFRP after 72 hours of SST	68
Table 11 - Synergistic effect for different coatings formulations in AA2024.....	78

1. Introduction

Metals and metallic alloys are currently widely used in different engineering applications. Consequently, corrosion is a big issue in the most engineering infrastructures (examples are in **Figure 1**) [1].



Figure 1 – Corrosion around: airplanes, cars and bridges

An innovative idea to corrosion mitigation is the use of active “smart” self-healing anti-corrosion protective coating [2,3]. These “smart” coatings are able to release inhibitors and prevent corrosion only when they are triggered by a stimulus linked to onset of corrosion processes.

The main objective of this work is the development of new protective self-healing coatings for aeronautic application where the material degradation can cause dramatic aftermaths not only for the used constructions but also for human lives.

Which materials are currently under interest for the aeronautic applications?

1. Light materials like aluminum alloys are well-known materials with good mechanical properties [4]: low weight, good corrosion resistance and relatively lower price in comparison with many other metals.
2. Carbon fiber reinforced plastic (CFRP) is a novel composite material, with extremely promising properties like high strength-to-weight ratio, and conductive properties [5].

The problem appears when these conductive materials are used in the electrical contact (requirement of thunderstorm protection). The more noble CFRP induces the extremely accelerated corrosion of aluminum due to galvanic coupling. To avoid this problem and prolong the life-time of proposed model system (aluminum alloy connected to

CFRP) a new active self-healing materials is going to be developed and applied in frame of this master project (performed in frame of PROAIR project for aeronautic industry).

1.1. Basics of protection with coatings

1.1.1. Corrosion processes

Corrosion of metals can be defined as the destructive attack of a metal through its interaction with environment [6]. It is a complex phenomenon which can occur into very different solutions [7]. Electrochemical corrosion is the most frequent nature of the chemical corrosion; usually it happens by the direct contact of the metal with the aggressive corrosive environment.

The electrochemical corrosion is normally characterized by the presence of aqueous solution in contact with the metal, thus providing an electrochemical system with movement of electrons near the metal surface and occurrence of the oxidation-reduction reactions at the respective electrodes. The most important dissolution of metal under these conditions can be presented by anodic reaction of metal oxidation:



where M is the original metal, M^{n+} is oxidized metal (can be in form oxide/hydroxide which represents the rust on the surface) and n are the number of electrons involved into the reaction (1) [6].

The cathodic reaction during the corrosion processes can be presented as reduction of hydrogen (reaction 2), oxygen (reaction 3) or water (reaction 4):



The reaction (2) occurs mainly in acidic media with low O_2 concentrations. The reaction (3) occurs preferably when high concentration of O_2 is available. The reaction (4) occurs in neutral or basic medium. The corrosion reactions may be accelerated by an increase of temperature, by increase amounts of oxidants (like oxygen), in high concentrations of corrosive species (like Cl^{-}), etc [6].

According to these reactions the cathodic area will be characterized by the increase of the pH near the metallic surface and into the solution around.

1.1.2. Typical protection mechanisms

For a better understanding of basics of protection for the substrate by coatings, possible types of corrosion protection should be mentioned. Commonly, the corrosion protection can be divided in three different types (**Figure 2**) [1,2,8]:

1. The barrier protection by the paint, which limits the transport of water and aggressive species to the metallic surfaces;
2. The sacrificial protection by active metal which present as a metal coating or as a pigment;
3. The protection by inhibitors (additives) which released during the contact of the coating with the environment.

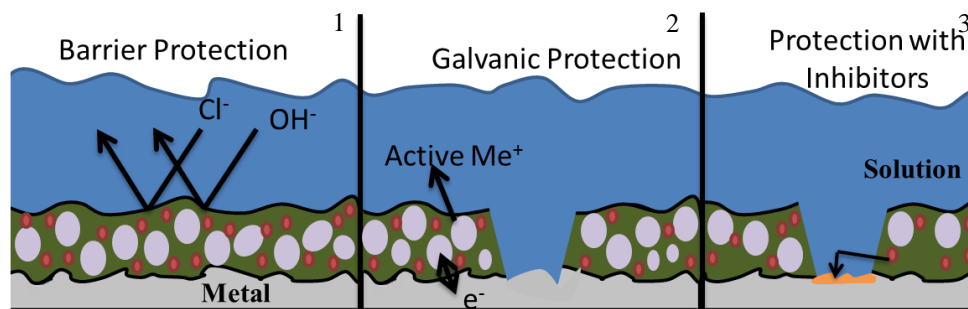


Figure 2 - Different mechanisms of corrosion protection

Moreover, all these types of protective coatings can be used in a multi-layer construction [9]. For example, the barrier protection is not sufficient in the presence of defects and on cut-edges, but it still can modify the active coating reactivity. Protective properties may be improved by galvanic protection or the use of inhibitors.

For better understanding, we will review the basic approaches for each protective mechanism separately.

1.1.3. Barrier protection

Barrier protection is typically offered by organic paints. The barrier coatings are used to suppress the corrosion reaction by limiting the diffusion of the electrolyte, oxygen and aggressive species like chloride to the surface of the substrate [2]. It also limits the

transport of electrons to the metal interface [2], suppressing the corrosion reactions. The weak point of the barrier protective coatings is the possible defect formation: as soon as the coating has any scratches, it stops being effective.

1.1.4. Galvanic protection

The second type of the protection, particularly important in the presence of defects in the coating, is the sacrificial protection by the more active metal. The sacrificial material for corrosion protection must have the following attributes [2]:

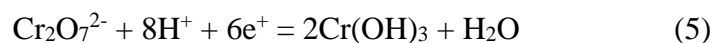
- (1) Excellent electrical contact,
- (2) A suitable electrochemical potential relative to the material, that is going to be protected,
- (3) Formation of suitable corrosion product layer(s) [10].

The possibility of magnesium (Mg) application for active galvanic protection of aluminum was reported [11]. In theory this can be a good solution however the main limitation of this method is the fire hazard associated to Mg metal, especially when it is used in form of powder [11]. In the case of aircrafts it is not sufficient.

1.1.5. Inhibitors

The protection with inhibitors was chosen in the frame of this master project.

For several decades the most used anti-corrosion inhibitor for aluminum in the presence of halide ions [12] was CrO_4^{2-} . Its action is still not completely understood but it is generally attributed to the formation of an oxide film on the metal surface (reaction 5), preventing the corrosion [12].



The necessity to exclude chromates from the surface treatment procedure has dramatically affected the aerospace industry due to its dependence on the use of aluminum based alloys in aircraft manufacturing. In order to replace chromate inhibitors, both organic and inorganic inhibitors were proposed [12].

1. Organic inhibitors. Although the mechanisms of protection with organic inhibitors are not completely understood, the basic principle associated with them is the adsorption of organic molecules on the surface of metallic substrate and the formation of a barrier which

prevent the contact between material and aggressive environment, leading to the decrease of corrosion activity [13].

Previous work with 2-mercaptobenzothiazole (MBT, **Figure 3-a**) and 1,2,3-benzotriazole (BTA, **Figure 3-b**) [6] has shown effective inhibition for galvanically coupled Al alloy with more noble material like steel or copper [8,14].



Figure 3 – Schematic presentation of 2-mercaptobenzothiazole (a) and 1,2,3-benzotriazole (b) molecules.

2. Inorganic inhibitors. As an alternative to organic inhibitors, some inorganic inhibitors have also been proposed for Al alloys. These inhibitors are cerium [2], lanthanum [6], molybdates [6], vanadates [6], phosphates [6] and silica-based inhibitors [2]. In previous work with cerium based inhibitors it was shown that this inhibitor creates a passive insoluble oxide layer that stops the oxygen diffusion from the aggressive environment to the surface [6, 15].

3. Synergistic mixture. In order to create a more effective inhibition system, mixtures of inhibitors have been used [6, 16, 17]. It was shown that the inhibiting actions of two compounds were not always additive: mutual increases or decreases in the inhibition effect were often observed [14]. For example, it was reported that a mixture of inhibitors (BTA + Ce^{3+}) is much more effective for protection of galvanic coupled (Zn+Fe) in comparison with the independent inhibition by BTA or Ce^{3+} compound [6].

For the effective protection of the material with an inhibitor, the easy access of the inhibitor to the surface is desirable. Originally, inhibitors were directly applied into the coating [6]. However, being applied directly, they could interact with the material of the coating and accelerate its destruction [18]. Due to this destruction the ability to keep inhibitors in the coating decreases. It leads to the loss of the inhibitor, decrease of the inhibition activity and possibly creates problems for people and for the environment.

In line with the idea of using environmentally friendly materials and processes, it is necessary to find a solution for controlling the release of the inhibitors. Two types of “smart” nanocontainers are promising for this aim: layer double hydroxides (LDH) [2] and bentonite [2].

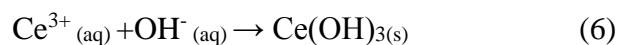
These nanocontainers are able to keep the inhibitors inside their structure and to prevent the contact between them and the coating; moreover the inhibitor release takes place only when the container is triggered.

4. **Layered double hydroxides** (LDH) are hydrotalcite-like compounds [2]. LDHs are known as a good anion-exchangers [19]. Between two positively charged layers of metallic cations/hydroxides there are negatively charged layers of anions. Using the LDH capability to anionic exchange some inhibitors, like MBT or BTA, could be included into the structure in anionic form.

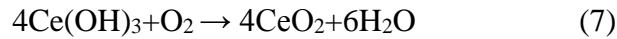
When LDH is loaded with inhibitors and inserted into the coating structure, it is placed near a metallic surface. When the substrate starts to corrode, the anions-exchange capability of LDH is used again: inhibitors are replaced by OH^- , formed by the cathodic reaction of water reduction, or by chloride anions available from the aggressive media. It leads to two advantages of LDH: controlled release of the inhibitor only when corrosion starts and absorbance of cathodically formed hydroxides, what is especially critical in case of aluminum corrosion.

5. **Bentonite** is a cation-exchanger, consisting of negatively charged aluminosilicate sheets, between which inhibiting cations can be intercalated [2, 20] Ce^{3+} loaded bentonite is promising to be dispersed in epoxy resin layers and to be applied to surface of coupled materials for the active anti-corrosion protection. The release of the inhibitor is triggered by metal cations available in the surroundings. In the case of the corrosion reaction of coupled aluminum alloy and CFRP the role of external cations can play Na^+ as a corrosion agent or Al^{3+} released from the material during its degradation.

Ce^{3+} is well-known as a corrosion inhibitor [2, 21, 22]. The effective inhibition happens because of the reaction between Ce^{3+} and hydroxides which leads to the formation of insoluble hydroxide [2]:



The further oxidation of $\text{Ce}(\text{OH})_3(\text{s})$ leads to the formation of CeO_2 according to the reaction (7). This compound is also insoluble and prevents the contact of the surface with aggressive environment [2].



1.1.6. Multi-layer construction

The most effective corrosion protection can be achieved by a combination of different protective mechanisms in the case of galvanically coupled aluminum alloys and CFRP, the barrier protection by organic or inorganic polymer (and corrosion products [9] and protection with inhibitors (Figure 4).

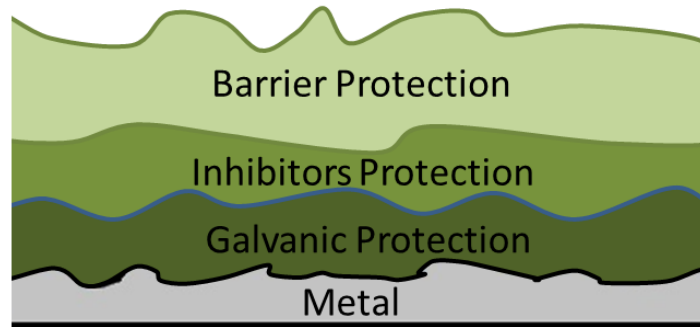


Figure 4 -Multilayer construction

1.2. Materials of the aeronautic industry

1.2.1. Aluminum

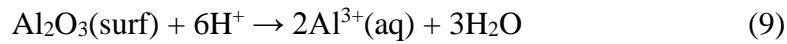
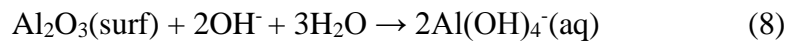
Aluminum alloys are well-known materials with good mechanical properties, low densities, good corrosion resistance and lower price in comparison with many other metals. They are widely used in many engineering applications and scientific technologies, such as aerospace, advanced nuclear reactor, surface coating, metal/air batteries, medicine, etc. [18,4,23].

The surface of aluminum (Al) is covered by a natural insoluble passive film [18]. It leads to a very low reactivity and corrosion rate of Al under neutral aqueous conditions. However, the presence of more noble components in electrical contact with aluminum accelerates its corrosion due to galvanic coupling [12]. It causes degradation of the material and accumulation of corrosion products which leads to the a reduction of the mechanical

properties. To avoid these unwanted processes, the fundamental mechanism of aluminum reactivity must be carefully understood.

1.2.2. Role of pH for the aluminum corrosion

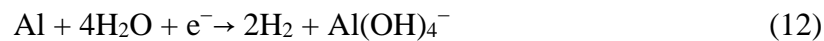
The pH has an important role for the aluminum corrosion: the thin protective insoluble aluminum oxide is present on the surface of material only in the pH range between 4.0 and 8.5. When the pH reaches 10 or decreases below 4 the dissolution of aluminum oxide starts according to the reactions (8) and (9) respectively.



The formation of hydroxides near the surface of aluminum takes place due to the cathodic reaction of water or oxygen reduction by reactions (10) and (11) respectively.



These reactions will take place either on the aluminum surface when it has no connection to other more noble material, or on the surface of the less active material. The increase of pH in aluminum surroundings leads to a higher solubility of the aluminum oxide/hydroxide film and its dissolution (reactions (3) and (4)). The simplified overall reaction of aluminum dissolution is the following:



The possible aluminum protection in this case can be performed by the formation of insoluble layer of inhibitor on the surface which will isolate the alloy from the aggressive environment, or by stabilizing the surrounding pH into neutral region.

1.2.3. Role of chloride for aluminum corrosion

Chloride ions are known to accelerate the pitting corrosion of aluminum [12]. It was shown [17] that chloride does not enter the oxide film but that it is chemisorbed onto the oxide surface and acts as a reaction partner, increasing Al dissolution due to the formation of soluble oxide–chloride complexes. The depression of pitting corrosion in aluminum alloys had a major importance in the last few years due to the important role of light materials in airspace and automotive industry.

A possible idea to control this corrosion is the utilization of anodic protective films which will interrupt the contact between aluminum and aggressive environment. It can be performed by organic inhibitors applications (like MBT [8] or BTA [18]), which will form a stable film on the surface [3]. The inhibitor can be intercalated into the protective coating and act only in case when corrosion starts.

1.2.4. Carbon fiber reinforced plastic

Nowadays, the carbon fiber reinforced plastic (CFRP) is an emergent composite material, with extremely promising properties like high strength-to-weight ratio, anti-corrosion and conductive properties (**Figure 5**) [13,24,25]. It is already used in several applications like aerospace (the wings of Airbus A350) [26], in sport equipment which are under higher levels of stress [25], etc.



Figure 5 - Carbon fiber for CFRP

Due to the favorable properties (like extremely high strength and rigidity of material, low density, high resistance to impact and good thermo-mechanical properties) for the aeronautic industry requirements, CFRP has a great potential to replace some of the aluminum parts of aircrafts [26]. For example, comparison of CFRP with aluminum alloy AA2024 shows these advantages:

1. The density of CFRP is lower (1.82 and 2.78 g / cm³ for CFRP and AA2024 respectively);
2. The strength of CFRP is higher (1440 and 320 MPa for CFRP and AA2024 respectively).

It provides a lighter airplane body or, in another words, it is possible to obtain higher values of strength with lower mass of material. The incorporation of CFRP during aircraft formation is expected to enable weight savings of up to 30% in comparison with the unmodified skin/stringer/frame system.

However, some properties of the new CFRP material are not completely understood and questions exist concerning its application and utilization. For example, the many applications of CFRP during aircraft manufacturing requires permanent control of conductivity between all parts of the machine in order to avoid the damage from lightning strike or from thunderstorm electric fields [25].

1.3. Objective of the work

The main objective of the work is the development of new protective self-healing coating for the galvanically coupled aluminum and carbon fiber reinforced plastic (CFRP). Synergistic mixtures of inhibitors are going to be intercalated into the coating formulation and self-healing ability is going to be analyzed. These new coatings are going to be used into the aeronautic industry and they are being developed in frame of PROAIR project (**Figure 6**).

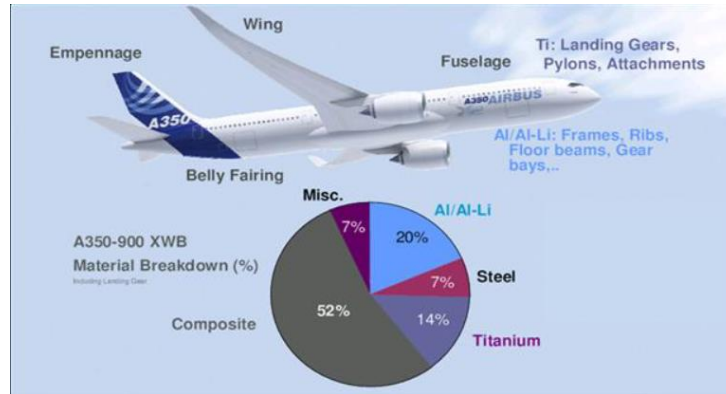


Figure 6 – Materials breakdown for Airbus A350 aircraft[ref]

Nowadays, aluminum alloys and CFRP are separated by insulation titanium layer to prevent electrical contact between them. The weak points of this solution are that titanium insulator is extremely difficult for treatment and expensive material. Moreover, in the presence of isolative materials the protection of aircrafts against thunderstorm strikes is not effective.

The idea of new “smart” self-healing coatings formation is to create effective protection even in the case when aluminum alloys have junction with noble carbon fiber reinforced plastic and increase the life-time of the system in the presence of aggressive environment.

The proposed master thesis has the objective to do work in the academic way and subsequently applying the results into the industrial environment. This work was done at University of Aveiro (Portugal) and in Airbus Group Innovations in Munich (Germany) where all knowledge previously obtained, was applied in industrial environment.

2. Experimental procedure and conditions used

2.1. Materials used

The materials used during the master thesis were:

AA2024 (Al 90.7-94.7%; Cr max 0.1%; Cu 3.8 - 4.9 %; Fe max 0.5%; Mg 1.2-1.8%; Mn 0.3 - 0.9%; Si max 0.5%; Ti max 0.15; Zn max 0.25, Other metals 0.20%) and CFRP.

Zinc nitrate hexahydrate, $Zn(NO_3)_2 \cdot 6H_2O$, ($\geq 99,0\%$); aluminum nitrate nonahydrate, $Al(NO_3)_3 \cdot 9H_2O$, ($\geq 98,5\%$); magnesium nitrate hexahydrate, $Mg(NO_3)_2 \cdot 6H_2O$, (99%), sodium hydroxide, NaOH, ($\geq 98\%$), sodium nitrate, $NaNO_3$, ($\geq 99,5\%$), cerium nitrate hexahydrate, $Ce(NO_3)_3$, (99%), bentonite, $H_2Al_2O_6S$; 2-mercaptobenzothiazol, $C_7H_5NS_2$, (97%); sodium molybdate dehydrate, $Na_2MoO_4 \cdot 2H_2O$ ($>99\%$), sodium metavanadate $NaVO_3$ (99,9 %), Sodium tungstate dehydrate $Na_2WO_4 \cdot 2H_2O$ (99%) all these materials are from Sigma-Aldrich (Germany); 1,2,3 – benzotriazole, $C_6H_5N_3$, ($>99\%$) is obtained from Riedel-de-Haën, Hydrochloric acid, HCl, (36.5% - 38.0%) is obtained from Alfa Aeser.

All chemicals were used without further purification. Deionized water was used as a solvent.

2.2. Type of coatings

The objective of this work was to study the effect of the inhibition during corrosion but not the barrier protection, by the coating, so the SEEVENAX 315-00 epoxy coating was chosen as a model and the formulation was filled with inhibitors inside. For loading the inhibitors inside the idea was to create nanocontainers and fill them with inhibitors because if the inhibitors would be applied directly in the material, they could start reacting with the material on the coating and destroy it, leading to the inhibitors release, decrease of inhibition efficiency and problems to the surround environment.

2.3. Techniques

In order to implement this work, firstly, the syntheses of “smart” nanocontainers: (1) Zn/Al and Mg/Al LDHs loaded with organic (MBT and BTA) and inorganic (Metavanadate, tungstate and molybdate) inhibitors and (2) bentonite loaded with Ce^{3+} cations were done.

The syntheses were performed in Aveiro University and in Airbus Group Innovations and the following techniques were used for characterization in both places.

The nanocontainers were characterized with:

1. **Scanning electron microscopy** (SEM) Hitachi S4100 which allows to analyze the typical size and shape of nanocontainers. The samples were immobilized with carbon glue.
2. **X-ray diffraction** (XRD) X'PERT-PRO from PANalytical which allows to analyze crystal structure of the nanocontainers in order to control their loading with chosen inhibitors. To perform the analysis, the samples were dried at 60° C during 12 hours (original LDH slurry contains about 80% of water).

After characterization the synthesized nanocontainers were applied into a model coated system formulation and were characterized with:

3. **Classical corrosion immersion test** gives an answer about general corrosion of the model system, covered by protective self-healing coatings. To perform the immersion test, a solution of 0,05 M NaCl was used. Photos of the sample surface were recorded every 24 h, until the first signs of corrosion appear.
4. **Electrochemical impedance spectroscopy** (EIS) which allows the discovering of the corrosion layer formation and the estimation of self-healing ability.

The electrochemical impedance measurements were performed in 0,05M NaCl. The perturbations of 10 mV vs. OCP were applied. The used frequency range was from 10 MHz to 100 kHz. The EIS measurements were carried out in a Faraday cage with the Gamry reference 600 ([Airbus group](#)) and the Gamry PCI 4 - 750 ([Aveiro University](#)).

5. **The scanning vibrating electrode technique** (SVET – **Figure 7**) which allows the quantification of corrosion current giving the information about local corrosion rate and degradation deceleration in the presence of the coating. It gives a key to input the fundamental mechanism of reactivity in the complex coupled system for the intelligent design of new effective protective coatings. A 0.05M

NaCl solution was used as an aggressive environment. The data were retrieved every 1hour, during 24 hours.

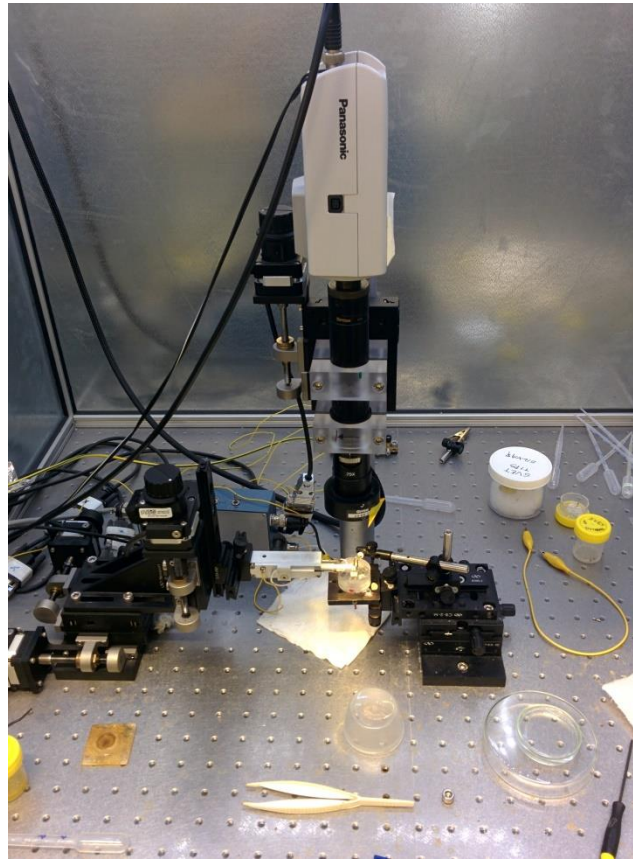


Figure 7 - SVET equipment

6. **Zero resistance ammetry (ZRA)** which allows measuring of the current between two galvanically coupled materials. The measured current is proportional to the rate of the reduction reaction on the surface of the cathodic member of the couple. These measurements were realized in Airbus group innovations in Munique, Germany. The measurements were performed during 24 hours (between the EIS analyses) and a 0.05M NaCl solution was used as an aggressive solvent. The measurements were performed inside a Faraday cage with the Gamry reference 600.
7. **Salt spray test (SST)** is the standardized method used for acceleration of corrosion processes. This technique produces dense saline fog in the chamber as a high corrosive environment.

The salt spray test was performed at 35°C with the salt fog of 1.5 ± 0.5 ml/h, using 0.86M solution of NaCl with pH between 6.5 and 7.2. The photos were recovered after 4h, 24h, 28h, 48, 72 h of exposure.

2.4. Samples and sample holder used

To perform the electrochemical tests in Aveiro University the used samples that had an area of $1 \pm 0.1 \times 10^{-5}$ cm² (1 cm x 1 cm) for each materials (**Figure 8**).

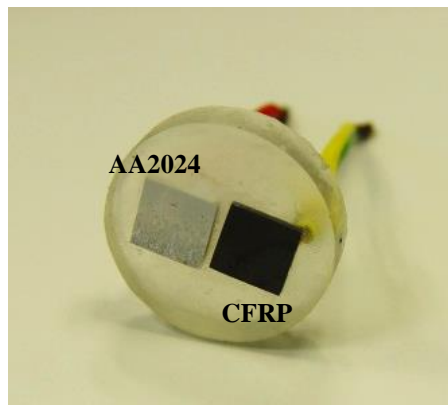


Figure 8 - Sample used for electrochemical tests in Aveiro University

In Airbus group the objective was to use samples with larger surface areas, 4.05 cm * 5.10 cm (or 20.65 cm²) for both materials (**Figure 9**).

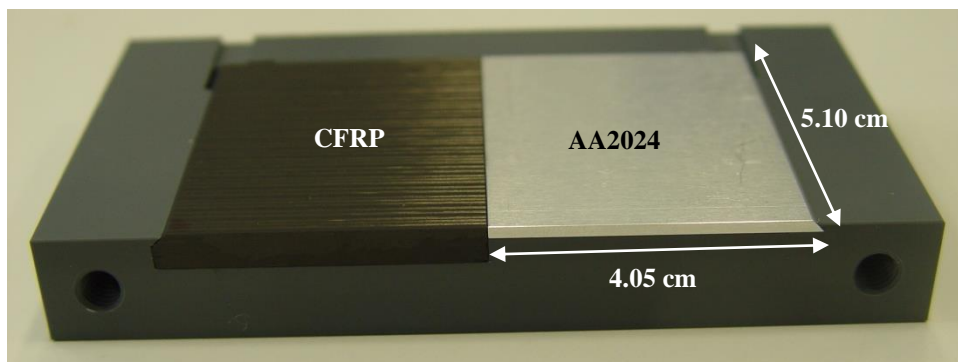


Figure 9 - Aluminum and CFRP Samples used in Airbus group

In order to properly connect both materials for the electrochemical tests, it was necessary to create a sample holder that keeps these two materials in contact during the test and avoids their separation, especially in the salt spray test where the samples are placed at an angle of 60 ° with the horizontal plane.

In order to solve this problem, the first aim was to draw the sample holder and the shape of the samples using the SolidWorks design program. In annex, the scheme of the sample holder and the measurements for the AA2024 and CFRP samples are represented. The sample holder was divided into two parts: one (Peca1_final) to apply the sample and the other to support and fix the sample to the holder (Peca2_final) using pressure, the final draw of both pieces are presented in Annex.

Figure 10 represents the final form of the holder for the samples. It consists on two different parts made of plastic and connected with 2 screws.

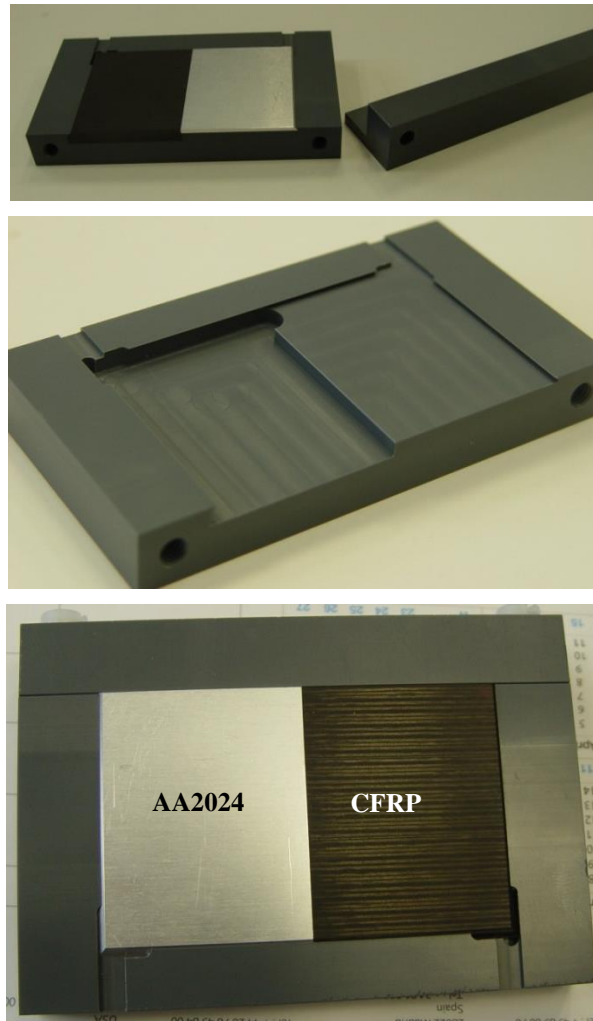


Figure 10 - Sample holder used in Airbus group

To design this sample holder it was necessary to consider some critical points, for example, make the surface completely flat, avoid the crevice corrosion between the two materials (CFRP and AA2024), create a way for solution flow through the sample holder and prevent the accumulation of solution inside the sample holder.

In order to solve some problems during the studying of corrosion processes, one point was to put both materials at the same level and to create a flat surface. For this, all the samples were cut with same height and the sample holder was made to compensate the difference of height between the aluminum (2mm) and CFRP (5mm) samples.

To fix the material into the sample holder, a chamfer was created in the both sides of each material directly in contact with the sample holder.

The way used to prevent the crevice corrosion between both materials, was to paint the sides of the materials which are directly in contact into each other. This prevented the direct contact and fast corrosion between two materials.

On the bottom of the sample holder a gap to facilitate the flow of any liquids presented in the samples was created, preventing the stagnation of solutions.

In order to connect both materials and create the galvanic couple, right next to the gap, into the sample-holder a part of the chamfer present in the sample was removed and the copper wire, which were placed using silver paint as a conductive material and super glue to fix the wires to the materials, first the area was painted with silver glue, than it was attached the wires and paint again with silver glue in order to have a good conduction and on top it was applied the super glue to fix to the holder the copper wires (**Figure 11**).

Some sealant was applied around the sample to prevent the solution enter to the backside of the sample.

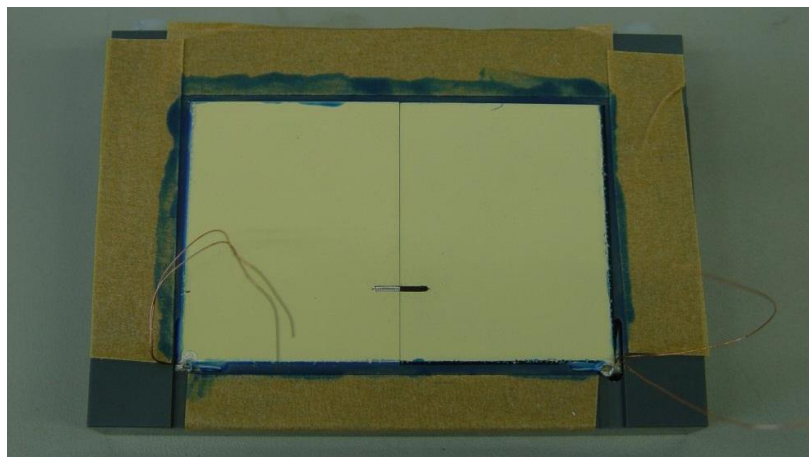


Figure 11 - Sample holder with the wires and the sealant already applied.

2.5. LDH synthesis

The first step of this work is the synthesis of “smart” nanocontainers and loading these nanocontainers with inhibitors (MBT, BTA, tungstate, metavanadate, molybdate in the case of Mg/Al LDH and Ce^{3+} cations in the case of bentonite).

The synthesis of LDH was effectuated according to the experimental procedure previously described [1]. Briefly, the LDH was prepared by slow adding a mixture of 0.5M magnesium nitrate and 0.25M aluminum nitrate deaerated solution ($V=200ml$) to 1.5M sodium nitrate deaerated solution ($V=400ml$) under continue stirring. The pH of the solution was controlled with 2M NaOH solution and kept between 7 and 9 during the synthesis. After this step, the LDH structure was formed under $100^{\circ}C$ during 4 hours, and the pH of this solution was kept between 9 and 10.

After the formation of LDH, in order to separate the slurry from the solution, the mixture was centrifuged at 10 000 rpm during 90 seconds. The obtained LDH precipitation was washed with deionized water and centrifuged again, this procedure was repeated two times in order to eliminate the presence of sodium nitrate into the slurry. Deionized deaerated water was used as a solvent for LDH synthesis, in order to prevent the formation of carbonates during the process. The deaeration of the solution was performed by N_2 (**Figure 12**).

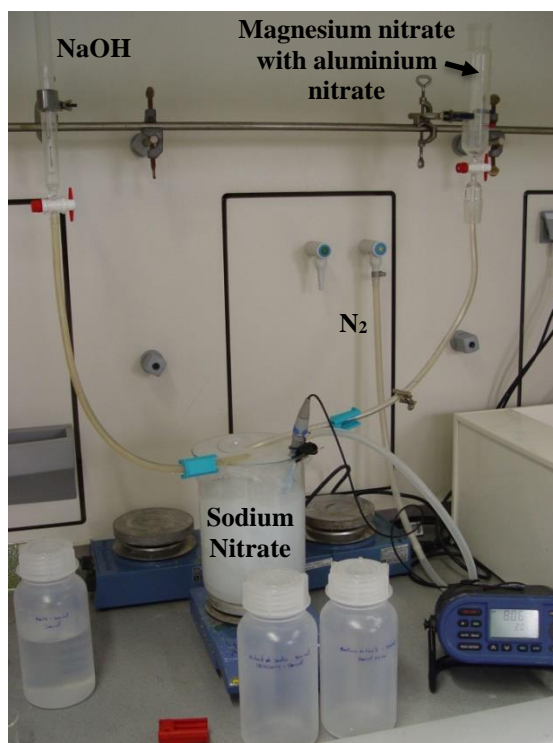


Figure 12 -LDH Synthesis

Bentonite was used as a nanocontainer for Ce^{3+} without any further treatment or purification.

Before the loading of nanocontainers with anti-corrosion inhibitors and their application into coating formulation, the characterization of empty nanocontainers was performed with

1. Scanning electron microscopy (SEM) in order to analyze their size and form, for this analysis all the samples were immobilized with carbon glue.
2. X-ray diffraction (XRD) in order to analyze the crystalline phases of the nanocontainers.

To perform these analyses the sample were dried at 60° C during 12 hours because the LDH slurry contains about 80% of water.

2.6. Inhibitors intercalation

The intercalation of the inhibitors was performed by anion-exchange method. Solutions with 0.1M concentration of the inhibitors were prepared. For the formation of the ionic form of the inhibitor, the pH of the solution was adjusted for each type of inhibitor (**Table 1**).

Table 1 - pH used for intercalation of different inhibitors into Mg/Al LDH

Inhibitors intercalated	pH (range)
MBT loaded into Mg/Al LDH	10.6 - 11
BTA loaded into Mg/Al LDH	10.5 -10.7
Tungstate loaded into Mg/Al LDH	10 – 10.5
Metavanadate loaded into Mg/Al LDH	9 - 9.5
Molybdate loaded into Mg/Al LDH	10.5 -11

To 125 ml of the formed solution, about 20 g of LDH slurry were added. The mixture was kept for 24 hours under continuous stirring. The formed slurry of LDH loaded with inhibitor was centrifuged at 10000 rpm during 90 sec and washed with deionized water three times (**Figure 13**). The work with MBT inhibitor was performed into the bottles covered with metallic foil in order to prevent MBT degradation from Sun light [27].



Figure 13- Inhibitors intercalation

In order to produce the bentonite nanocontainers loaded with Ce^{3+} , firstly a solution of Ce^{3+} (0.56 mol/L) in deionized water was prepared (40 ml) and stirred until all the salt is completely dissolved. The obtained solution was combined with bentonite (2 g) and continuously stirred during 24 hours. After this, the solution was filtered with vacuum filtration technique and washed with deionised water. The synthesized nanocontainers with inhibitors were also characterized with SEM and XRD methods in order to confirm the successful inhibitors intercalation.

2.7. Synergistic mixtures

Synergistic mixture is a mixture of several inhibitors in which the inhibition efficiency (IE) of the mixture of inhibitors is higher than the sum of inhibition efficiencies of included components.

The values of the IE is calculated using **equation 13**:

$$IE = \frac{CR_0 - CR_{inh}}{CR_0} \quad (13)$$

where CR_0 is the corrosion rate in the non-inhibited medium and CR_{inh} is the corrosion rate in the presence of inhibitor. The synergistic parameter (S) is calculated using equation suggested [6] (**equation 14**):

$$S = \frac{1 - IE_{1+2}}{1 - IE_{12}} \quad (14)$$

where $IE_{1+2} = (IE_1 + IE_2) - (IE_1 \cdot IE_2)$. The parameters IE_1 , IE_2 and IE_{12} are calculated inhibition efficiencies for inhibitors 1, 2 and the mixture of 1 and 2, respectively. Values of $S > 1$ indicate the synergistic behavior of selected inhibitors in combination.

In order to find the most effective inhibitive combinations some mixtures of organic and inorganic inhibitors were tested during this work of this Master thesis (**Table 2**).

Table 2 – Synergistic mixtures produced in Aveiro University and Airbus Group.

Synergistic mixtures
MBT loaded into Mg/Al LDH mixed with Ce^{3+} loaded into bentonite
BTA loaded into Mg/Al LDH mixed with Ce^{3+} loaded into bentonite
Metavanadate loaded into Mg/Al LDH mixed with Ce^{3+} loaded into bentonite
Tungstate loaded into Mg/Al LDH mixed with Ce^{3+} loaded into bentonite
Molybdate loaded into Mg/Al LDH mixed with Ce^{3+} loaded into bentonite

3.Results

3.1.Research laboratory

3.1.1. Nanocontainer characterization

3.1.1.1. Scanning electron microscopy (SEM)

Figure 14 shows as an example of the typical results for Mg/Al LDH (a), Zn/Al LDH (b), Mg/Al LDH loaded with MBT (c) and Zn/Al LDH loaded with MBT (d). The typical size of LDH crystal does not depend on the inhibitors inside and it is defined by the cationic composition of the layers.

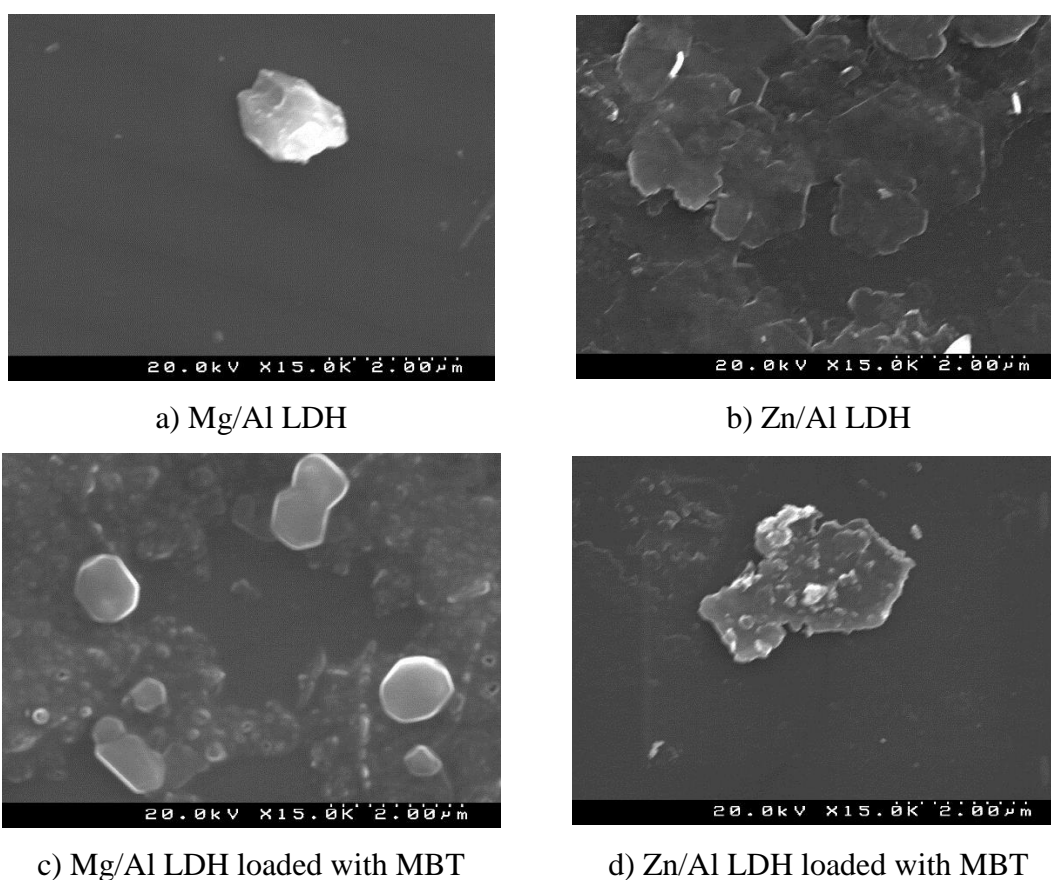


Figure 14 - SEM images for the different types of nanocontainers, used in this work

3.1.1.2. X-ray diffraction (XRD)

Figure 15 represents the XRD patterns of Mg-Al LDH before (a) and after intercalation with 1,2,3-benzotriazole (BTA, b) and with 2-mercaptobenzothiazole (MBT, c).

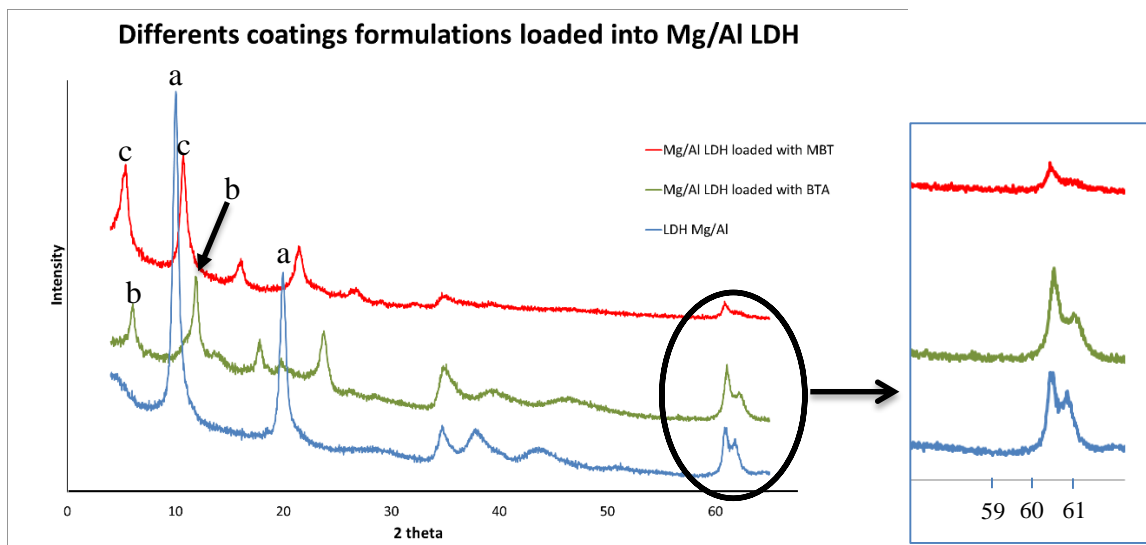


Figure 15 - XRD patterns of Mg/Al LDH before (a), and after intercalated with BTA (b) and MBT (c)

In the XRD pattern of the parental Mg-Al LDH, one can see two characteristics peaks of the LDH structure, at 2 Theta (2θ) equal to 9.83° and 19.80° , marked as “a”. These reflections correspond to a basal spacing of 8.94 \AA . Taking into account the thickness of Mg/Al hydroxide layer (4.77 \AA^{23}), the space available for NO_3^- is 4.17 \AA .

In the XRD pattern of Mg/Al LDH loaded with MBT, it is possible to observe that the main LDH reflections are shifted to the smaller 2 Theta range can be found at 5.19° and 10.58° respectively (marked “c”). These angles correspond to the basal spacing of 16.67 \AA and 17.03 \AA respectively. Hence the gallery height available for MBT is equal to 11.63 \AA .

In the pattern of Mg/Al LDH loaded with BTA (“b”), the characteristic peaks are also shifted to smaller values of 2θ in comparison with those of the parental LDH structure. The two peaks, representative for this material, located at 5.75° and 11.50° , respectively, which gives the basal spacing equal to 15.5 \AA and the gallery height available for BTA anions equal 10.44 \AA .

The diffraction reflection at 2θ of about 61° (inset in Figure 15), does not depend on the nature of intercalated anions and corresponds to the planes perpendicular to double cations layers [28]. One can see that the anion exchanges resulted in no change in position of this reflection thereby indicating that the exchange reactions do not affect composition and structure of the double cations layer.

Figure 16 represents the XRD patterns of the parental Zn/Al NO_3^- LDH (a) in comparison with ZN/AL LDH loaded with MBT (b).

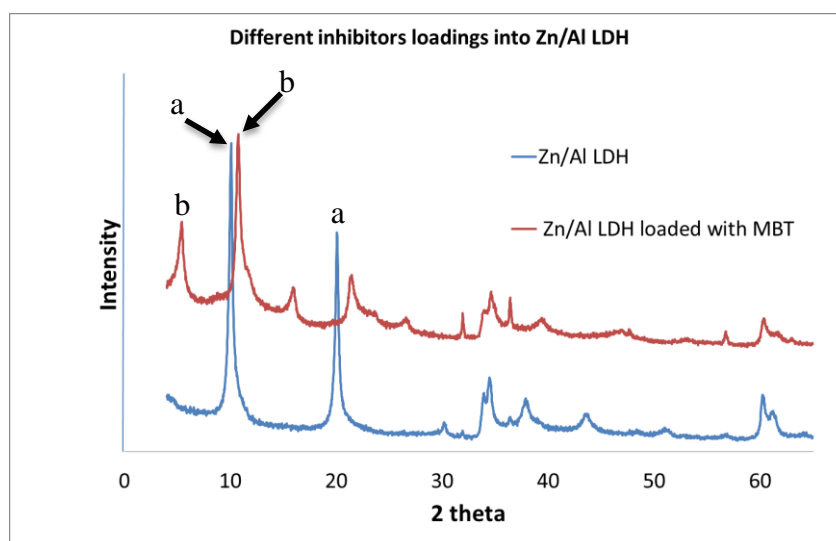


Figure 16 – XRD of Zn/Al LDH loaded with MBT (b) as compared with XRD the parental Zn/Al LDH (a) (intercalated with the nitrate)

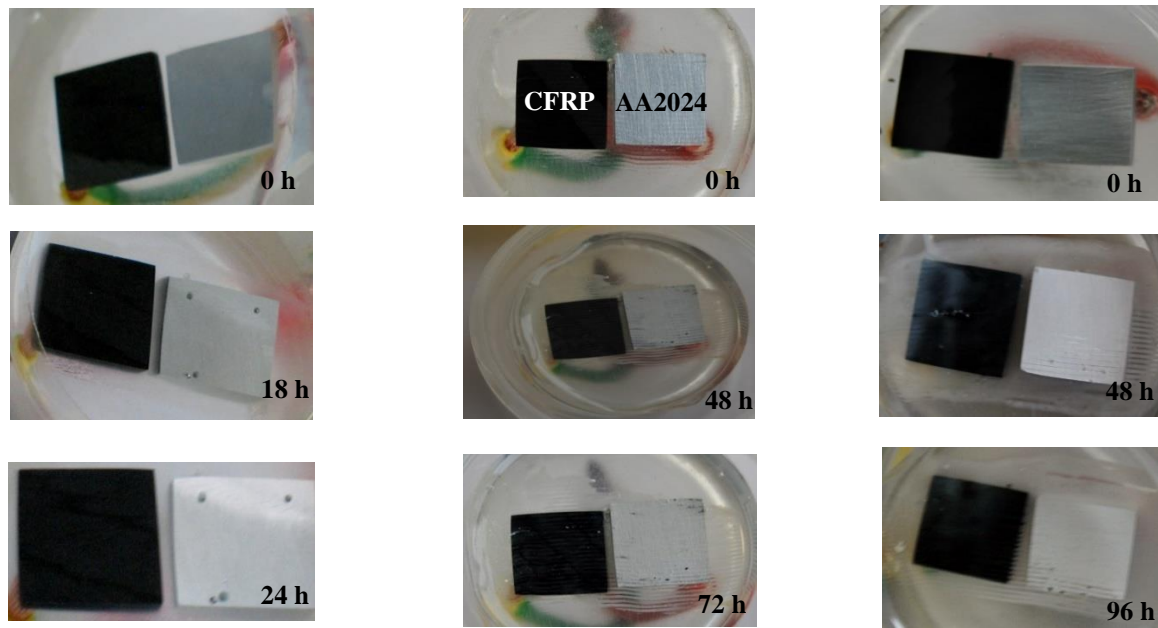
In the XRD pattern of the parental Zn/Al LDH, there are two peaks at 2 Theta about 9.87° and 19.90° corresponding to the basal spacing value of 8.91 Å. The thickness of Zn/Al hydroxide layer is about 4.71 Å, then gallery height available for NO³⁻ anions equals 4.20 Å. This value is very similar to the respective value for the parental Mg/Al LDH.

In the case of Zn/Al LDH loaded with MBT, these two characteristic peaks in the XRD pattern are shifted to smaller values of 2θ and located at 5.13° and 10.53°, corresponding to the basal spacing value equal to 16.78 Å. The height of the gallery space occupied by MBT⁻ anions and water molecules is 12.07 Å.

3.1.2. Results of the different types of coated formulations

3.1.2.1. Immersion test

The immersion tests of galvanically coupled CFRP and AA2024 were performed into aqueous 0.5M NaCl solution. The obtained results show that the corrosion of the samples with the different types of coating formulation starts at different times (**Table 3** and **Figure 17**). **Figure 17** shows the sample with the minimum of resistance against corrosion and the sample with the maximum resistance to corrosion. **Table 3** shows the amount of time in hours, which is required for each type of coating formulation to present the first signs of corrosion on sample.



a) Without inhibitors in the coating formulation (0, 18, 24 h)

b) BTA loaded into Mg/Al LDH mixed with cerium loaded into bentonite (0, 48, 72 h)

c) MBT loaded into Mg/Al LDH mixed with cerium loaded into bentonite (0, 48, 96 h)

Figure 17 - Corrosion tests for different types of coating

In **Figure 17** it is observed that corrosion starts to appear from 18 hours (coating without any inhibitors) up to 96 hours (synergistic mixture of MBT loaded into Mg/Al LDH mixed with cerium loaded into bentonite).

In sample (a) is showed as a reference: it does not contain any additives inside the paint. The corrosion of this sample starts very fast (after 18 hours of immersion).

Samples (b) and (c) in **Figure 17** represent the mixture of inhibitors loaded into “smart” nanocontainers and applied into coating formulation (about 16% of the coating formulation). **Figure 17 -b** represents the sample of which the coating contains BTA loaded into Mg/Al LDH mixed with Ce^{3+} loaded into bentonite. The corrosion of this sample appears after 72h of immersion. **Figure 17-c** represents the coating formulation containing MBT loaded into Mg/Al mixed with Ce^{3+} loaded into bentonite. In this case one observes that the corrosion starts to appear after 96 hours of immersion.

In some cases some corrosion spots are viewed on the surface of the samples very earlier. The reason for this behavior can be explained with poor application of the coating by a bar-coater (40 μ m of raw material) and low reproducibility of the experiments (immersion test) during laboratory tests.

Table 3 - Time needed to corrosion initiation for samples with different coatings

Type of coating	Time needed to starts corrosion (h)
Simple coating	18
Mg/Al LDH	24
Zn/Al LDH	24
Bentonite	24
Cerium loaded into bentonite	24
MBT loaded into Mg/Al LDH	48
BTA loaded into Mg/Al LDH	48
MBT loaded into Zn/Al LDH	24
MBT loaded into Mg/Al LDH mixed with Ce ³⁺ loaded into bentonite	96
BTA loaded into Mg/Al LDH mixed with Ce ³⁺ loaded into bentonite	72
MBT loaded into Zn/Al LDH mixed with Ce ³⁺ loaded into bentonite	72

3.1.2.2. Electrochemical impedance spectroscopy (EIS)

Figure 18 represents the electrochemical impedance results for scratched and non-scratched reference samples (no inhibitors in the coating formulation). From **Figure 18** it can be seen that the decrease of resistance for the sample without scratch happens immediately between 1h and 5 hours of immersion. On the other hand, for the sample with the scratch, the values of resistance decrease between 5 hours and 10 hours of immersion.

However it should be mentioned that at the beginning of the measurement the resistance in the reference coating without any artificial scratch is lower than in the scratched sample. This could be explained by a poor quality of the paint on the non-scratch sample and a good application on scratched sample at the same time.

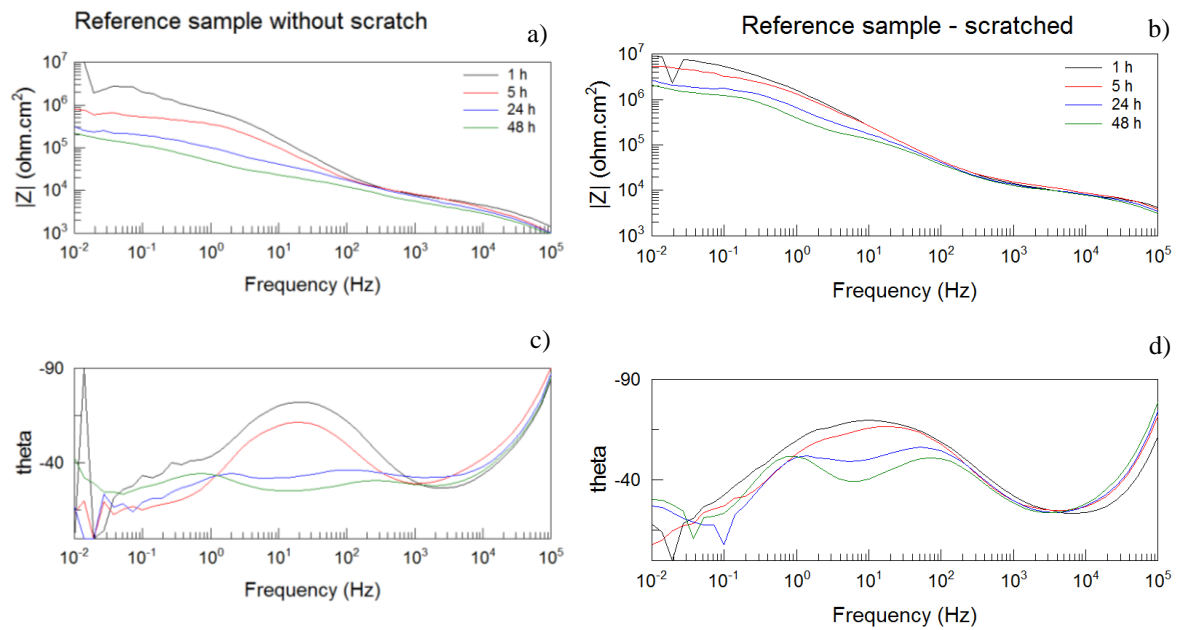


Figure 18 – EIS for reference sample, a) without scratch, b) scratched.

Figure 19 represents the comparison between the reference sample (with scratch) and the sample coated with tungstate loaded into Mg/Al LDH mixed with cerium loaded into bentonite in the coating formulation (without scratch).

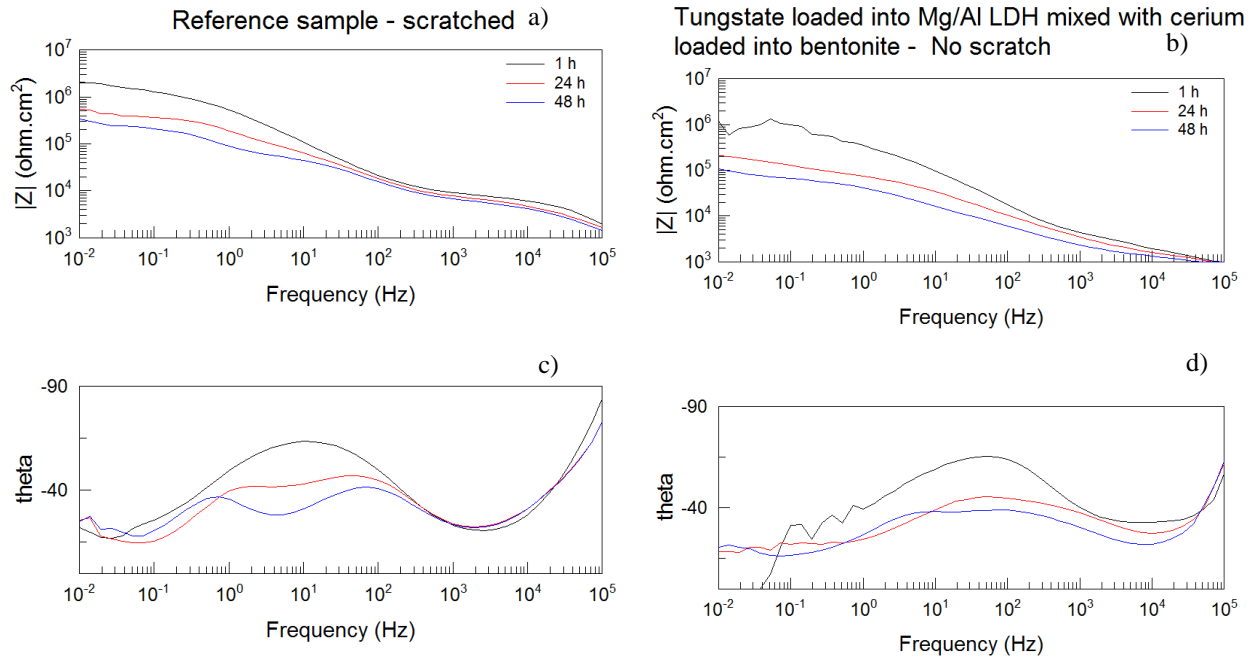


Figure 19 – EIS for a) Reference sample (scratched) and b) Tungstate loaded into Mg/Al LDH mixed with Ce^{3+} loaded into bentonite (no scratch).

The analysis of these graphics, shows that after 1 hour of immersion the reference sample with scratch has values of $|Z|$ and theta in same order of magnitude as the sample

without any scratch but coated with synergistic mixtures of inhibitors loaded into nanocontainers. This can mean that all the micro-scratches naturally formed between the nanocontainers and the coating could be represented with more or less comparable size with the artificial defect which was created with the needle into reference coating.

This intermediate **conclusion** had effect on the next measurements where all the impedances tests were realized without any artificial defect because all of them have nanocontainers with inhibitors in the coating formulation.

Figures 20 - 23 represent the impedance measurements for the samples which contain the mixture of inhibitors into the coating formulation without any artificial defects:

1. MBT loaded into Mg/Al LDH together with Ce^{3+} loaded into bentonite (**Figure 20-a**).
2. MBT loaded into Mg/Al LDH (**Figure 20-b**).
3. BTA loaded into Mg/Al LDH together with Ce^{3+} loaded into bentonite (**Figure 21-a**).
4. Cerium loaded into bentonite (**Figure 21-b**).
5. Metavanadate loaded into Mg/Al LDH together with Ce^{3+} loaded into bentonite (**Figure 22-a**).
6. Metavanadate loaded into Mg/Al LDH (**Figure 22-b**).
7. Tungstate loaded into Mg/Al LDH together with Ce^{3+} loaded into bentonite (**Figure 23-a**).
8. Tungstate loaded into Mg/Al LDH (**Figure 23-b**).

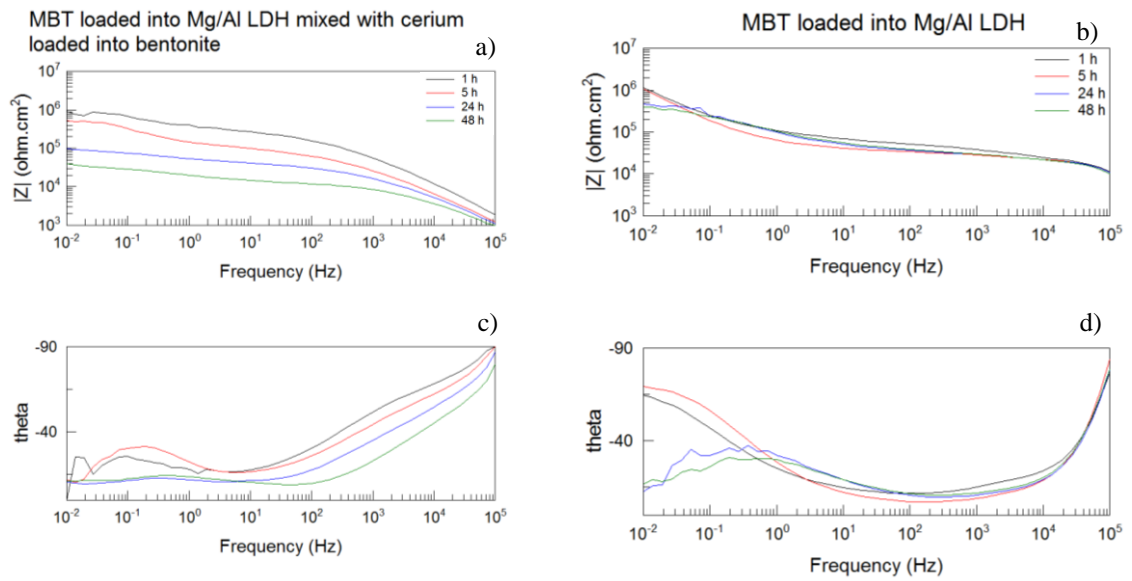


Figure 20 – EIS analyses for a) MBT loaded into Mg/Al mixed with cerium loaded into bentonite, b) MBT loaded into Mg/Al LDH.

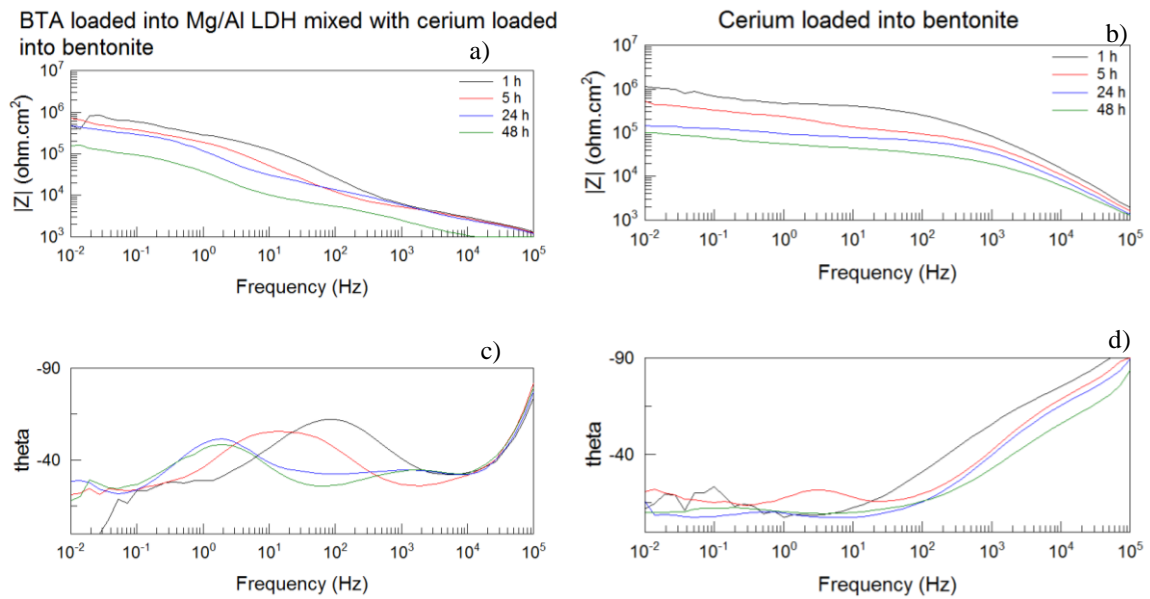


Figure 21 - EIS analyses for a) BTA loaded into Mg/Al mixed with cerium loaded into bentonite, b) cerium loaded into bentonite.

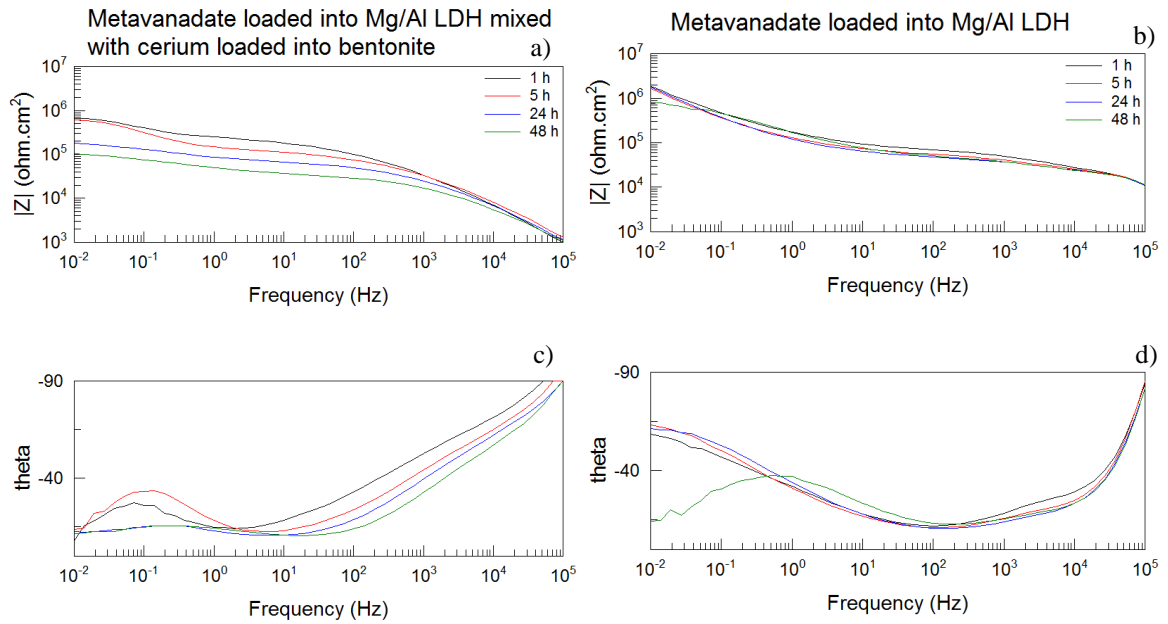


Figure 22 - EIS analyses for a) Metavanadate loaded into Mg/Al mixed with cerium loaded into bentonite, b) metavanadate loaded into Mg/Al LDH.

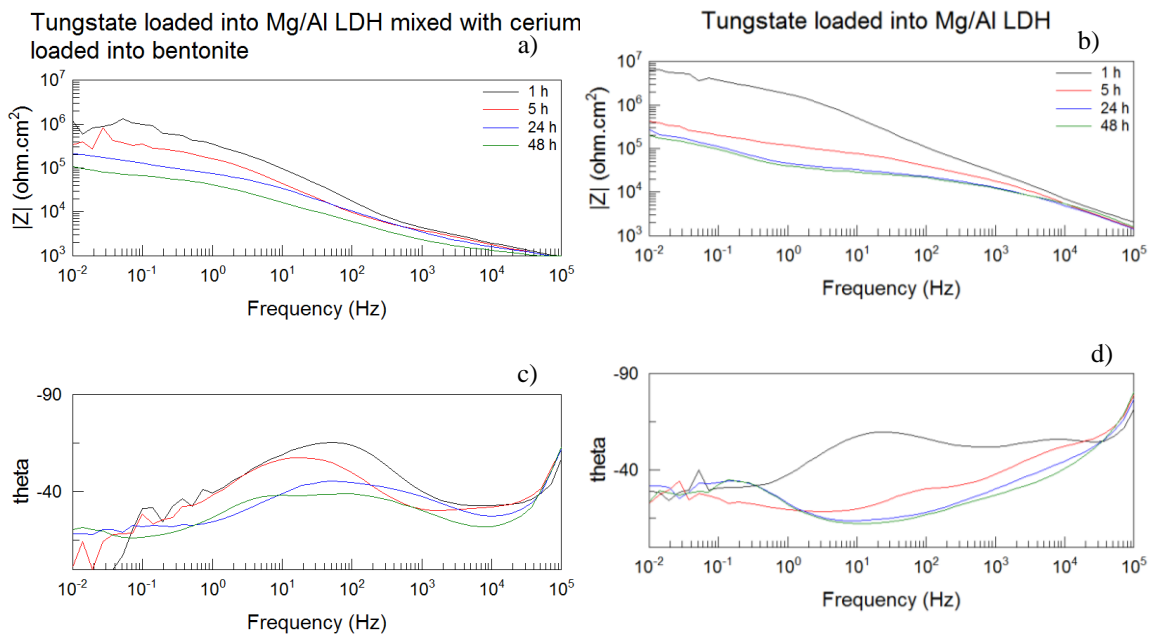


Figure 23 - EIS analyses for a) Tungstate loaded into Mg/Al mixed with cerium loaded into bentonite, b) tungstate loaded into Mg/Al LDH.

Based on the previous figures (20 to 23), the synergistic mixture of MBT loaded into Mg/Al LDH together with Ce³⁺ loaded into bentonite shows a constant decrease of resistance during 48 hours in comparison with the single inhibitor MBT loaded into Mg/Al LDH. However analysis of both coatings shows the same value of resistance after 48 hours

of immersion (resistance decrease about one order of magnitude). Comparison of all figures showed that the MBT loaded nanocontainers mixed with Ce^{3+} loaded nanocontainers and standalone MBT loaded into Mg/Al LDH implement a higher resistance of the sample to the corrosion environment.

Figure 21-b represents the standalone Ce^{3+} inhibitor loaded into bentonite. These results show a slow and a gradual decrease of resistance during 48 hours (one order of magnitude in the summing during 48 hours).

The obtained values for the BTA loaded into Mg/Al LDH show a slowly decrease during the first 24 hours, however after this period the resistance suffer a drop.

The interesting result appears with metavanadate loaded into Mg/Al LDH nanocontainers. The resistance of the coating remains very stable during 24 hours, however between 24 hours and 48 hours the resistance significantly decreases.

The sample with the higher resistance against corrosion during the 48 hours is the one with the coating formulation containing metavanadate loaded into Mg/Al mixed with cerium loaded into bentonite the result. It shows a good resistance to corrosion during the first 24 hours of immersion, but between 24 - 48 hours the resistance significantly decreases accomplishing the values of resistance equal for the other coatings formulations. This result matches the results obtained in Airbus Group Innovations, where, during the immersion test, the coating with metavanadate mixed with cerium inhibitors showed a really shiny surface for up to 24 hours of immersion. However after 48 hours the sample started to corrode. The ZRA measurements for this sample also show a decrease of corrosion during first-hours of experiment (see **chapter 3.2.2.1**).

Figure 23-a represents the EIS measurements for the coating formulation containing tungstate loaded into Mg/Al mixed with cerium loaded into bentonite. The initial resistance ($10^6 \Omega.cm^2$) is lower than the resistance in the standalone inhibitor ($10^7 \Omega.cm^2$), of tungstate loaded into Mg/Al LDH. However after 48 hours of immersion both samples show the same order of magnitude for resistivity against corrosion.

3.1.2.3. Scanning vibrating electrode technique (SVET)

For a general acknowledgement the SVET results usually can be presented in two different ways, **Figure 24** show the graphic obtained in 2D and 3D from the sample surface.

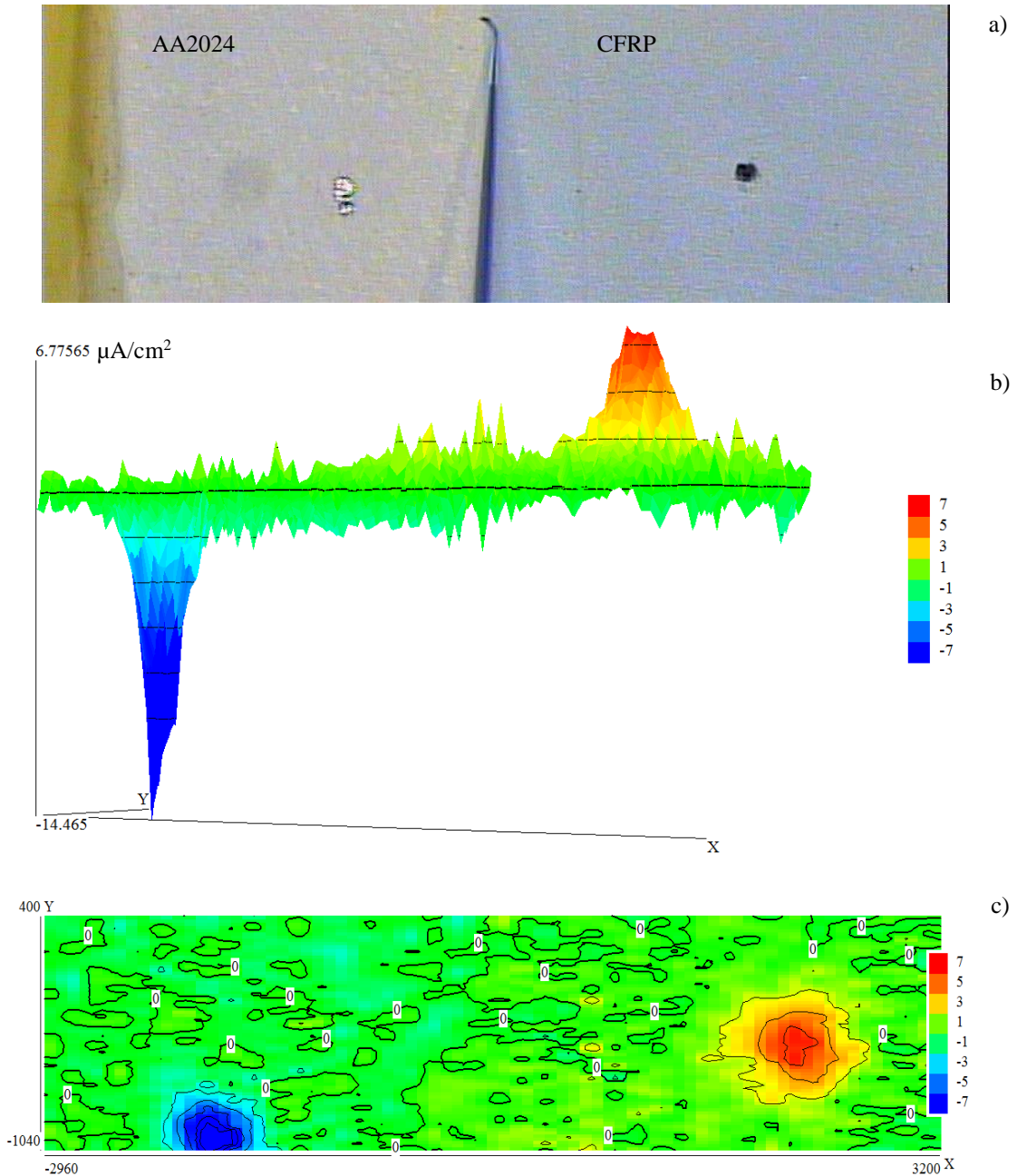


Figure 24 - SVET general results a) photo from the reference sample, b) SVET measurement result in 3D, c) SVET measurement result in 2D

The results demonstrated in **Figure 24** show 2 peaks which are located in places of the needle defects: the anodic one (AA2024, red right peak) and cathodic one (CFRP, blue

left peak). These peaks represent the corrosion currents from the sample. The objective of the application of SVET technique is to quantify the corrosion currents and to analyze their decreases through the time in the presence of inhibitors.

Table 4 and **Table 5** represent the SVET analyses for the model reference sample (1), for a single inhibitor MBT loaded into Mg/Al LDH (2) and tungstate loaded into Mg/Al LDH (3) both added into coating formulation and for two different examples of inhibitive mixture (MBT loaded into Mg/Al LDH mixed with Ce^{3+} loaded into bentonite(4) and tungstate loaded into Mg/Al LDH mixed with Ce^{3+} loaded into bentonite (5)) at the beginning, after 10 and 24 hours of immersion. **Tables 4** and **5** represent the coating loaded with inhibitors which showed the best results during previous tests such as Salt spray test, immersion test, Zero resistance ammeter (ZRA) and EIS made in Airbus Group.

Table 4 – SVET map's for different types of coating formulation using MBT as inhibitor after 0h, 10h and 24h of immersion.

	0 hours	10 hours	24 hours
Reference sample	<p>12.61 $\mu\text{A}/\text{cm}^2$ -26.38 $\mu\text{A}/\text{cm}^2$</p>	<p>8.58 $\mu\text{A}/\text{cm}^2$ -13.34 $\mu\text{A}/\text{cm}^2$</p>	<p>9.77 $\mu\text{A}/\text{cm}^2$ -12.01 $\mu\text{A}/\text{cm}^2$</p>
MBT loaded into Mg/Al LDH	<p>5.43 $\mu\text{A}/\text{cm}^2$ -2.54 $\mu\text{A}/\text{cm}^2$</p>	<p>3.43 $\mu\text{A}/\text{cm}^2$ -3.62 $\mu\text{A}/\text{cm}^2$</p>	<p>2.57 $\mu\text{A}/\text{cm}^2$ -1.50 $\mu\text{A}/\text{cm}^2$</p>
MBT loaded into Mg/Al LDH mixed with Ce ³⁺ loaded into bentonite	<p>2.26 $\mu\text{A}/\text{cm}^2$ -2.41 $\mu\text{A}/\text{cm}^2$</p>	<p>2.95 $\mu\text{A}/\text{cm}^2$ -1.33 $\mu\text{A}/\text{cm}^2$</p>	<p>2.36 $\mu\text{A}/\text{cm}^2$ -1.37 $\mu\text{A}/\text{cm}^2$</p>

Table 5 - SVET map's for different types of coating formulation using tungstate as inhibitor after 0h, 10h and 24h of immersion.

	0 hours	10 hours	24 hours
Reference sample	<p>12.61 $\mu\text{A}/\text{cm}^2$ -26.38 $\mu\text{A}/\text{cm}^2$</p>	<p>8.58 $\mu\text{A}/\text{cm}^2$ -13.34 $\mu\text{A}/\text{cm}^2$</p>	<p>9.77 $\mu\text{A}/\text{cm}^2$ -12.01 $\mu\text{A}/\text{cm}^2$</p>
Tungstate loaded into Mg/Al LDH	<p>182.12 $\mu\text{A}/\text{cm}^2$ -25.19 $\mu\text{A}/\text{cm}^2$</p>	<p>123.58 $\mu\text{A}/\text{cm}^2$ -29.09 $\mu\text{A}/\text{cm}^2$</p>	<p>122.09 $\mu\text{A}/\text{cm}^2$ -19.45 $\mu\text{A}/\text{cm}^2$</p>
Tungstate loaded into Mg/Al LDH mixed with Ce ³⁺ loaded into bentonite	<p>14.89 $\mu\text{A}/\text{cm}^2$ -3.31 $\mu\text{A}/\text{cm}^2$</p>	<p>12.00 $\mu\text{A}/\text{cm}^2$ -4.88 $\mu\text{A}/\text{cm}^2$</p>	<p>12.74 $\mu\text{A}/\text{cm}^2$ -3.84 $\mu\text{A}/\text{cm}^2$</p>

These results show a predictable output, where the standalone inhibitors have higher values of current in comparison with the synergistic mixture values. For the reference sample the current can be either higher in comparison with loaded coating formulation (as in the case the standalone MBT loaded into Mg/Al LDH) or lower (as in the case of standalone tungstate loaded into Mg/Al LDH).

Table 6 presents the average of the maximum and minimum peak values for all the inhibitors and their mixtures analyzed with SVET during this work (last 5 hours of measurement are counted). The maximum correspond to the AA2024 sample corrosion peak and the CFRP sample cathodic reaction correspond to the negative peak value.

Table 6 – Maximum and minimum average of the corrosion peaks and average total currents.

Type of coating formulation (single inhibitors)	Average value ($\mu\text{A}/\text{cm}^2$)	Total current value ($\text{A} \cdot 10^{-8}$)	Type of coating formulation (reference sample / synergistic mixtures)	Average value ($\mu\text{A}/\text{cm}^2$)	Total current value ($\text{A} \cdot 10^{-8}$)
Reference sample	Max: 8.24 Min: -10.84	Max: 11.38 Min: -5.52	Ce^{3+} loaded into Bentonite	Max: 58.82 Min: -25.36	Max: 9.33 Min: -11.71
MBT loaded into Mg/Al LDH	Max: 2.38 Min: -2.23	Max: 0.91 Min: -0.87	MBT loaded into Mg/Al LDH mixed with Ce^{3+} loaded into bentonite	Max: 2.63 Min: -1.69	Max: 0.72 Min: -6.76
BTA loaded into Mg/Al LDH	Max: 28.80 Min: -29.73	/	BTA loaded into Mg/Al LDH mixed with Ce^{3+} loaded into bentonite	Max: 6.67 Min: -4.22	Max: 2.43 Min: -2.51
Metavanadate loaded into Mg/Al LDH	Max: 18.30 Min: -3.39		Max: 9.68 Min: -9.21	Metavanadate loaded into Mg/Al LDH mixed with Ce^{3+} loaded into bentonite	Max: 19.32 Min: -3.62
Tungstate loaded into Mg/Al LDH	Max: 140.02 Min: -22.34	Max: 27.15 Min: -22.88	Tungstate loaded into Mg/Al LDH mixed with Ce^{3+} loaded into bentonite	Max: 13.17 Min: -4.27	Max: 9.86 Min: -6.37
			Molybdate loaded into Mg/Al LDH mixed with Ce^{3+} loaded into bentonite	Max: 12.63 Min: -6.26	Max: 2.37 Min: -4.93

From **Table 6**, it is evident that the average values of the corrosion currents decrease for the mixture of inhibitors in comparison with standalone inhibitors. One exception is the metavanadate inhibitor loaded into Mg/Al LDH. However even in this case the values remain very similar to the metavanadate synergistic mixture.

The average values of corrosion current show a higher inhibitive effect in the case of two combined inhibitors in the same coating formulation. The highest effect is observed for the mixture of MBT loaded into Mg/Al LDH together with Ce^{3+} loaded into bentonite.

In the case of molybdate loaded into Mg/Al LDH mixed with cerium loaded into bentonite, the result shows a low average corrosion current. However from the comparison of all entire results, it's possible to conclude that the molybdate was release from the coating not only in the place of artificial defects but also in a large amount from all the coating (**Figure 25**) making the solution rich in molybdate.

This solution creates the inhibitive protection effect in the case of stationary conditions and becomes not effective in the case of flow solution.

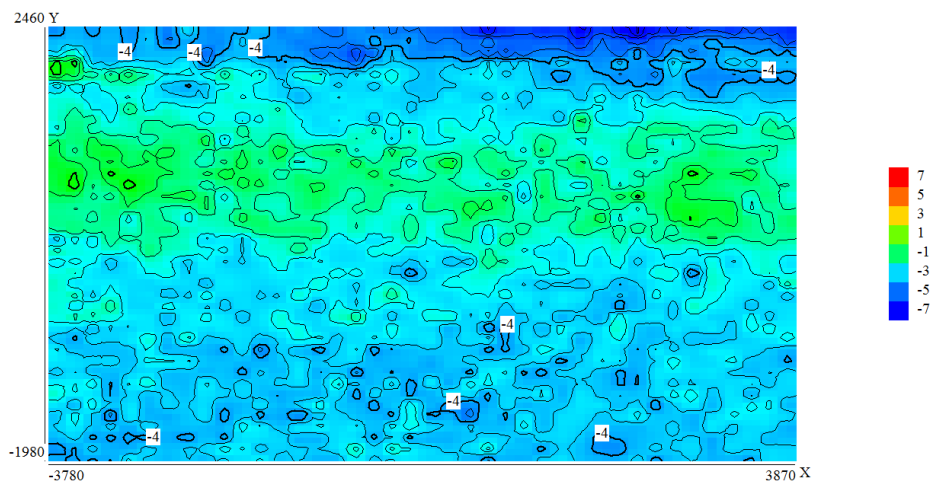


Figure 25 - SVET measurement from coating formulation molybdate loaded into Mg/Al LDH mixed with cerium loaded into bentonite (2 hours of immersion)

Figure 26 represents the variation of corrosion currents during 24 hours for the reference sample, for four different types of coating formulation (standalone MBT loaded into Mg/Al LDH, cerium loaded into bentonite, the synergistic mixture MBT loaded into Mg/Al LDH together with cerium loaded into bentonite and the reference coating without any inhibitors).

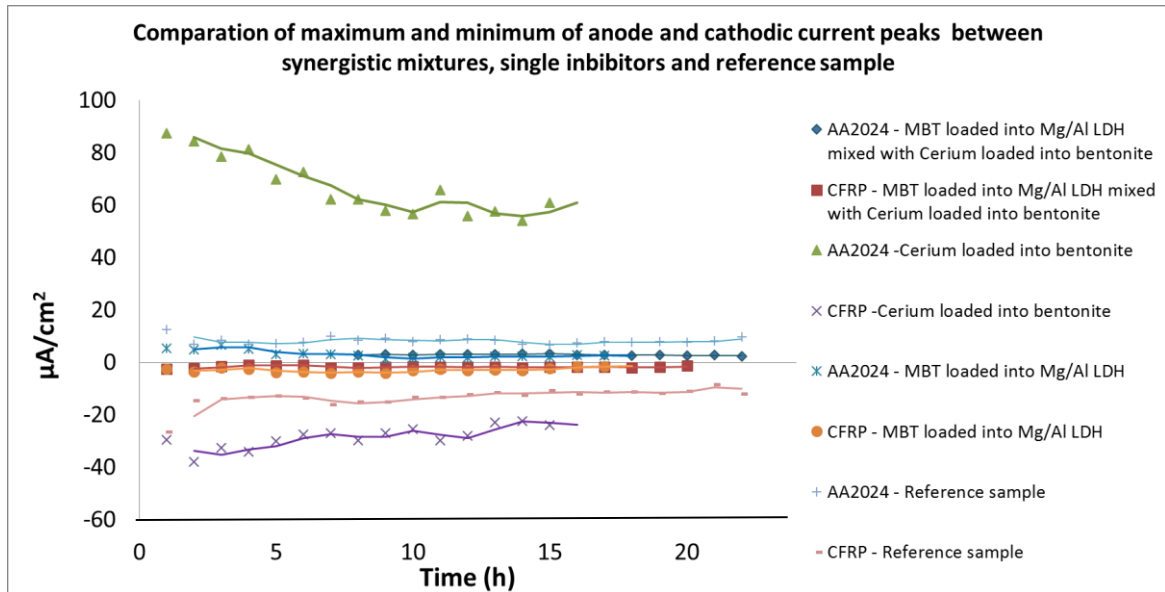


Figure 26 – Maximum and minimum peaks of corrosion between samples during 24h, a) MBT loaded into Mg/Al LDH mixed with cerium loaded into bentonite, b) MBT loaded into Mg/Al LDH, c) Cerium loaded into bentonite and d) reference sample.

The graphic in **Figure 26** shows a significant increase of corrosion current for the standalone cerium loaded into bentonite in comparison with the reference sample. This can be explained by the significant increase of the ionic strength of the solution due to the release of Ce^{3+} .

In contrast, the coating containing MBT loaded into Mg/Al LDH mixed with Ce^{3+} loaded in bentonite mixture of inhibitors shows the lowest corrosion current in both anodic and cathodic part of the system. In comparison with standalone inhibitor MBT loaded into Mg/Al LDH the difference is negligible; however the mixture of inhibitors shows very stable decreased corrosion current throughout the entire test.

The calculations based on maximal SVET detection of ionic currents can be overestimated due to unevenly distributed corrosion activities which results in a several multiple current maximums.

The integrated ionic currents I_{intAN} and I_{intCAT} are independent from the number of observed data points and can be calculated by (**equation 15**):

$$I_{int} = \sum_{k=1}^N I_n * A_n \quad (15)$$

Where I_n is the SVET current density measured in point n (at 200 μm above the surface), A_n is the surface area (mm^2) corresponding to one data point and N is the total number of data points (anodic and cathodic, respectively) considered for calculation. In frame of this work this calculation method will called as “**Total corrosion current**”.

Figure 27 and **Figure 28** represent the corrosion current calculated through the volume method during 24 hours on anodic and cathodic area of the model samples for different coating formulations. **Figure 27** represents the tungstate loaded into Mg/Al LDH mixed with cerium loaded into bentonite the results for the coating formulations and **Figure 28** show the results for the MBT loaded into Mg/Al LDH mixed with cerium loaded into bentonite. These systems were chosen due to the best results in previous analyzes. They were also compared with standalone inhibitors MBT loaded into Mg/Al LDH and tungstate loaded into Mg/Al LDH respectively, with standalone Ce^{3+} loaded into bentonite and with the reference sample.

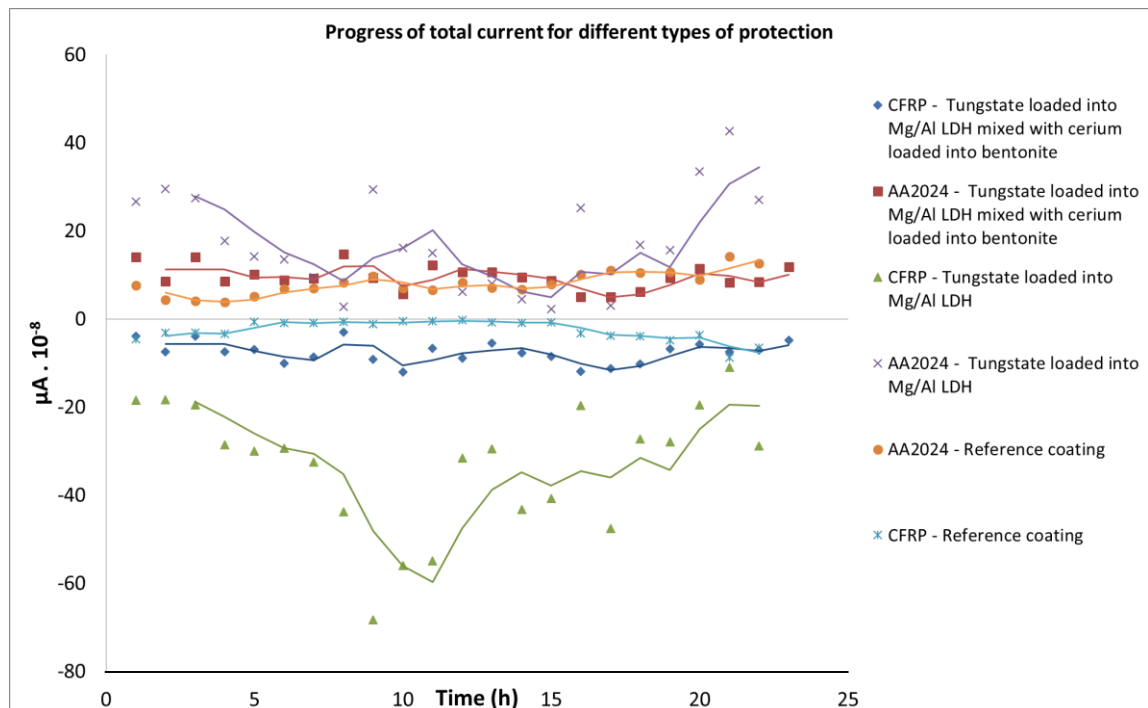


Figure 27 – Total corrosion current calculated for different coatings formulations during 24h, a) Tungstate loaded into Mg/Al LDH mixed with Ce^{3+} loaded into bentonite, b) Tungstate loaded into Mg/Al LDH and c) Reference sample without any inhibitors.

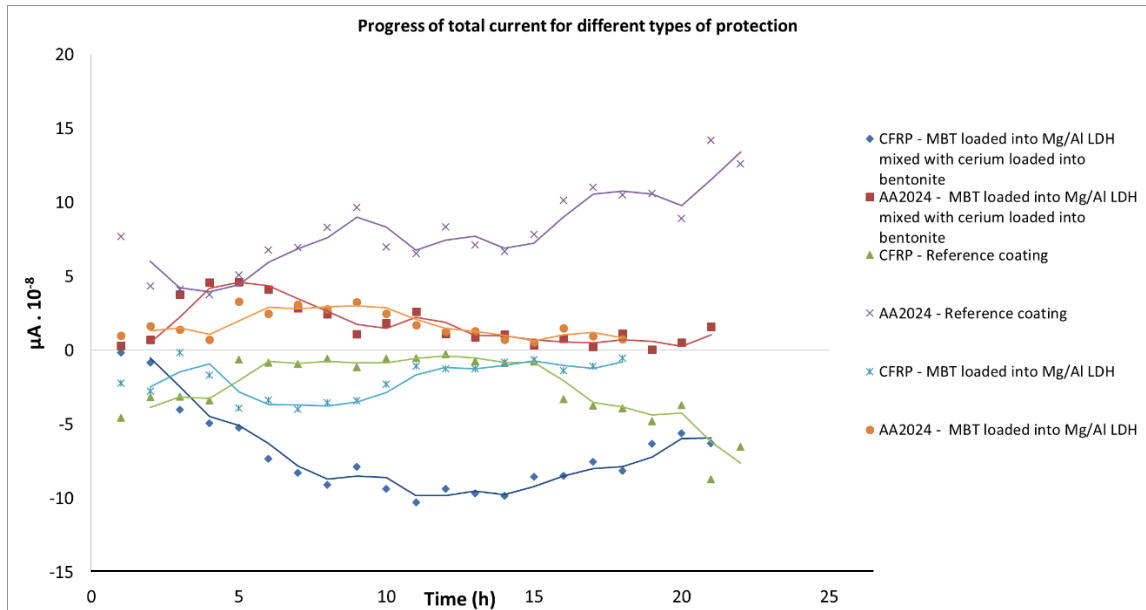


Figure 28 – Total corrosion currents calculated for different coating formulations during 24h, a) MBT loaded into Mg/Al LDH mixed with Ce^{3+} loaded into bentonite, b) MBT loaded into Mg/Al LDH and c) reference sample.

The results presented show the stabilization of corrosion currents after 10 hours of immersion. In both cases the AA2024 with the coating formulation containing MBT loaded into Mg/Al LDH mixed with cerium loaded into bentonite and tungstate loaded into Mg/Al LDH mixed with cerium loaded into bentonite show the best results.

Figure 29 represents the comparison between the two mixtures introduced above

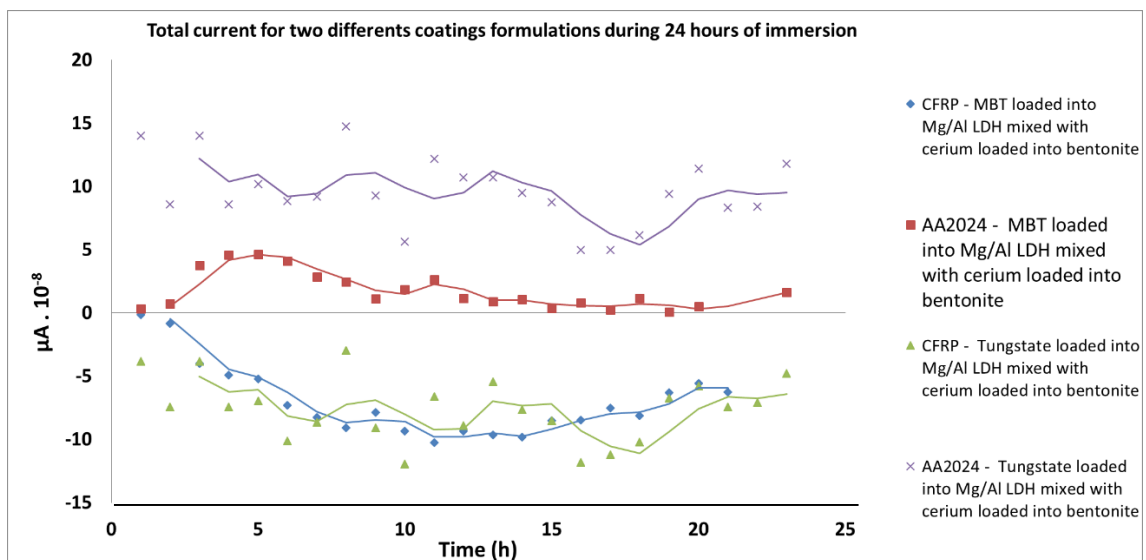


Figure 29 – Total corrosion current during 24 hours between a) MBT loaded into Mg/Al LDH mixed with cerium loaded into bentonite and b) tungstate loaded into Mg/Al LDH mixed with cerium loaded into bentonite.

The information present in the previous graphic (**Figure 28**) show a notable inhibitive effect in anodic and cathodic sample for MBT loaded into Mg/Al LDH mixed with cerium loaded into bentonite in comparison with reference sample. In the case of anodic AA2024, the difference of corrosion current became about $13 \mu\text{A} \times 10^{-8}$.

3.2.Industrial results

3.2.1. X-ray diffraction (XRD)

In Airbus group, it was planned to produce Mg/Al LDH and perform some new intercalations. Before the application of nanocontainers into the model coated system, it was necessary to confirm that inhibitors are successfully intercalated.

The results represented in next figures (**Figure 30 – Figure 34**), correspond to the intercalations made in Airbus.

Figure 30 represents original Mg/Al LDH with NO_3^- (Mg/Al – NO_3) and Mg/Al LDH intercalated with BTA: Mg/Al LDH – BTA.

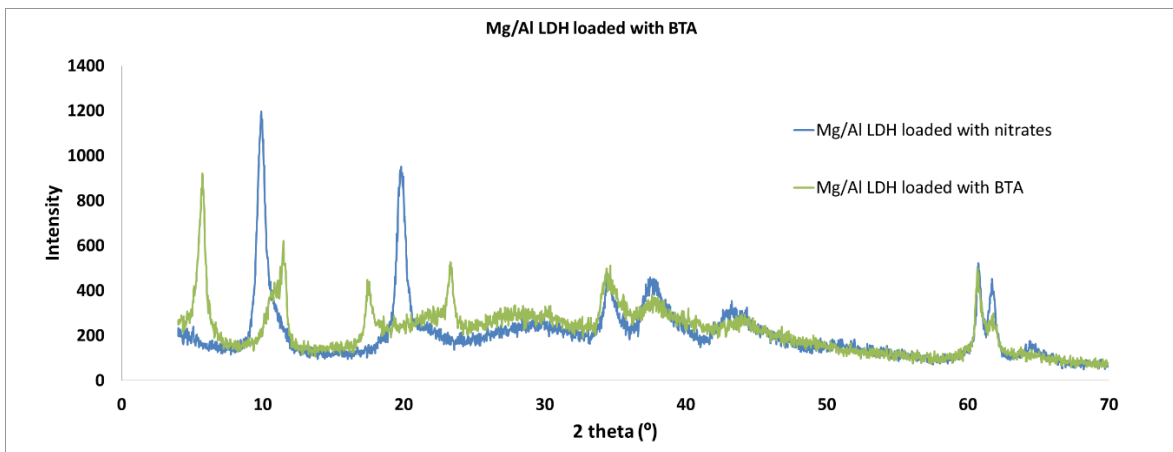


Figure 30 – XRD pattern of BTA intercalated into Mg/Al LDH

Figure 31 represents the intercalation of MBT into Mg/Al LDH structure.

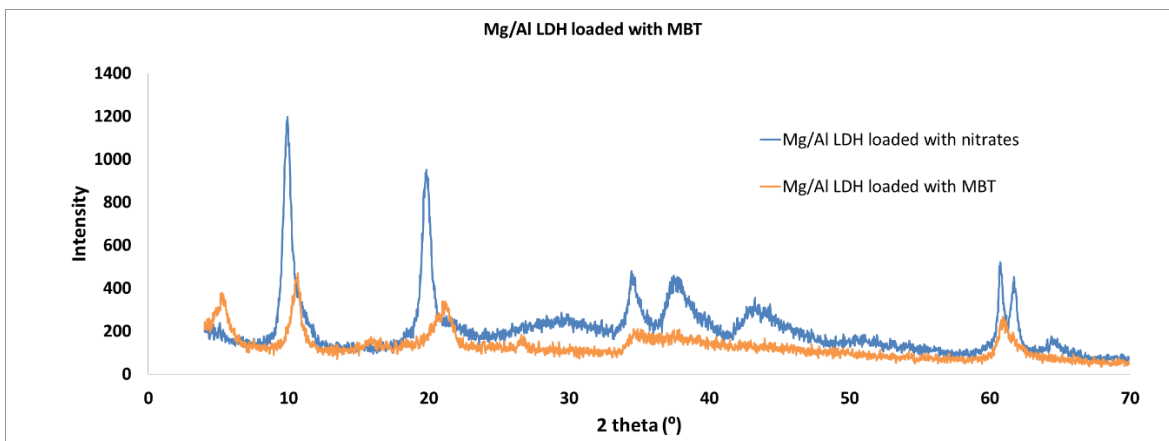


Figure 31 – XRD pattern of MBT intercalated into Mg/Al LDH

The XRD study revealed that the LDH samples loaded with MBT and BTA inhibitors prepared in Aveiro university and in Airbus groups were identical.

The XRD pattern of Mg/Al LDH intercalated with vanadate is represented in **Figure 32**.

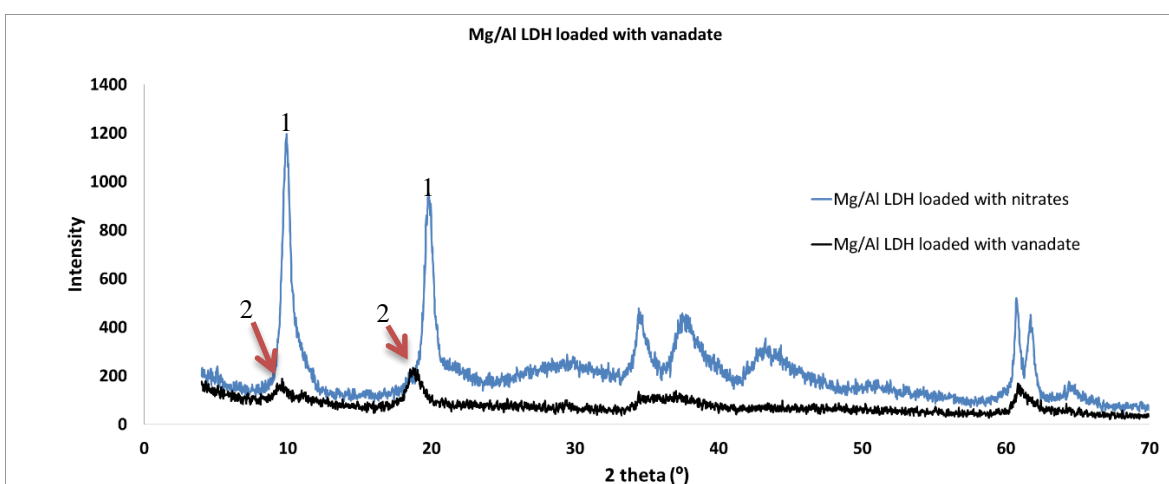


Figure 32 - XRD pattern of 1) Mg/Al LDH loaded with nitrates and 2) vanadate intercalated into Mg/Al LDH

It can be seen from the XRD pattern that the two characteristic peaks, are shifted to a lower 2 Theta values: 5.03° and 9.12°, respectively (marked as “2” in pattern). The gallery height corresponds to 4.08 Å.

The XRD represented in **Figure 33** indicates intercalation of molybdate into Mg/Al LDH structure.

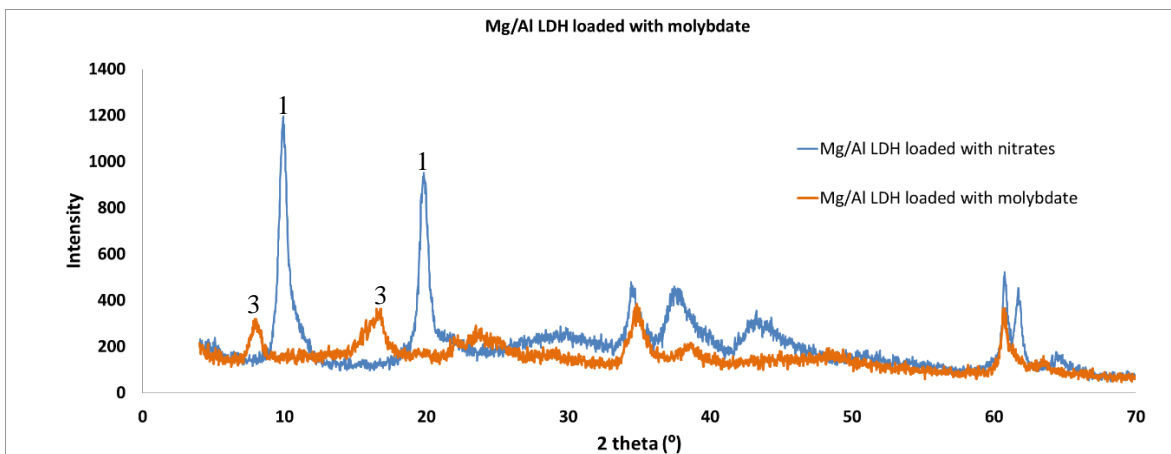


Figure 33 – XRD pattern of 1) Mg/Al LDH loaded with nitrates and 3) Mg/Al LDH intercalated with molybdate

This case is very similar to the previous. The peaks are shifted to smaller values of 2 theta angles. The positions of these two peaks (marked as “3” in the pattern) are 9.24° and 18.79°, corresponding to gallery height of 4.86 Å.

The last intercalation was tungstate into Mg/Al LDH structure (**Figure 34**).

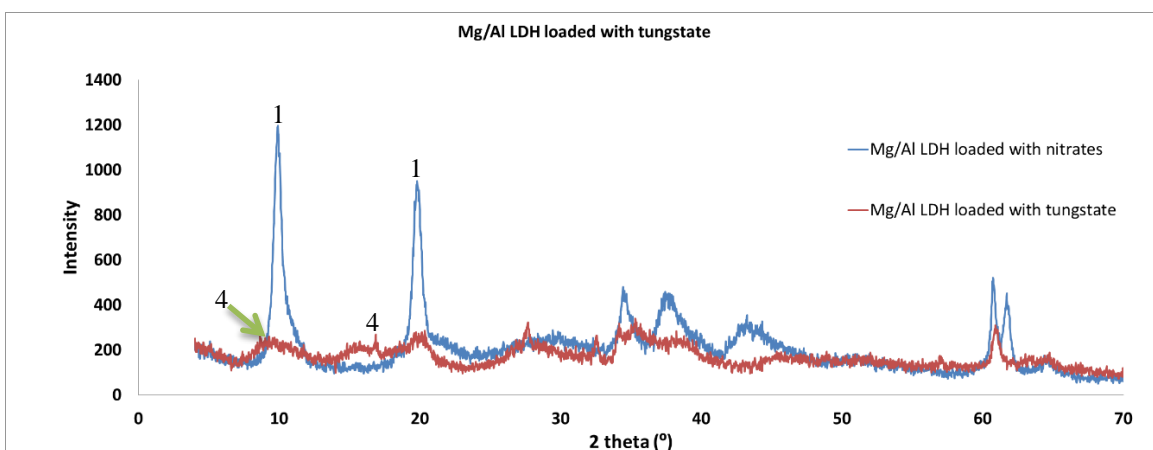


Figure 34 –XRD pattern of 1) Mg/Al LDH loaded with nitrates and 4) Mg/Al LDH loaded with tungstate.

In the case of tungstate loaded into Mg/Al LDH (**Figure 34**), there are no well defined diffraction peaks of LDH; only the small peaks show a intercalation, these two peaks (marked as “4” in pattern) are represented at 2 Theta equal to 4.46° and 9.20°, and corresponds to a gallery height of 5.19 Å.

3.2.2. Electrochemical tests

For better understanding of the results, different types of reference samples were analysed (called as “Old reference”, “new samples – 1 test” and “new samples – 2 test”). This coating does not contain any inhibitor and consists on a mixture of resin (SEEVENAX 315-02) with hardener, without any inhibitors inside.

The samples named, “Old reference”, are the first sample made in Airbus (**Figure 35**). They have different surface area, the coating was applied manually and with the only objective to test the equipment, confirm some initial results and get familiarized with the Gamry software.

The analyses of “new samples – 1 test” and the “new samples – 2 test” were made using the sample holder described in 2.4 (**Figure 11**).

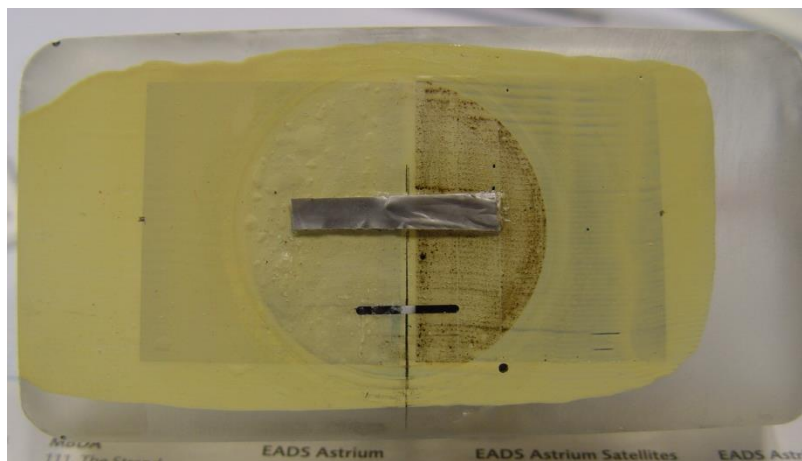


Figure 35 - Old Reference used in the electrochemical tests

It should be mentioned that the ways how the coatings were applied in both cases are different. **Figure 36-a** represents the coating applied with bar-coater in the Aveiro University, while **Figure 36-b** represents the coating which was industrially applied in the Airbus group.

However, the final result in both cases was very similar: the most effective anti-corrosion protection was performed by coating formulation containing MBT loaded into Mg/Al LDH mixed with Ce^{3+} loaded into bentonite.

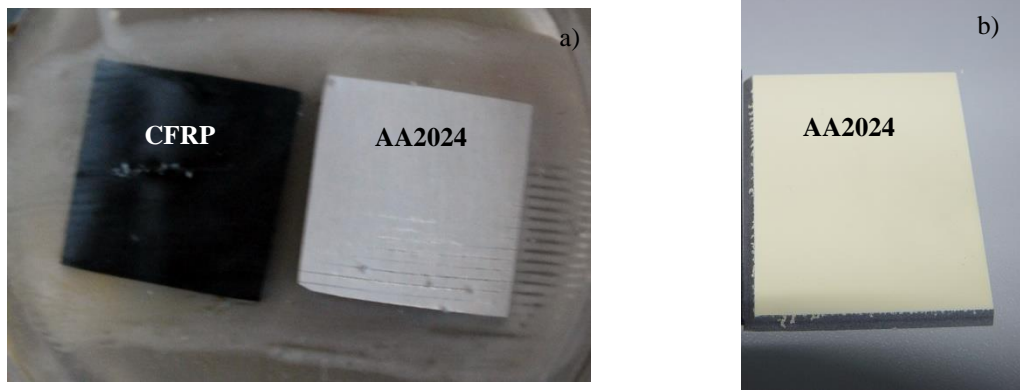


Figure 36 – Different types of coating application, a) Aveiro university, b) Airbus group

3.2.2.1. Zero Resistance Ammeter (ZRA)

Figure 37, represents the results for the zero resistance ammeter, the result is the average value of the four ZRA measurements made in Airbus.

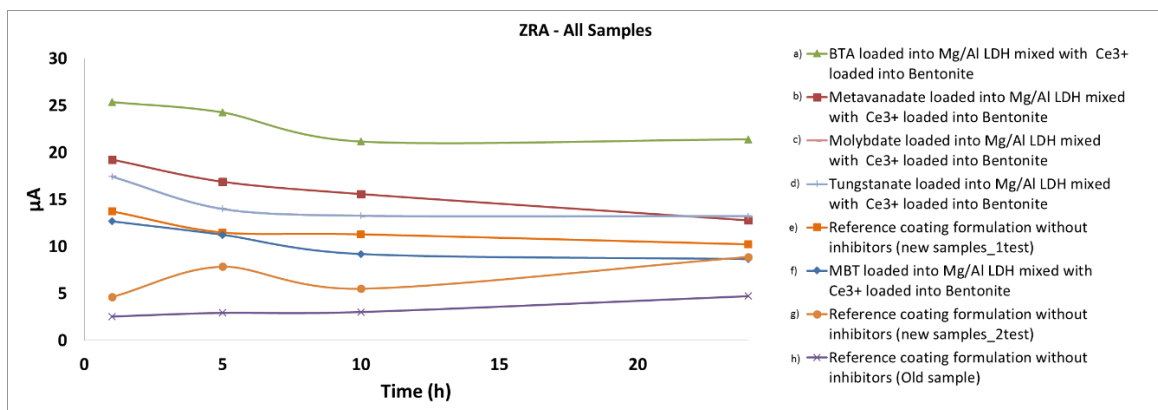


Figure 37 - ZRA measurements of all samples: a) BTA loaded into Mg/Al LDH mixed with Ce^{3+} loaded into bentonite, b) metavanadate loaded into Mg/Al LDH mixed with Ce^{3+} loaded into bentonite, c) molybdate loaded into Mg/Al LDH mixed with Ce^{3+} loaded into bentonite, d) tungstate loaded into Mg/Al LDH mixed with Ce^{3+} loaded into bentonite, e) reference coating formulation (new samples_1test), f) MBT loaded into Mg/Al LDH mixed with Ce^{3+} loaded into bentonite, g) reference coating formulation (new samples_2test) and h) reference coating formulation (old sample)

A brief analysis of these results makes evident the difficulties about the understanding the real result of different inhibitors: every analysis starts and finishes at different points during the corrosion process. However it is possible to observe the difference of performance during the 24 hours of immersion with and without the inhibitive mixtures.

All samples coated with inhibitive mixtures show a decrease of current during the first 24 hours (with the exception of molybdate loaded into Mg/Al LDH mixed with Ce^{3+} loaded into bentonite). The samples without any inhibitors show the evident increase of current.

For a better understanding of the results, **Figure 38** represents a graphic where the evolution through the time of the corrosion in percentage is shown.

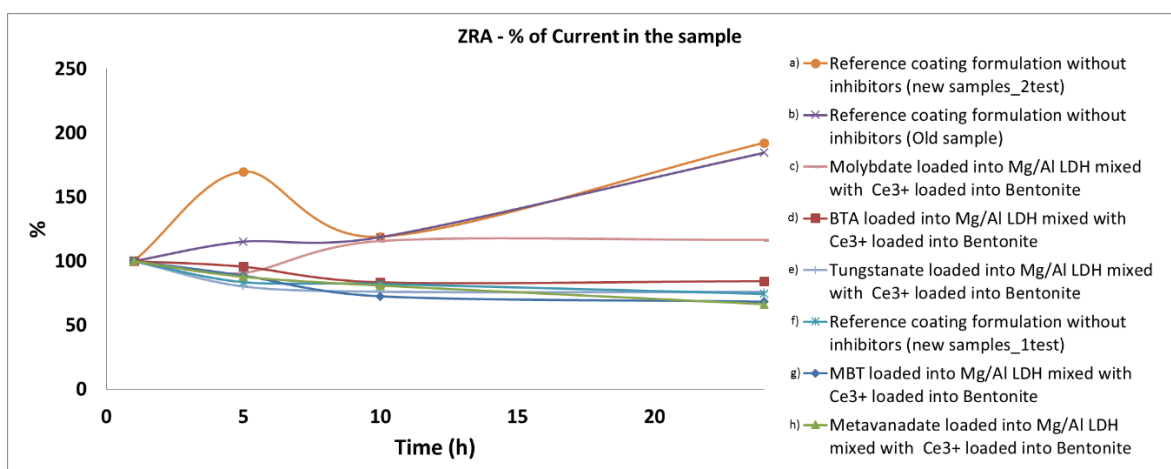


Figure 38 - ZRA analyses in percentage of efficiency: a) reference coating formulation (new sample_2test), b) reference coating formulation (old sample), c) molybdate loaded into Mg/Al LDH mixed with Ce^{3+} loaded into bentonite, d) BTA loaded into Mg/Al LDH mixed with Ce^{3+} loaded into bentonite, e) tungstate loaded into Mg/Al LDH mixed with Ce^{3+} loaded into bentonite, f) reference coating formulation (new sample_1test), g) MBT loaded into Mg/Al LDH mixed with Ce^{3+} loaded into bentonite, h) metavanadate loaded into Mg/Al LDH mixed with Ce^{3+} loaded into bentonite.

From the **Figure 38**, is possible to conclude that without any inhibitors the current increases with the time (92% of total increases during 24h of experiment). The exception of the reference (new samples_1test) can be correlated with experimental errors done during the preparation.

The current increases as well in the sample with the coating (16% of increase), which contains the mixture of inhibitor: molybdate loaded into Mg/Al LDH nanocontainers and Ce^{3+} loaded into bentonite. It means that this inhibitor doesn't properly work for this type of galvanically couple system.

The evident influence of inhibitors from the coating is observed for all other samples. A decrease of corrosion current was observed in the first 24 hours with special emphasis for metavanadate loaded into Mg/Al LDH in mixture with Ce^{3+} loaded into bentonite (34% decrease) (**Figure 38**).

The good results are also evident for the mixture of MBT loaded into Mg/Al LDH with Ce^{3+} loaded into bentonite (32 % decrease) and tungstate loaded into Mg/Al LDH in the mixture with Ce^{3+} loaded into bentonite (24 % decrease), same **Figure 38**.

3.2.2.2. Electrochemical impedance spectroscopy (EIS)

The electrochemical impedance spectroscopy was performed for two types of samples, with and without scratches (1mm * 5mm * 0,1mm).

In order to compare EIS results for different samples, their normalization in concordance to the active area was performed. In the case of scratched samples the anode area (AA2024, 0.05 cm²) and the cathode area (CFRP, 0.05 cm²) were used. The total area of normalization was defined as 0.1 cm². However, as the analyses were made only for low frequencies measurements, it was choose to normalize the EIS spectra only with the anode area.

For the EIS measurements without scratch the analysed area was defined as 1.57 cm². This area is calculated from the cell used during the test.

Figure 39-a represents the EIS for the original coating without any artificial defects and **Figure 39-b** represents the coating with scratch.

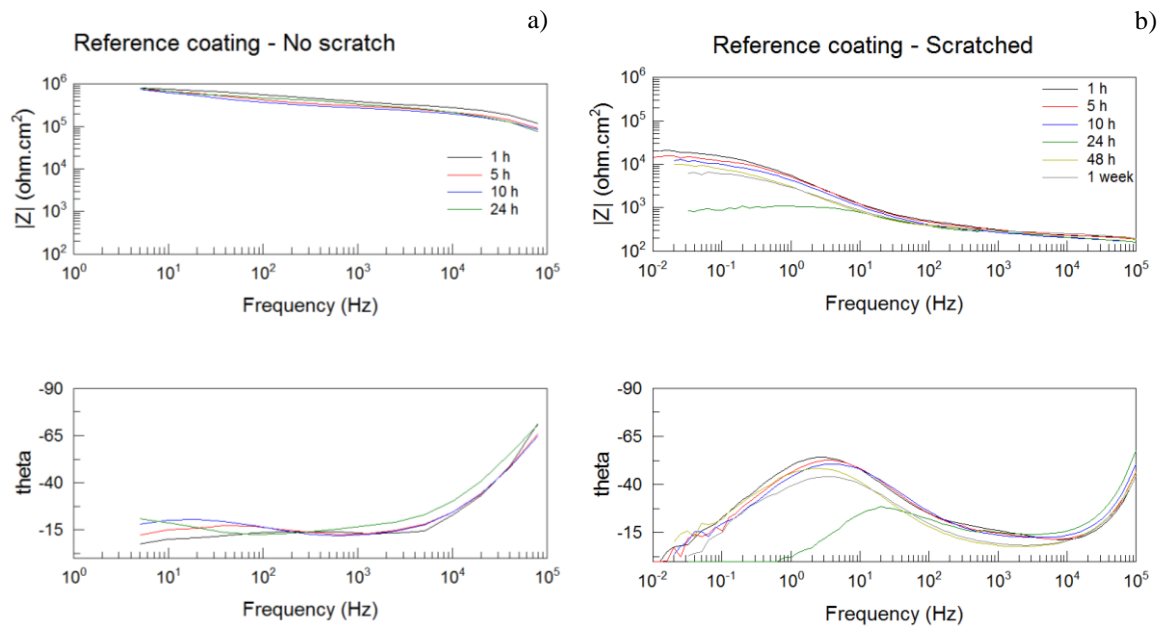


Figure 39 – EIS Reference coating without any inhibitors, a) no scratch, b) artificial scratch

The difference between typical impedance spectra for the coupled AA2024 and CFRP with and without scratch is based on the signal from the coating. From **Figure 39** it can be seen that resistivity of the coating significantly decreases after the formation of the artificial defect.

The equivalent circuit, which corresponds to the type of system used in Aveiro University and in Airbus group, can be presented as follows (**Figure 40**).

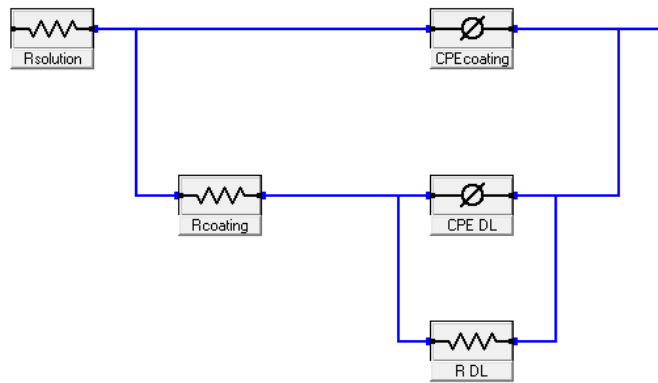


Figure 40 - Equivalent circuit used during the measurements

Where R_{solution} is the resistivity of the solution, CPE_{coat} is the constant phase element for the used epoxy coating, R_{coat} is the resistivity of the epoxy coating, CPE_{DL} is the constant phase element for double layer capacitance and R_{DL} is the resistivity of the double layer (charge transfer resistance).

After the formation of artificial scratch the resistivity and the capacitance of the epoxy coating become negligible and the equivalent circuit can be presented as in the following (**Figure 41**):

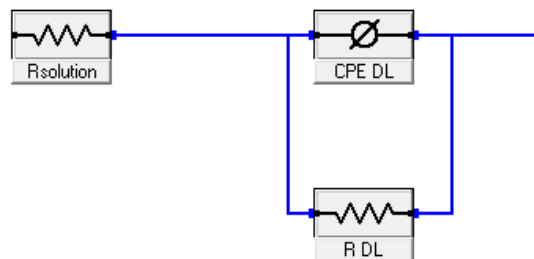


Figure 41 - Equivalent circuit after the formation of artificial scratch

The alteration of the spectra between 0 and 24 hours can be interpreted in the frame of technical deviation of the measurements and could not be uniquely attributed to any additional layer formation.

Figures 42-46 represent the impedance measurements for the samples, which contain different mixture of inhibitors into the coating formulation:

1. MBT loaded into Mg/Al LDH together with Ce^{3+} loaded into bentonite without artificial defects (**Figure 42-a**) and with scratch (**Figure 42-b**).

2. BTA loaded into Mg/Al LDH together with Ce^{3+} loaded into bentonite without artificial defects (**Figure 43-a**) and with scratch (**Figure 43-b**).
3. Metavanadate loaded into Mg/Al LDH together with Ce^{3+} loaded into bentonite without artificial defects (**Figure 44-a**) and with scratch (**Figure 44-b**).
4. Tungstate loaded into Mg/Al LDH together with Ce^{3+} loaded into bentonite without artificial defects (**Figure 45-a**) and with scratch (**Figure 45-b**).
5. Molybdate loaded into Mg/Al LDH together with Ce^{3+} loaded into bentonite without artificial defects (**Figure 46-a**) and with scratch (**Figure 46-b**).

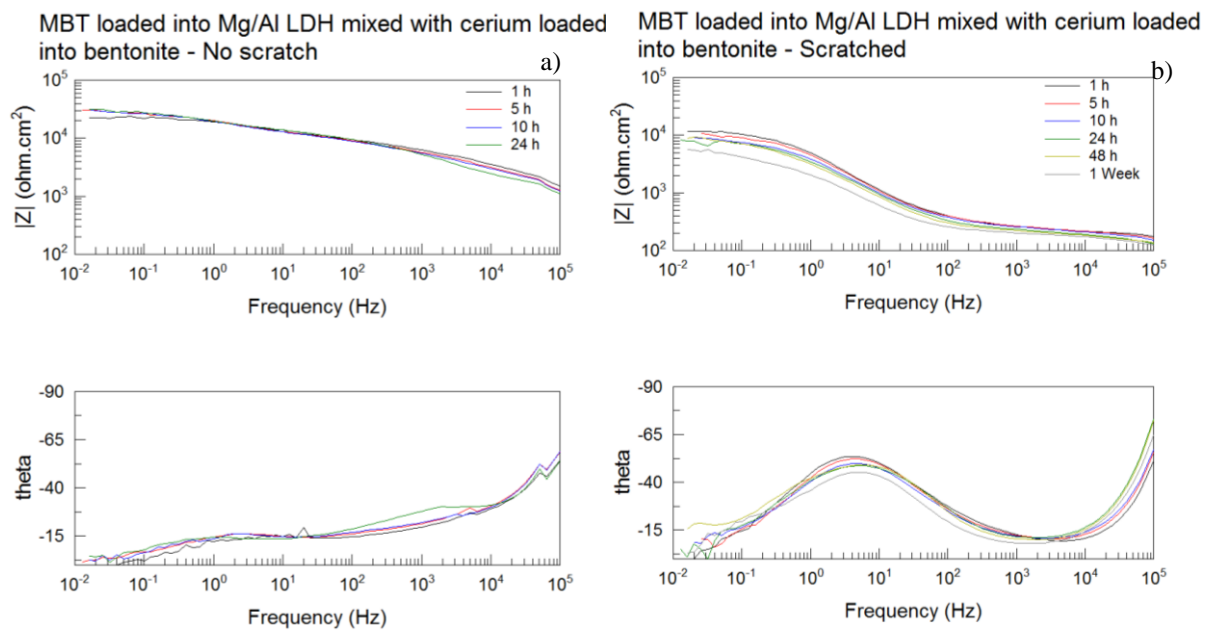


Figure 42 - EIS spectra obtained from galvanically coupled AA2024 and CFRP coated with epoxy coating containing mixture of MBT loaded into Mg/Al LDH and Ce^{3+} loaded into bentonite: a) without artificial defects, b) with scratch. The measurements were performed after 1, 4, 24, 48 hours and 1 week.

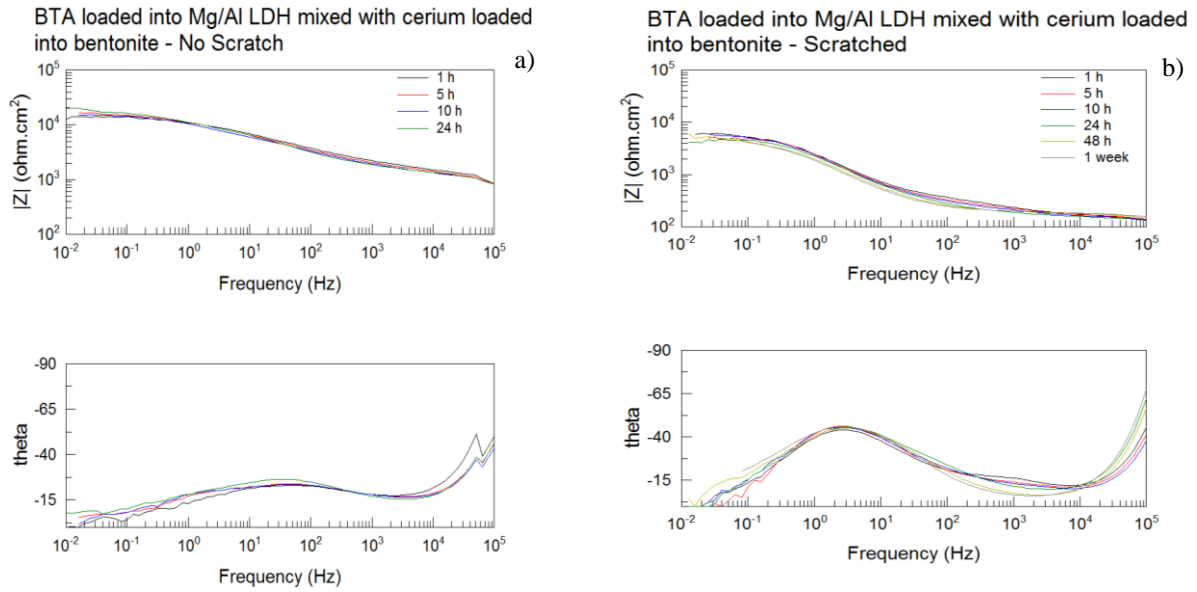


Figure 43 - EIS spectra obtained from galvanically coupled AA2024 and CFRP coated with epoxy coating containing mixture of BTA loaded into Mg/Al LDH and Ce³⁺ loaded into bentonite: a) without artificial defects, b) with scratch. The measurements were performed after 1, 4, 24, 48 hours and 1 week.

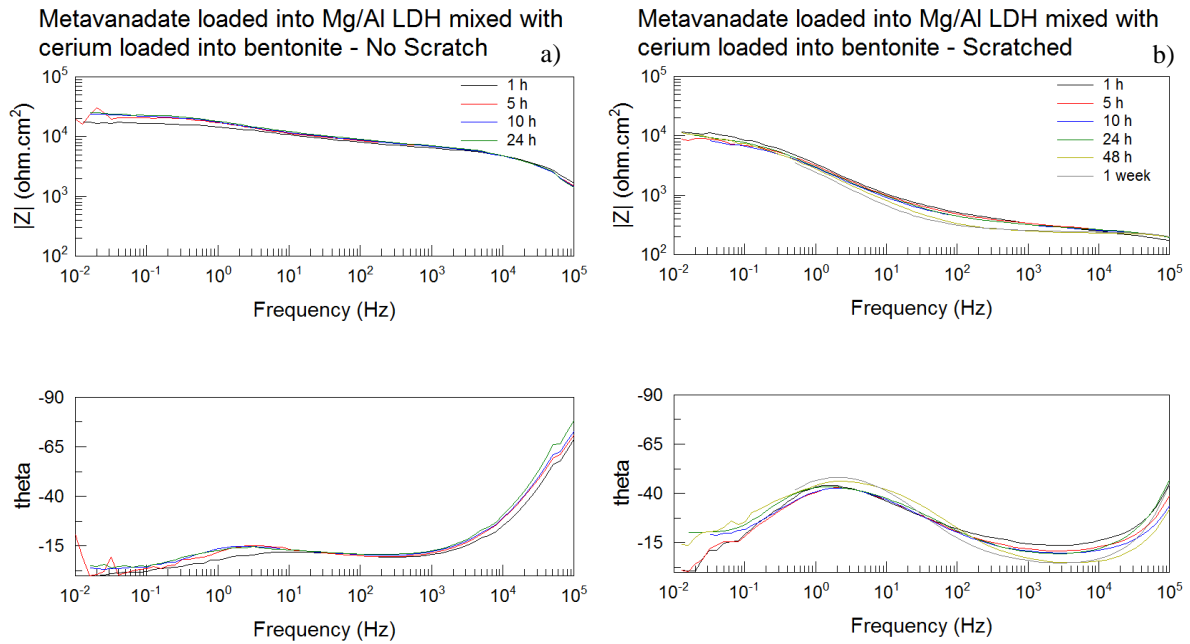


Figure 44 - EIS spectra obtained from galvanically coupled AA2024 and CFRP coated with epoxy coating containing mixture of metavanadate loaded into Mg/Al LDH and Ce³⁺ loaded into bentonite: a) without artificial defects, b) with scratch. The measurements were performed after 1, 4, 24, 48 hours and 1 week.

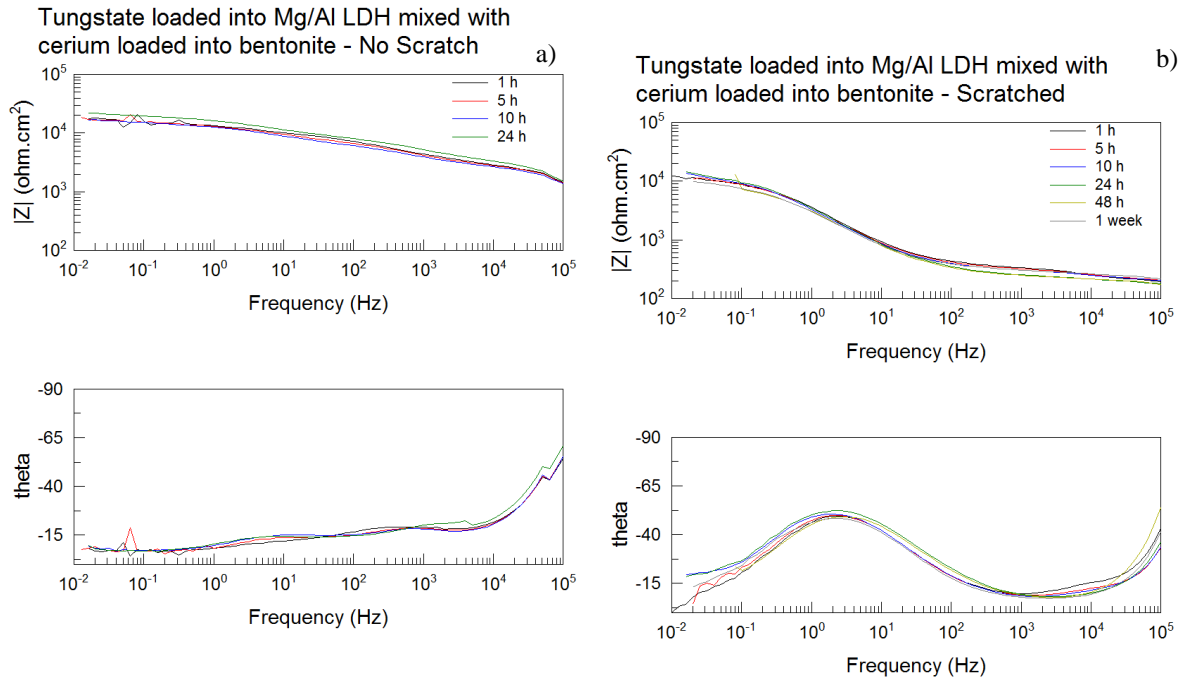


Figure 45 - EIS spectra obtained from galvanically coupled AA2024 and CFRP coated with epoxy coating containing mixture of tungstate loaded into Mg/Al LDH and Ce3+ loaded into bentonite: a) without artificial defects, b) with scratch. The measurements were performed after 1, 4, 24, 48 hours and 1 week.

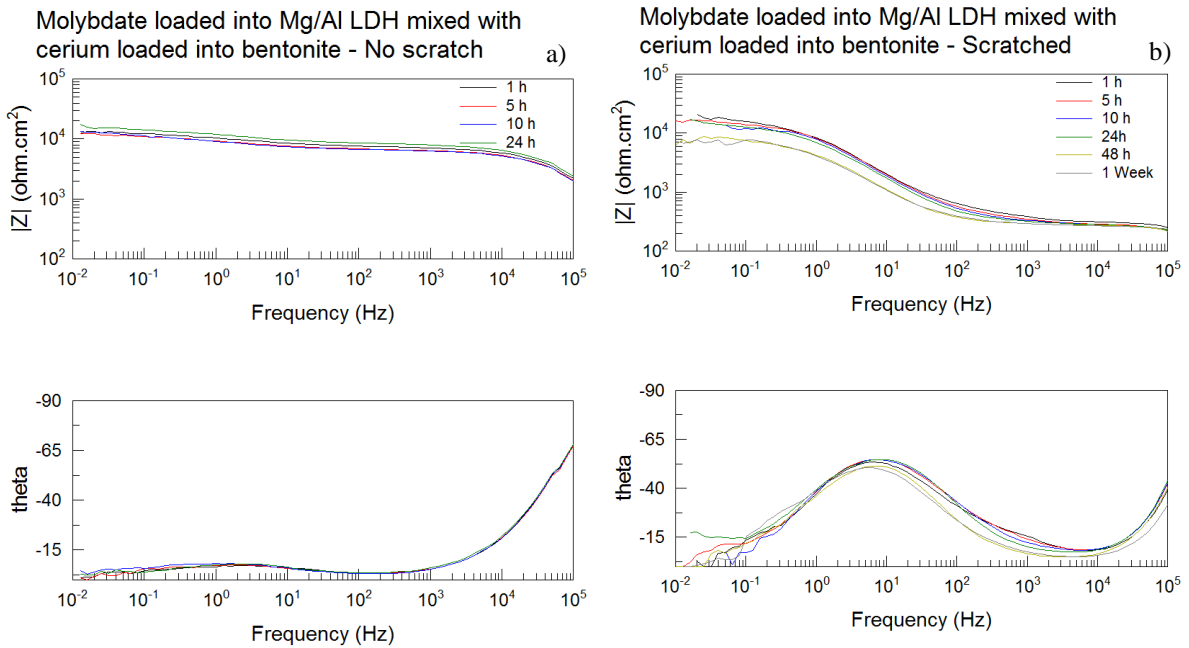


Figure 46 - EIS spectra obtained from galvanically coupled AA2024 and CFRP coated with epoxy coating containing mixture of molybdate loaded into Mg/Al LDH and Ce3+ loaded into bentonite: a) without artificial defects, b) with scratch. The measurements were performed after 1, 4, 24, 48 hours and 1 week.

As it can be seen from **Figures 42 -46**, the total resistivity of the coating decreases (from about 10^6 to 10^4 Ohm.cm²) for the coating formulation containing nanocontainers. It

can be explained by the formation of micro-cracks into the coating in presence of loaded nanocontainers inside. The alteration of the EIS signal from one coating formulation to another one is negligible between 1h and 24h of immersion and can be explained by the deviation during the measurements (**Figure 47**).

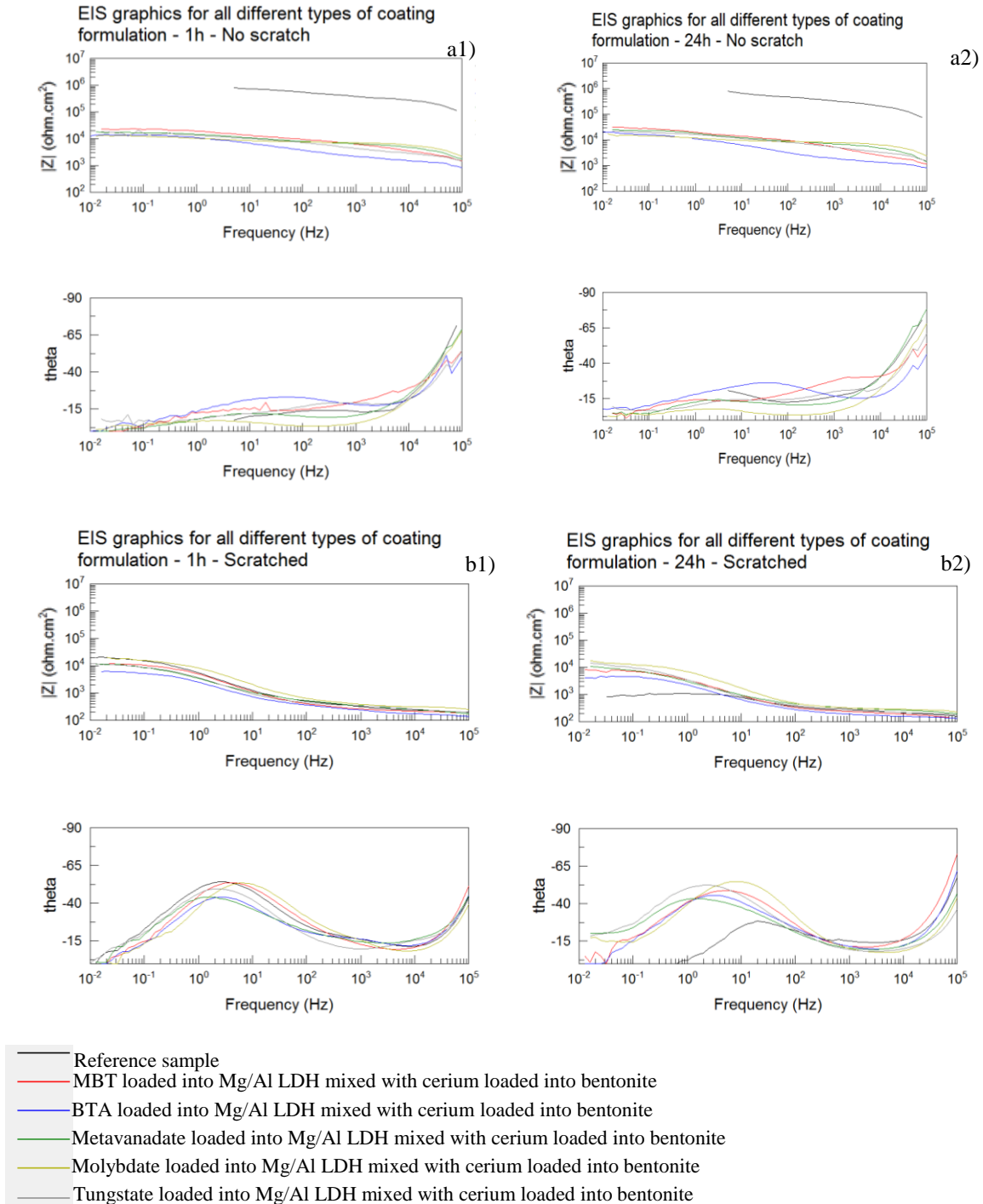


Figure 47 - Comparison of EIS results for a1) 1 hour without scratch, a2) 24 hours without scratch, b1) 1 hour with scratch and b2) 24 hours with scratch, for the different coating formulations

3.2.2.3. Optical microscopy

The optical analysis is an adequate way to check the progress of corrosion during time. For each sample several photos were taken, after 24h / 48h/ 72h and 1 week. The test was performed using 0,05M of NaCl solution.

Figure 48 represents the photos for the sample without any inhibitors, (reference coating) inside SEEVENAX 315-00 epoxy resin.

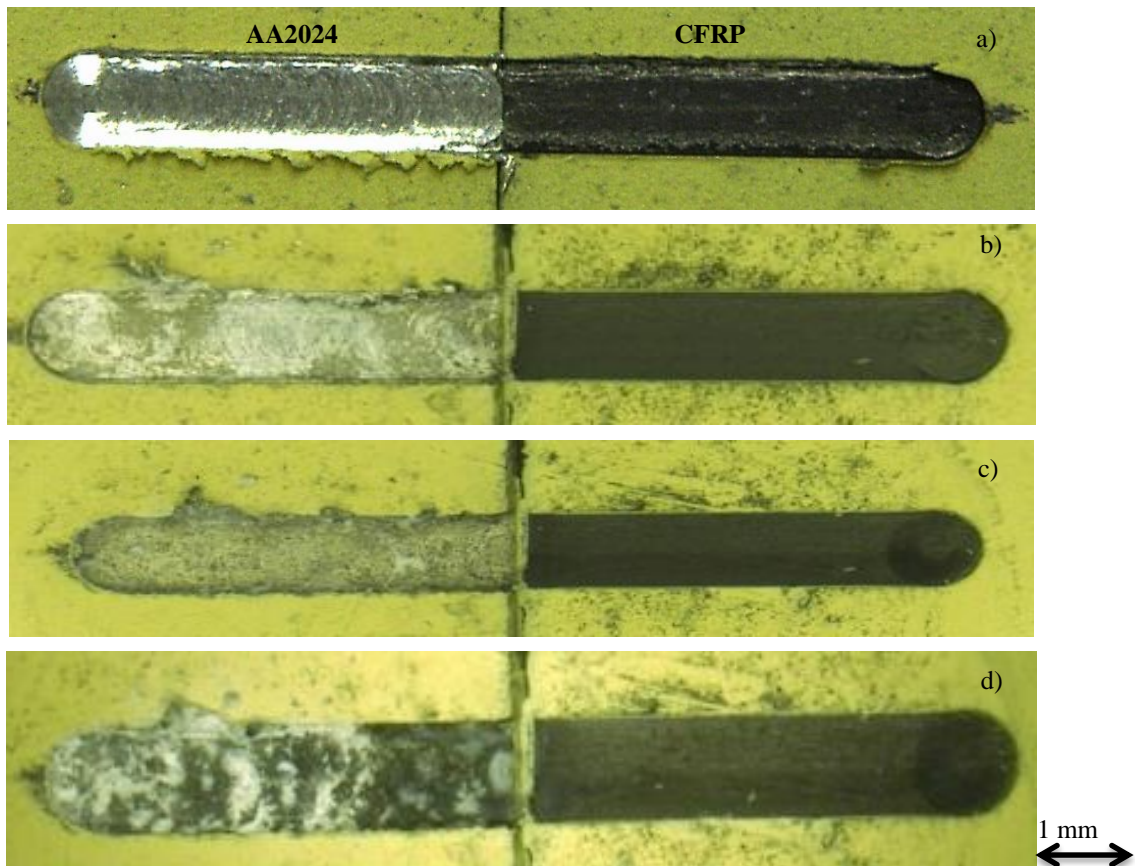


Figure 48 - Photos of the corroded reference sample during the immersion test through time (0.05M NaCl solution), a) 0h, b) 48h, c) 72h and d) 168 h

It is evident to see that only the epoxy coating without any inhibition inside is not effective against galvanic corrosion: there is visual notice of the corrosion after 24 hours of immersion with the formation of pitting corrosion, **Figure 48b**.

To improve the protection of the galvanically coupled systems, the inhibitors were added to the coating formulation. **Figure 49** represents the corrosion progress for the mixture of inhibitors MBT loaded into Mg/Al LDH mixed with Ce^{3+} loaded into bentonite.

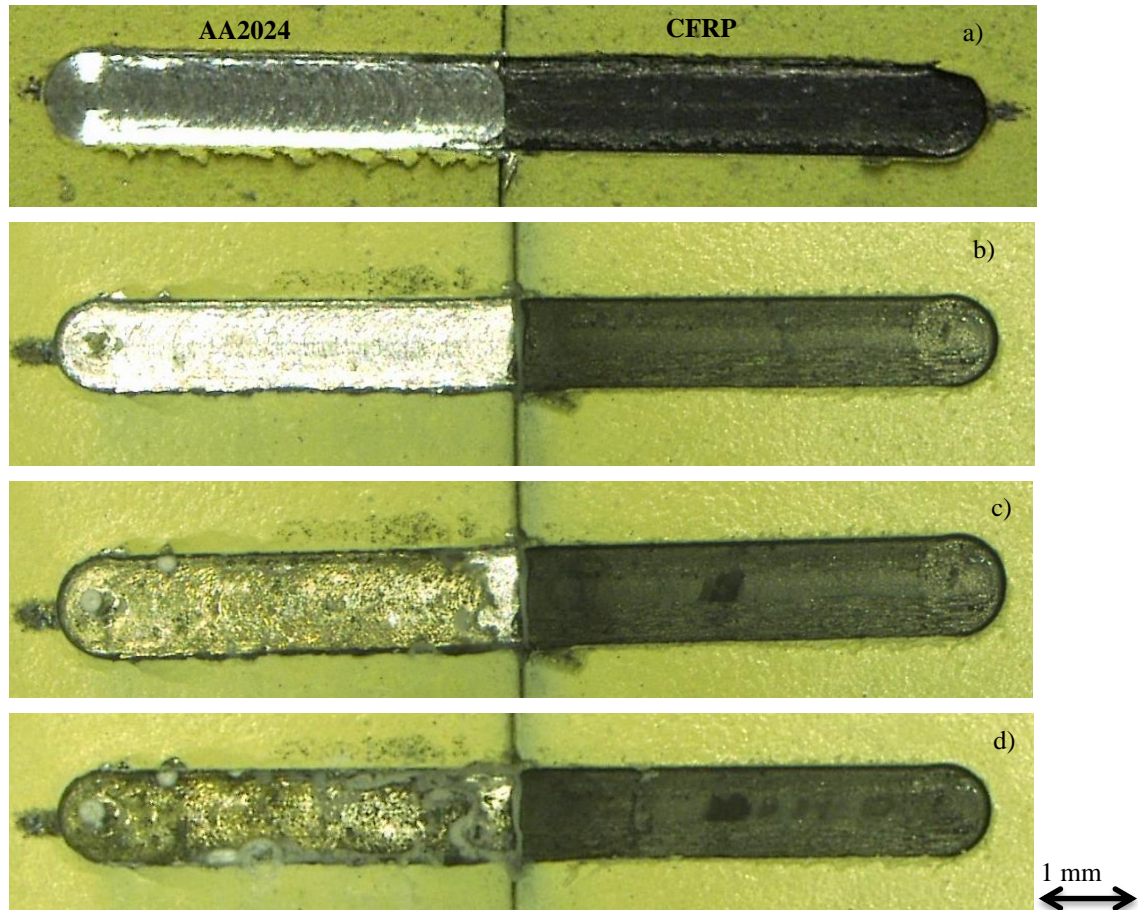


Figure 49 - Photos of the corrosion processes of the sample coating the mixture of inhibitors (MBT loaded into Mg/Al IDH together with the Ce^{3+} loaded into bentonite) during the immersion test (0.05 M NaCl solution), a) 0 h, b) 48 h, c) 72 h and d) 168 h

In this case the photos reveal the significant corrosion protection against the aggressive environment during the first 48 hours of immersion. Only after 72 hours signs of corrosion are observed in **Figure 48c**). After 1 week of immersion the corrosion becomes completely visible but it is possible as well to see some shiny parts of the preserved aluminium.

Figure 50 represents another mixture of inhibitors, BTA loaded into Mg/Al LDH together with Ce^{3+} loaded into bentonite.

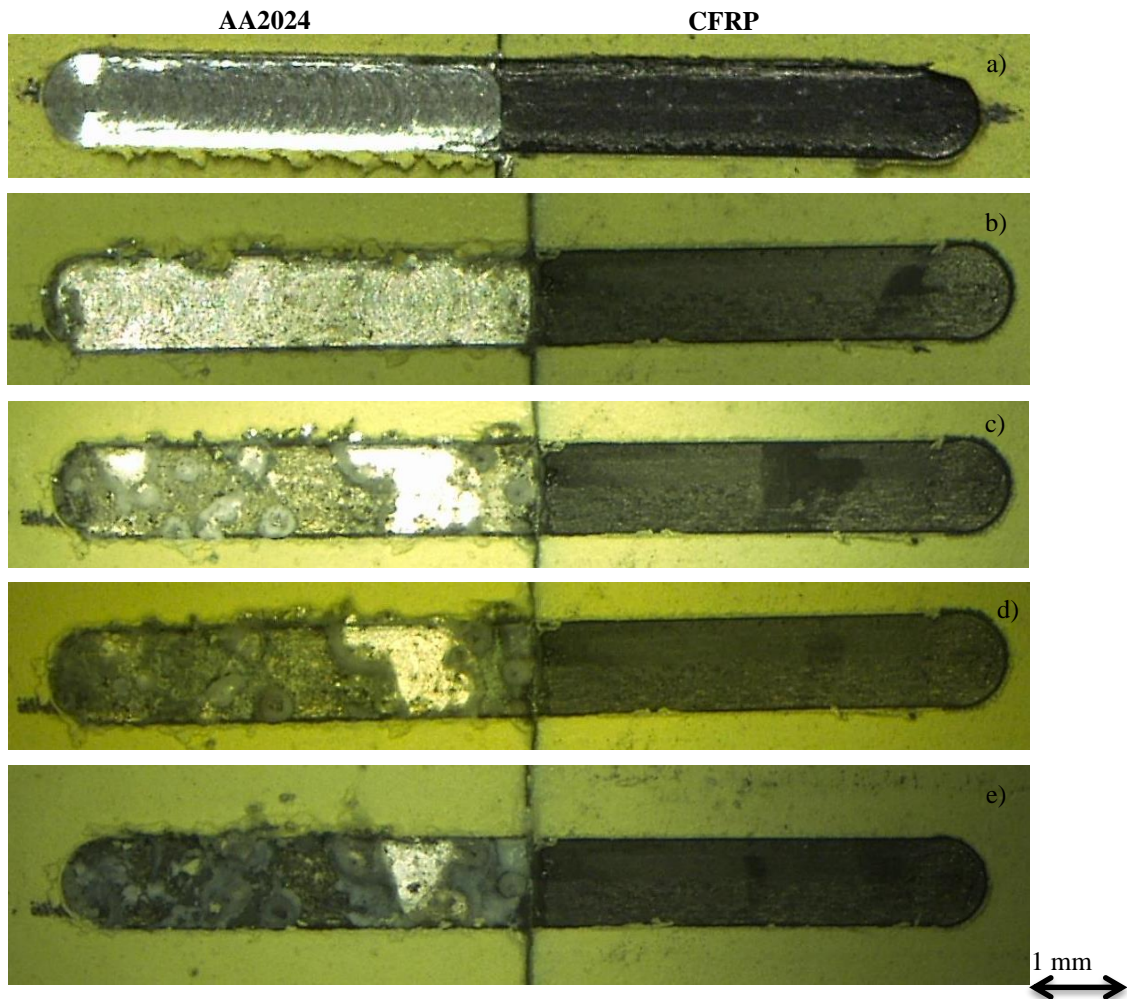


Figure 50 - Photos of the corrosion processes of the sample containing the mixture of inhibitors (BTA loaded into Mg/Al LDH together with Ce^{3+} loaded into bentonite) during the immersion test (0.05 M NaCl solution), a) 0 h, b) 24 h, c) 48 h, d) 72 h and e) 168 h

For this sample, containing the mixture metavanadate loaded into Mg/Al LDH mixture with Ce^{3+} loaded into bentonite, the visible corrosion starts to appear after 48h of immersion with already some relevant pitting corrosion in aluminum part. However, the close analysis of the immersed sample with the optical microscope (magnification 50x) after 24h of immersion already shows the presence of some pitting corrosion. After 72 hours of immersion the aluminum part of the sample (anode) is completely corroded.

Figure 51 represents the coating formulation loaded with metavanadate into Mg/Al LDH together with Ce^{3+} loaded into bentonite.

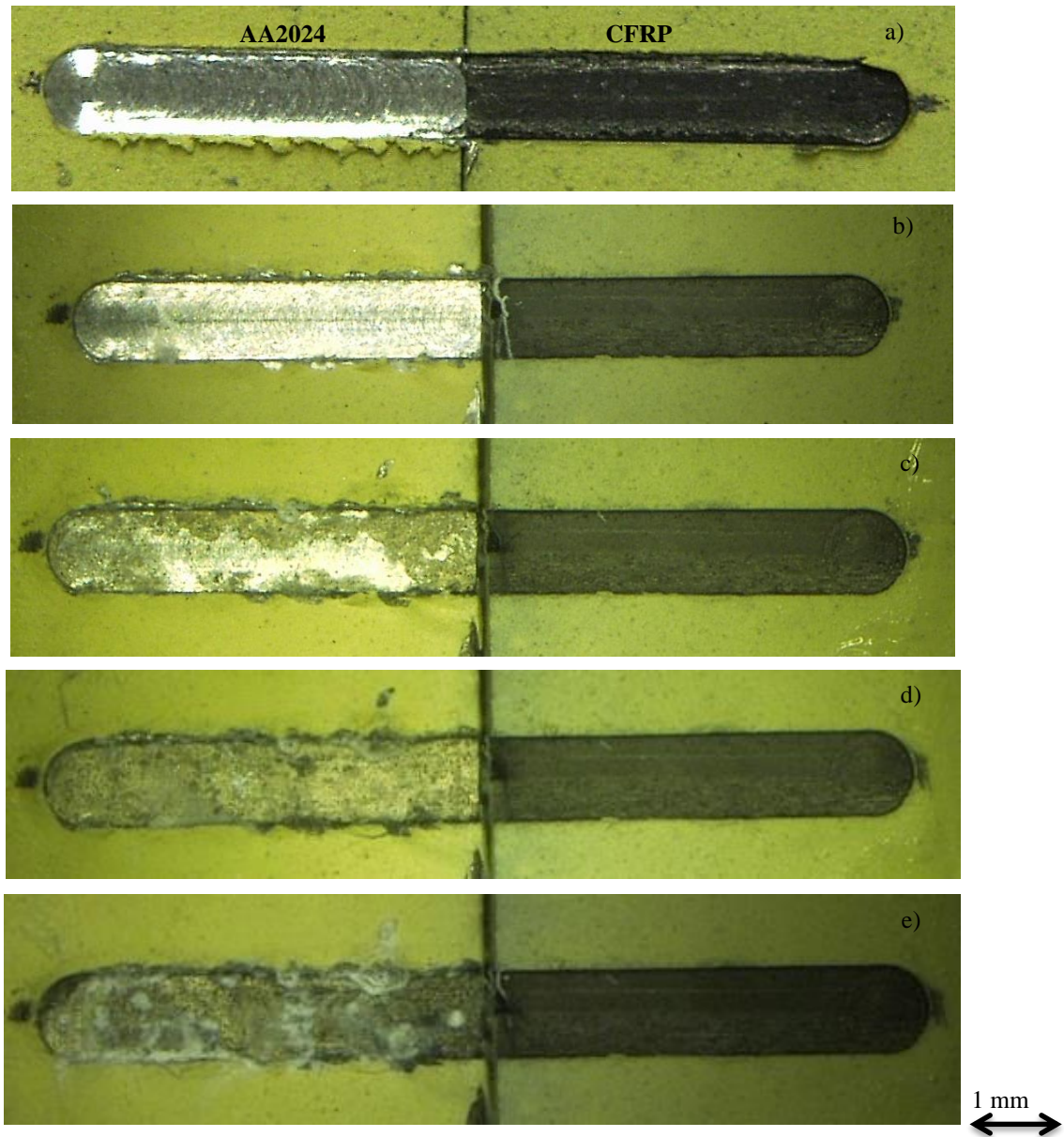


Figure 51 - Photos of the corrosion processes of the sample containing the mixture of inhibitors (metavadate loaded into Mg/Al LDH together with Ce^{3+} loaded into bentonite) during the immersion test (0.05M NaCl solution), a) 0 h, b) 24 h, c) 48 h, d) 72 h and e) 168 h.

Figure 51 shows relatively good corrosion inhibition during the first 24h and the aluminum parts (anode) remains completely shiny. Between 24 - 48 hours the corrosion starts and the pitting corrosion became evident. After 72 hours the sample is completely corroded.

Figure 52 represents the sample containing tungstate loaded into Mg/Al LDH together with Ce^{3+} loaded into bentonite mixture into coating formulation.

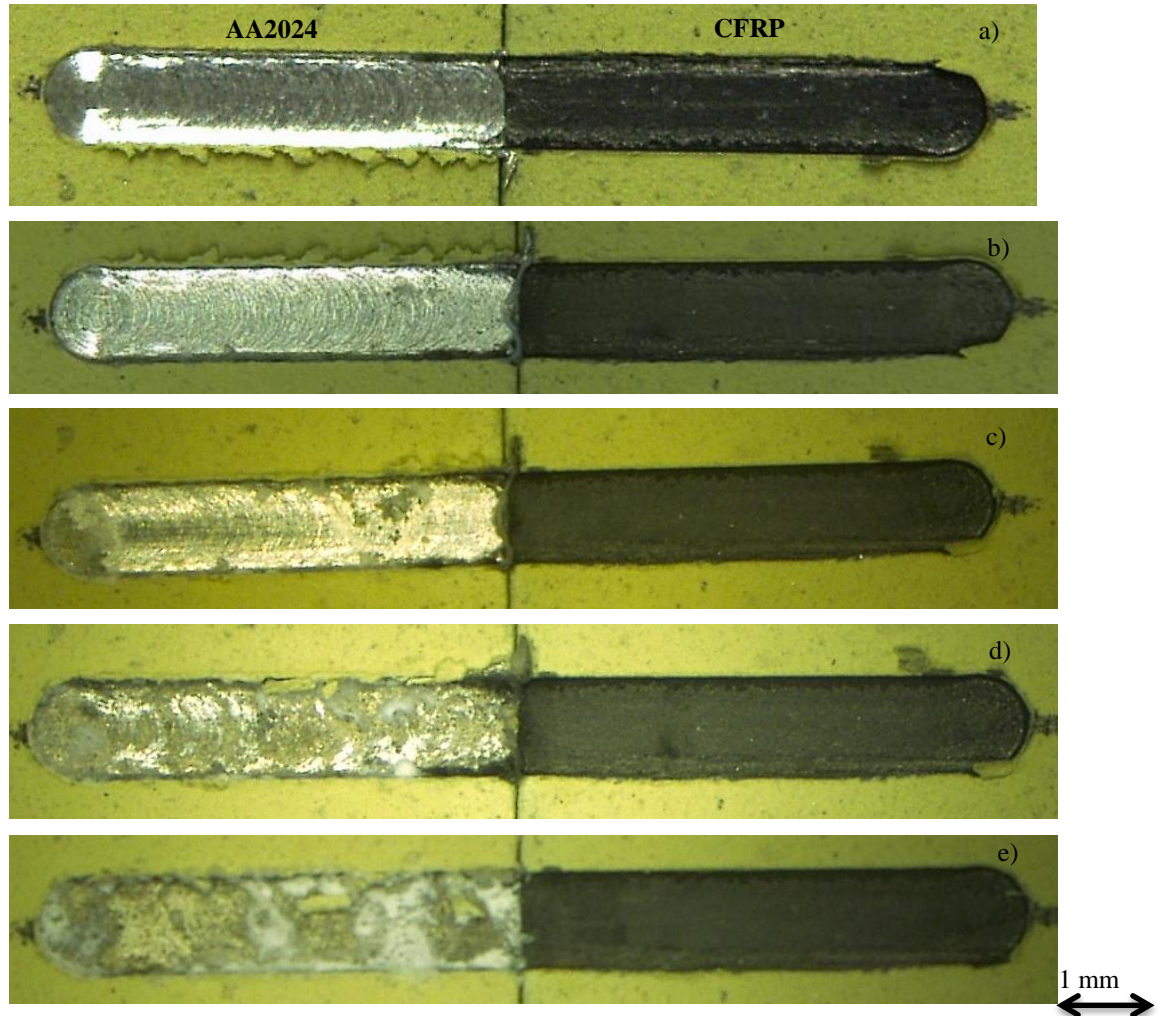


Figure 52 - Photos of the corrosion processes of the sample containing the mixture of inhibitors (Tungstate loaded into Mg/Al LDH together with Ce^{3+} loaded into bentonite) during the immersion test (0.05M NaCl solution), a) 0 h, b) 24 h, c) 48 h, d) 72 h and e) 168 h.

In the case of this sample containing tungstate loaded into Mg/Al LDH mixture with Ce^{3+} loaded into bentonite a significant response from point of corrosion protection of AA2024 is observed: during the first 24 hours the sample remains completely shiny and protected.

After 48 hours of immersion in the aggressive environment the weak presence of pitting corrosion in the aluminum part is observed. After 72 hours the aluminum displays a large big presence of pitting corrosion and after 1 week the aluminum sample is completely corroded.

Figure 53 represents the sample containing following the mixture of inhibitors into coating formulation: molybdate loaded into Mg/Al LDH together with Ce^{3+} loaded into bentonite.

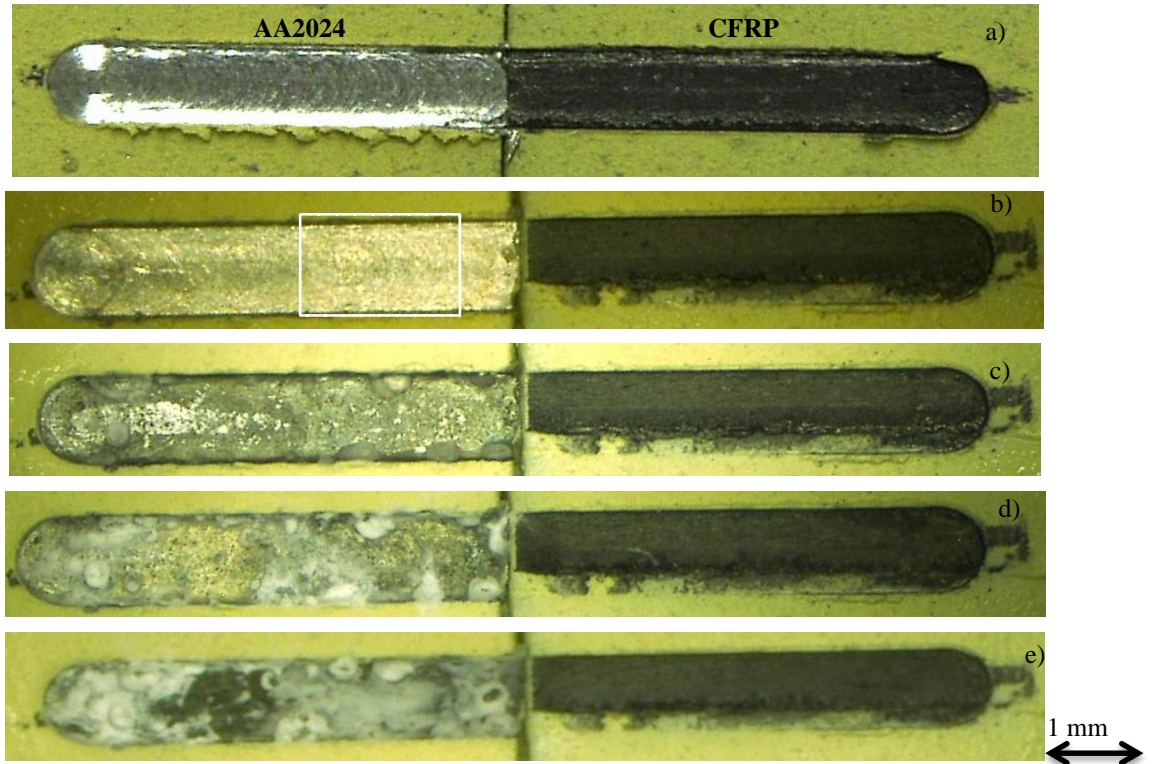


Figure 53 - Photos of the corrosion processes of the sample containing the mixture of inhibitors (molybdate loaded into Mg/Al LDH together with Ce^{3+} loaded into bentonite) during the immersion test (0.05M NaCl solution), a) 0 h, b) 24 h, c) 48 h, d) 72 h and e) 168 h.

For the case of the sample containing molybdate loaded into Mg/Al LDH together with Ce^{3+} into bentonite into coating formulation the aluminum anode is almost completely protected during first 24 hours. However on close analysis of the sample, already shows the beginning of a small spot of pitting corrosion (**Figure 54**).

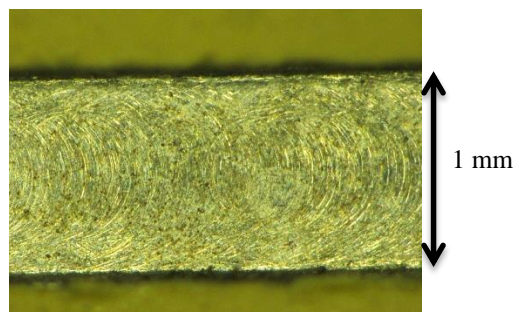


Figure 54 - 200x times magnification of the corroded zone of aluminum of the sample in figure 52 after 24h of immersion

To summarize the obtained results of the anti-corrosion protection tests of galvanically couples AA2024 with CFRP, **Figure 55** represents the corroded surface of the samples after the same time of immersion (48 hours).

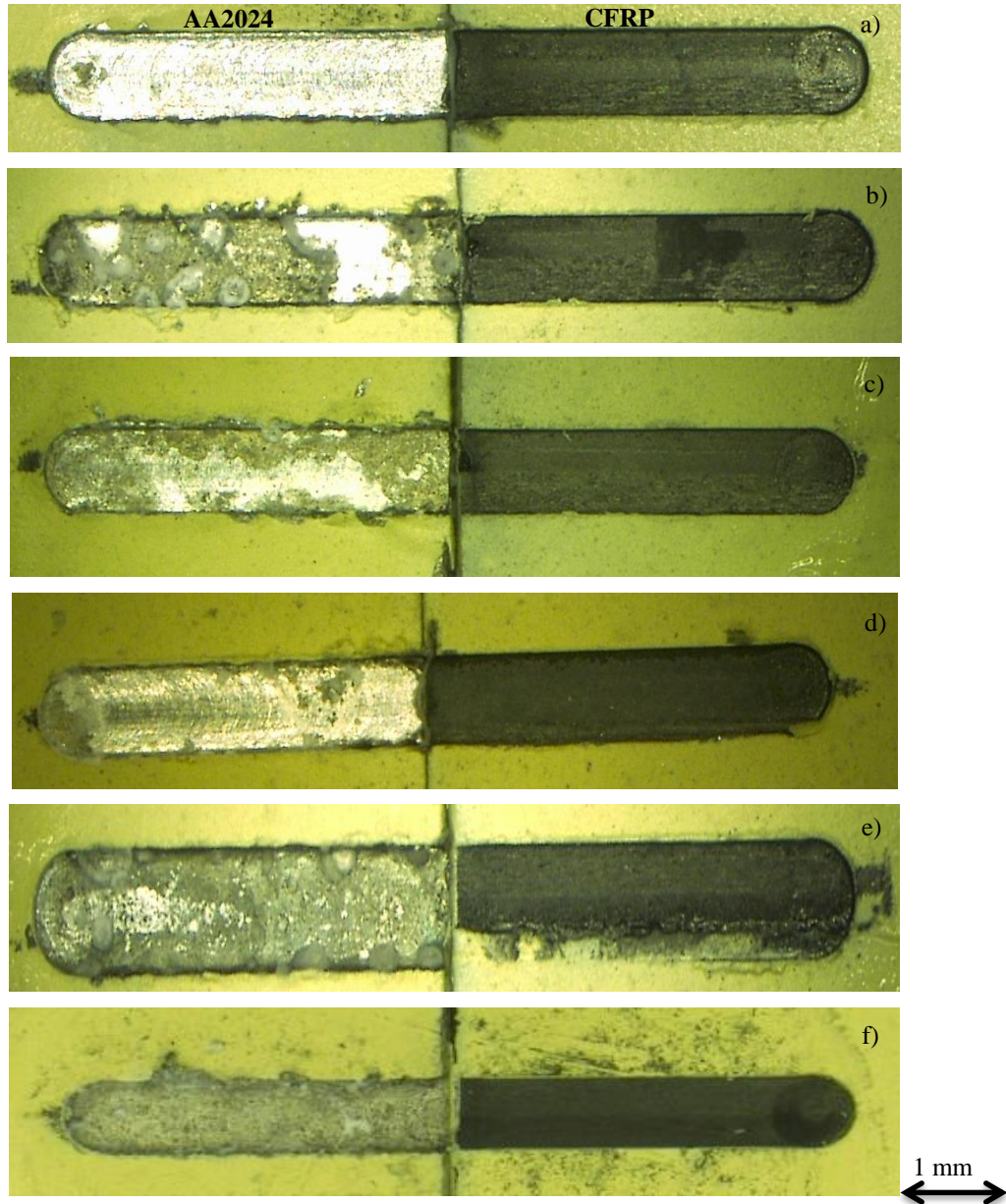


Figure 55 - Photos of all samples of the set with different mixtures of inhibitors (see above) into the coating formulation after 48 hours of immersion, a) MBT loaded into Mg/Al LDH mixed with Ce^{3+} loaded into bentonite, b) BTA loaded into Mg/Al LDH mixed with Ce^{3+} loaded into bentonite, c) metavanadate loaded into Mg/Al LDH mixed Ce^{3+} loaded into bentonite, d) tungstate loaded into Mg/Al LDH mixed Ce^{3+} loaded into bentonite and e) molybdate loaded into Mg/Al LDH mixed Ce^{3+} loaded into bentonite and f) reference without inhibitors into the coating formulation.

There are evident differences in **Figure 55** between mixtures of anti-corrosion inhibitors used in this work. The mixture of MBT loaded into Mg/Al LDH together with Ce^{3+} loaded into bentonite (**Figure 55 – a**) and the mixture tungstate loaded into Mg/Al LDH

together with Ce^{3+} loaded into bentonite (**Figure 55 –d**) are the two most effective corrosion inhibiting mixtures. The mixture of molybdate loaded into Mg/Al LDH mixture with Ce^{3+} loaded into bentonite as well as the reference sample are completely corroded. After 48 hours, the corrosion processes becomes significant for all samples and after 1 week the corrosion completely covers the surface of all samples.

3.2.2.4.Salt Spray test (SST)

3.2.2.4.1.Aluminum alloy 2024

In order to study the inhibitive effect of coating formulation containing the proposed mixtures of inhibitors and understand their role for the anti-corrosion protection, the salt spray tests for the AA 2024 aluminum alloy with the different coating formulations were performed. The photos are taken after 4, 24, 28, 48 and 72 hours. For this analysis the scratches were made with a scalpel; this lead to a not perfect and completely reproducible scratch. However, the objective to create as smaller as possible defect (less than 1 mm) was achieved. 0.86 M NaCl was used as an aggressive environment at 35°C.

Figures 56, 57 and 58 represent the results of SST after 24, 48 and 72 hours (respectively) for AA2024 aluminum alloy.

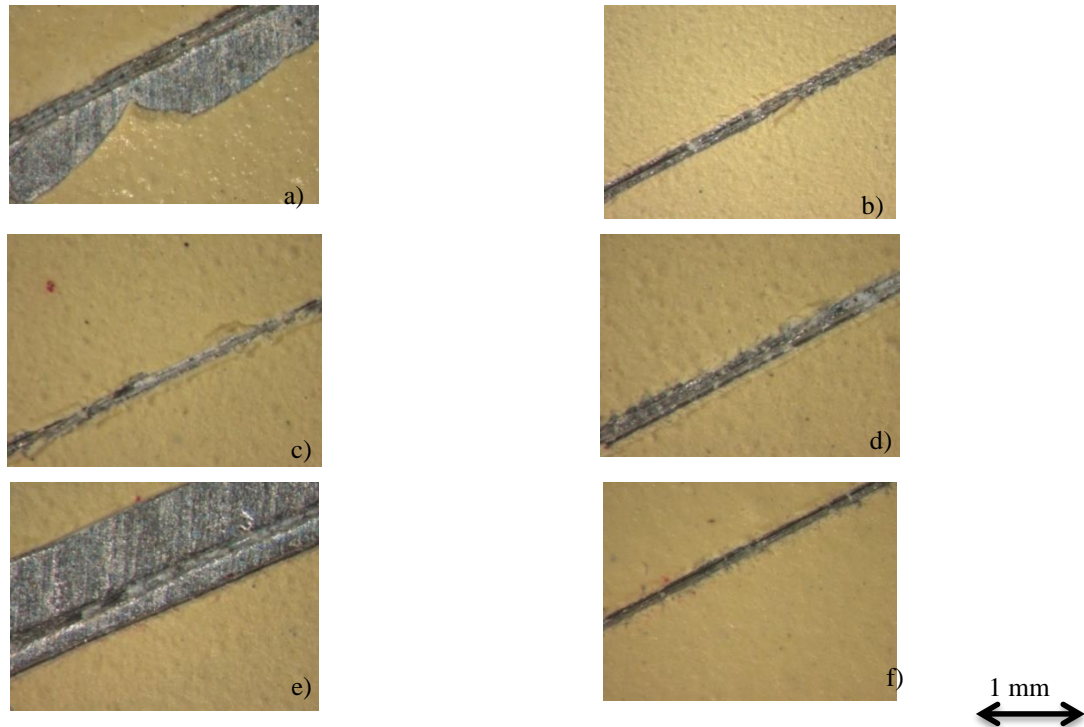


Figure 56 - Photos of AA2024 aluminum alloy protected by coating containing mixture of inhibitors into the formulation (after 24 hours of SST), a) MBT loaded into Mg/Al LDH mixed with Ce^{3+} loaded into bentonite, b) BTA loaded into Mg/Al LDH mixed with Ce^{3+} loaded into bentonite, c) metavanadate loaded into Mg/Al LDH mixed Ce^{3+} loaded into bentonite, d) tungstate loaded into Mg/Al LDH mixed Ce^{3+} loaded into bentonite and e) molybdate loaded into Mg/Al LDH mixed Ce^{3+} loaded into bentonite and f) Reference without inhibitors into coating formulation

From previous **Figure 56** it is possible to observe that after 24 hours of SST the AA2024 remains completely shiny for all coating formulations.

In the case of molybdate loaded into Mg/Al LDH mixed with Ce^{3+} loaded into bentonite the scratch is wider: the reason is that during the passage of the scalpel into the coating of AA2024, some of the coating delaminated from the sample.

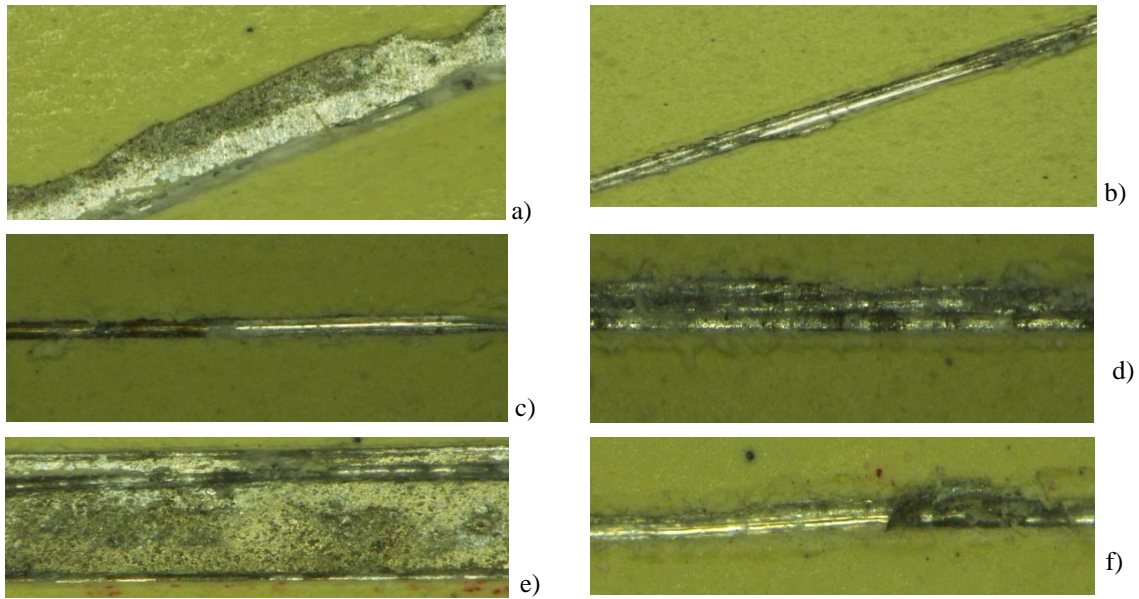


Figure 57 - Photos of AA2024 aluminum alloy protected by coating containing mixture of inhibitors into the formulation (after 48 hours of SST), a) MBT loaded into Mg/Al LDH mixed with Ce^{3+} loaded into bentonite, b) BTA loaded into Mg/Al LDH mixed with Ce^{3+} loaded into bentonite, c) Metavanadate loaded into Mg/Al LDH mixed Ce^{3+} loaded into bentonite, d) tungstate loaded into Mg/Al LDH mixed Ce^{3+} loaded into bentonite and e) molybdate loaded into Mg/Al LDH mixed Ce^{3+} loaded into bentonite and f) reference without inhibitors into coating formulation.

After 48 hours of exposure in SST, in general, the samples show a slow progress of corrosion. However the molybdate loaded into Mg/Al LDH mixed with Ce^{3+} loaded into bentonite and the reference sample show the highest presence of corrosion.

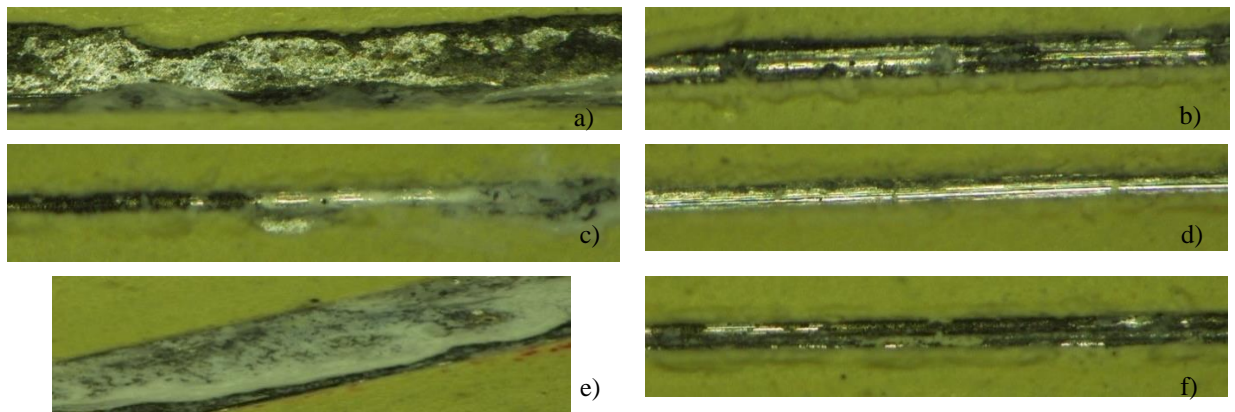


Figure 58 - Photos of AA2024 aluminum alloy protected by coating containing mixture of inhibitors into the formulation (after 72 hours of SST), a) MBT loaded into Mg/Al LDH mixed with Ce^{3+} loaded into bentonite, b) BTA loaded into Mg/Al LDH mixed with Ce^{3+} loaded into bentonite, c) metavanadate loaded into Mg/Al LDH mixed Ce^{3+} loaded into bentonite, d) tungstate loaded into Mg/Al LDH mixed Ce^{3+} loaded into bentonite and e) molybdate loaded into Mg/Al LDH mixed Ce^{3+} loaded into bentonite and f) reference without inhibitors into coating formulation.

After 72 hours of corrosion, only the coating with MBT loaded into Mg/Al LDH mixed with Ce^{3+} loaded into bentonite and tungstate loaded into Mg/Al LDH mixed with Ce^{3+} loaded into bentonite show a shiny aluminum surface with special reference to the last

coating formulation. The remaining samples show a high presence of corrosion in the scratch.

3.2.2.4.2. Galvanic couple

During this electrochemical test the sample with the mixture of inhibitors molybdate loaded into Mg/Al LDH mixture with Ce^{3+} loaded into bentonite in the coating formulation was not tested because after the results of EIS and ZRA it was concluded that this synergistic mixture is not effective against the corrosion for this type of galvanic couple.

For a more careful analysis of the AA2024 corrosion in the couple with CFRP and the photos of corroded samples were taken near the contact with CFRP (Zone1) and at some distance from CFRP (Zone 2, about 4 mm from the contact point), the scratch applied for this test was made with a scalpel (**Figure 59**). The obtained results were recorded after 4h, 24h, 28h, 48h and 72 hours of SST.

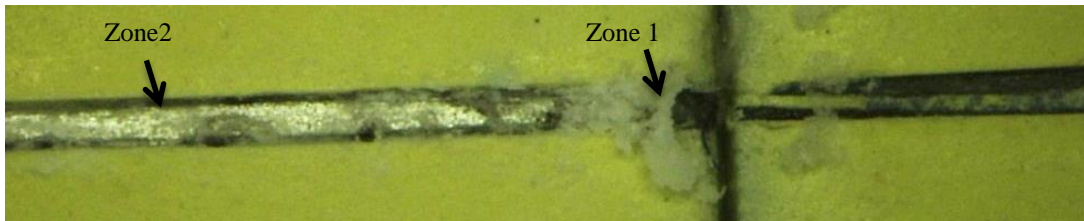


Figure 59 - “Zone1” (near CFRP) and “Zone 2” (about 4 mm from CFRP)

Figure 60 represents the results of the SST for the galvanically coupled AA2024 and CFRP with different mixtures of inhibitors into coating formulation after 4 hours of analysis.

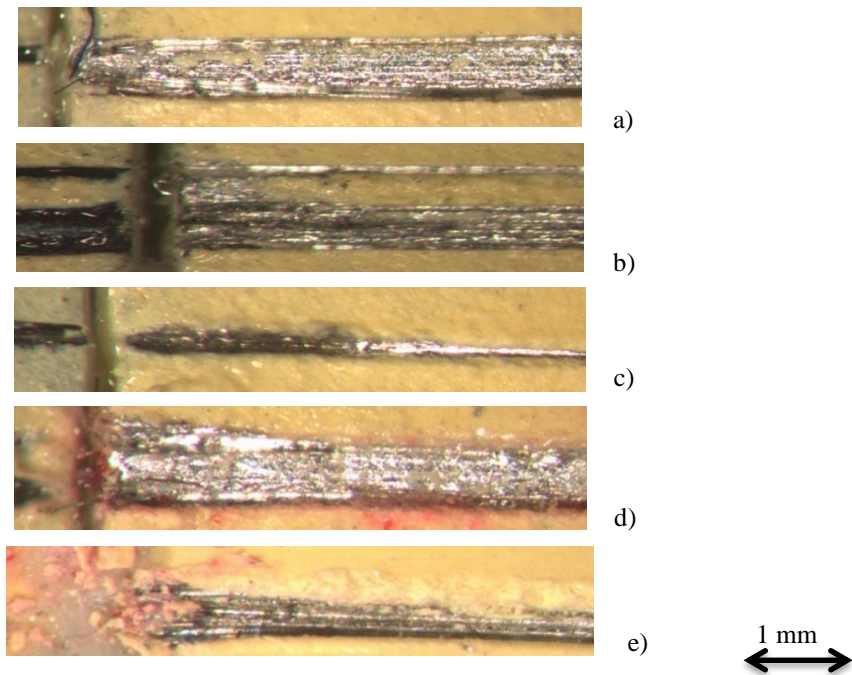
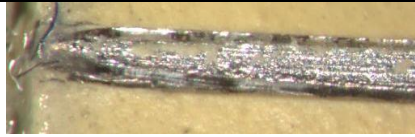

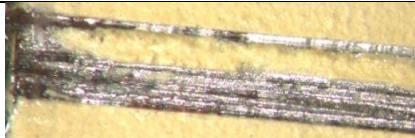


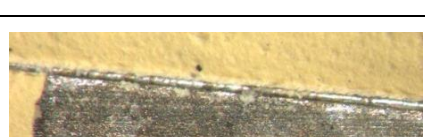






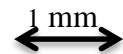
Figure 60 - Photos of galvanically coupled AA2024 and CFRP after 4 hours in SST (*Zone1*), a) MBT loaded into Mg/Al LDH mixed with Ce^{3+} loaded into bentonite, b) BTA loaded into Mg/Al LDH mixed with Ce^{3+} loaded into bentonite, c) metavanadate loaded into Mg/Al LDH mixed Ce^{3+} loaded into bentonite, d) tungstate loaded into Mg/Al LDH mixed Ce^{3+} loaded into bentonite and e) reference without inhibitors into coating formulation.

From these photos in **Figure 60** it can be seen that after 4 hours of SST all samples remains completely shiny without visible corrosion defects into the aluminum surface.

Table 7 shows, the results of SST after 24 hours of analysis for the same mixtures on inhibitors. Photos were taken into *zone 1* and *zone 2* from the aluminium sample surface.

Table 7 - Photos of galvanically coupled AA2024 and CFRP after 24 hours of SST (zone 1 and zone 2)


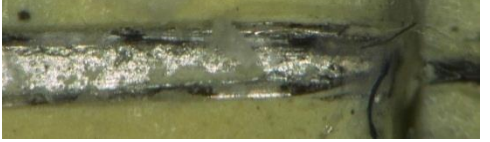
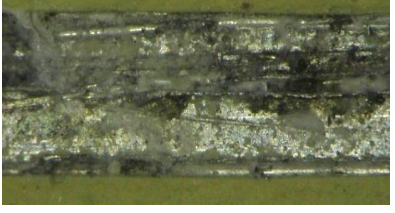
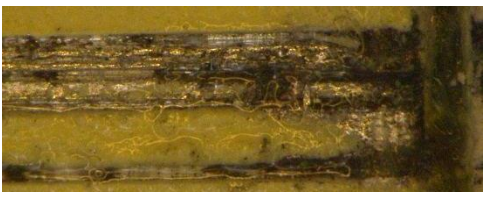
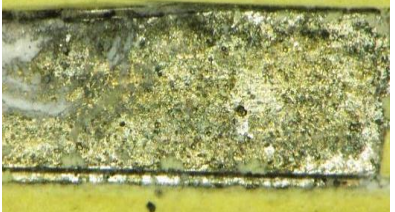


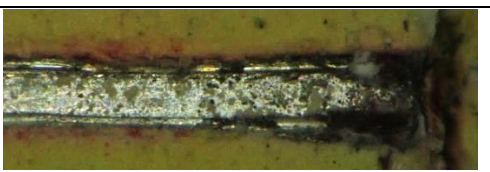

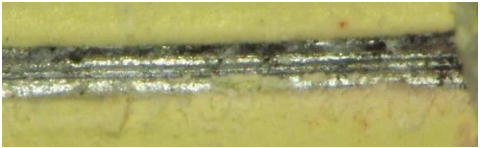
Mixture of inhibitors into the coating formulation	After 24 hours of SST (Zone 1)	After 24 hours of SST (Zone 2)
MBT loaded into Mg/Al LDH mixed with Ce ³⁺ loaded into bentonite		
BTA loaded into Mg/Al LDH mixed with Ce ³⁺ loaded into bentonite		
Metavanadate loaded into Mg/Al LDH mixed with Ce ³⁺ loaded into bentonite		
Tungstate loaded into Mg/Al LDH mixed with Ce ³⁺ loaded into bentonite		
Reference coating without inhibitors		

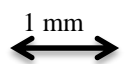


After 24 hours of SST the reference sample and the sample containing metavanadate loaded into Mg/Al LDH mixture with Ce³⁺ loaded into bentonite show presence of corrosion processes. The other samples remain without visible corrosion.

Table 8 shows the results of SST after 28 hours of analysis. Photos were taken into *zone 1* and *zone 2* from the aluminum part of sample surface.

Table 8 - Photos of galvanically coupled AA2024 and CFRP after 28 hours of SST (zone 1 and zone 2)

Mixture of inhibitors into the coating formulation	After 28 hours of SST (Zone 2)	After 28 hours of SST (Zone 1)
MBT loaded into Mg/Al LDH mixed with Ce ³⁺ loaded into bentonite		
BTA loaded into Mg/Al LDH mixed with Ce ³⁺ loaded into bentonite		
Metavanadate loaded into Mg/Al LDH mixed with Ce ³⁺ loaded into bentonite		
Tungstate loaded into Mg/Al LDH mixed with Ce ³⁺ loaded into bentonite		
Reference coating without inhibitors		



After 28 hours inside the salt spray chamber, the increase of AA2024 corrosion near the CFRP is evident and in the opposite side the corrosion is not so evident.

At this point only two samples, those containing MBT loaded into Mg/Al LDH mixture with Ce³⁺ loaded into bentonite and tungstate loaded into Mg/Al LDH combined with Ce³⁺ loaded in bentonite, into the coating formulation remain relatively shiny, the others coating formulations show presence of AA2024 corrosion.

Figure 61 represents one aspect present in all samples after 48 hours of salt spray test: at this moment the corrosion is observed in all samples; these is evident increase of corrosion of AA2024 near the CFRP but less corrosion is observe as distance increase from CFRP.



Figure 61 - General view of the AA2024 sample after 48 hours in SST

Table 9 presents the results after 48 hours of salt spray test for the same mixtures of inhibitors in the coating formulation. This time the photos were taken near the CFRP sample and in the opposite place away from CFRP. It is evident the higher presence of corrosion near the CFRP and less corrosion in opposite part of AA2024. This can be explained by the increase of distance and consequently by ionic transport limitations in the electrolyte.



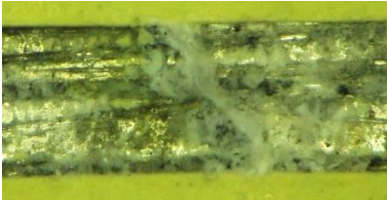
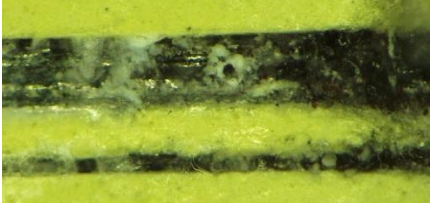
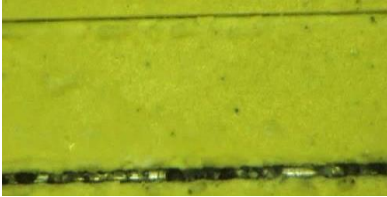
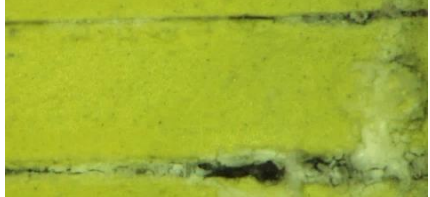

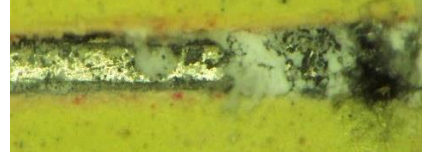

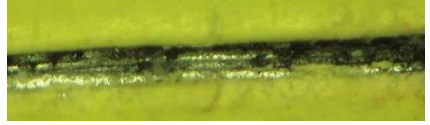
Table 9 - Photos of galvanically coupled AA2024 and CFRP after 48 hours of SST (zone 1 and zone 2)

Mixture of inhibitors into the coating formulation	After 48 hours of SST (Zone 2)	After 48 hours of SST (Zone 1)
MBT loaded into Mg/Al LDH mixed with Ce ³⁺ loaded into bentonite		
BTA loaded into Mg/Al LDH mixed with Ce ³⁺ loaded into bentonite		
Metavanadate loaded into Mg/Al LDH mixed with Ce ³⁺ loaded into bentonite		
Tungstate loaded into Mg/Al LDH mixed with Ce ³⁺ loaded into bentonite		
Reference coating without inhibitors		

1 mm
↔

Table 10 represents the results after 72 hours of salt spray test for the same mixtures of inhibitors

Table 10 - Photos of galvanically coupled AA2024 and CFRP after 72 hours of SST (zone 1 and zone 2)

Mixture of inhibitors into the coating formulation	After 72 hours of SST (Zone 2)	After 72 hours of SST (Zone 1)
MBT loaded into Mg/Al LDH mixed with Ce ³⁺ loaded into bentonite		
BTA loaded into Mg/Al LDH mixed with Ce ³⁺ loaded into bentonite		
Metavanadate loaded into Mg/Al LDH mixed with Ce ³⁺ loaded into bentonite		
Tungstate loaded into Mg/Al LDH mixed with Ce ³⁺ loaded into bentonite		
Reference coating paint without inhibitors		

1 mm
↔

3.2.2.5. Salt spray test and electrochemical impedance spectroscopy

The next series of experiments was performed in order to understand qualitatively if the inhibitors remain in the coating after a long time exposure into aggressive environment without the artificial defects formation into the protective coating.

Taking into account the previous results, the following samples were chosen for these tests:

1. The reference sample without inhibitors into the coating formulation;
2. The samples with MBT loaded into Mg/Al LDH mixed with Ce^{3+} loaded into bentonite into the coating
3. The sample with tungstate loaded into Mg/Al LDH mixed with Ce^{3+} loaded into bentonite into the coating.

The proposed scheme of the experiments can be presented as following:

1. Immersion into 0.05 M NaCl with EIS of a non-scratch area at 1h, 5h, 10h and 24 h (**Figure 62-a** for the reference sample, **Figure 62-b** for the samples with MBT loaded into Mg/Al LDH mixed with Ce^{3+} loaded into bentonite and **Figure 62-c** for the sample with tungstate loaded into Mg/Al LDH mixed with Ce^{3+} loaded into bentonite into the coating)
2. SST (0.86M NaCl) of the same non-scratch area for 72 hours and a new EIS measurement (0.05M NaCl) at the end of SST (**Figure 63-a**, **63-b** and **63-c** respectively).
3. Application of a scalpel scratch at the same place;
4. SST of scratched area during 24 hours and visual comparing of obtained corroded surface (after 96 hours) with routinely corroded samples after 24 hours (**Figure 63**).

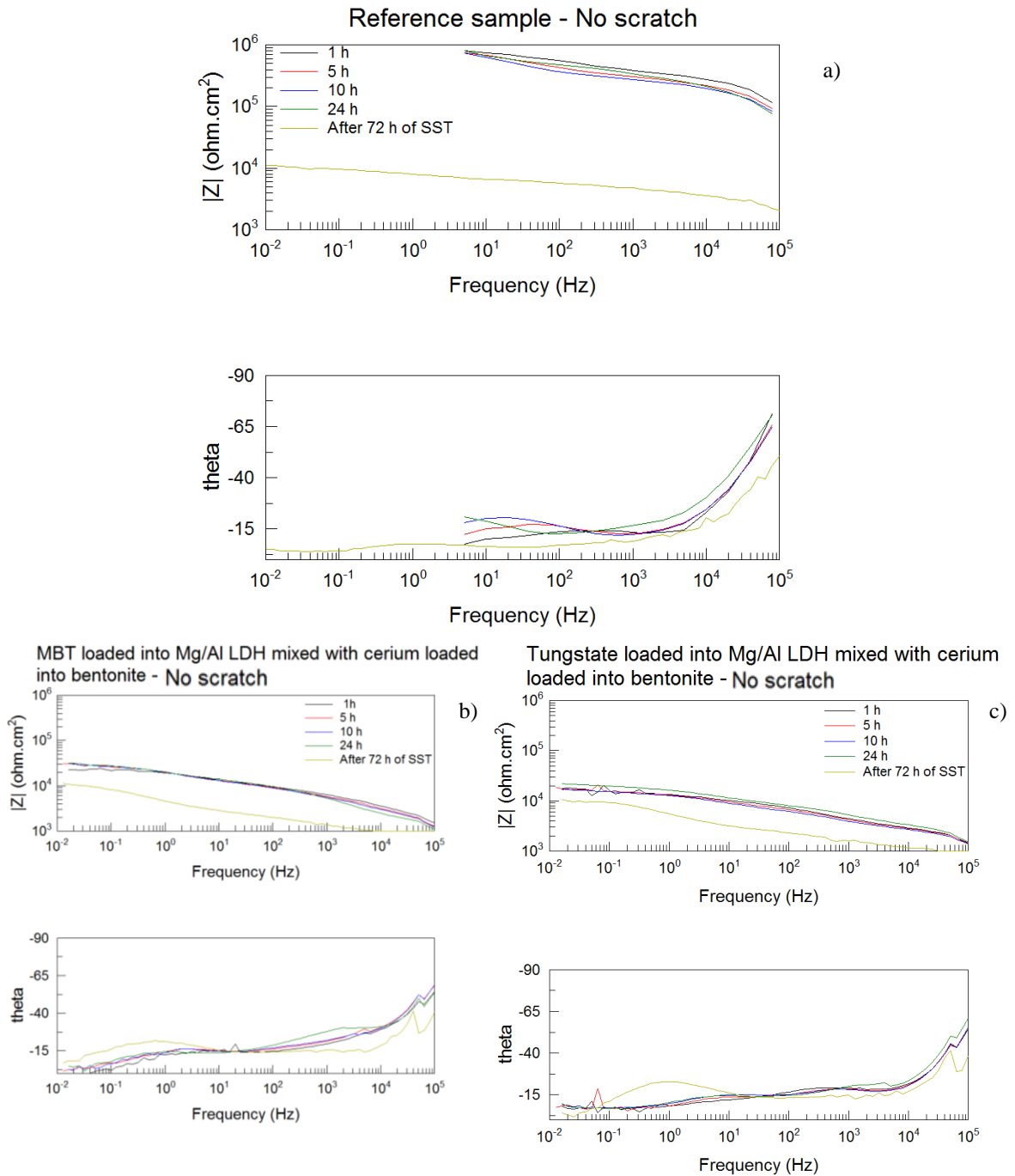


Figure 62 - EIS results for 24 hours of immersion test and after 72 hours of SST: a) reference coating, b) coating's formulation with MBT loaded into Mg/Al LDH mixed with Ce^{3+} loaded into bentonite, c) tungstate loaded into Mg/Al LDH mixed with Ce^{3+} loaded into bentonite.

The results presented show that the reference coating makes a significant decrease of resistance after 72 hours of salt spray test (10^6 ohm/cm² at the beginning and after 24 hours of immersion and around 10^4 ohm/cm² after 72 hours of SST).

For the coating formulations with mixture of inhibitors inside the decrease of resistance was not so significant, but have absolute values much smaller. After 72 hours of

SST the resistance is similar to the same measurement for the reference sample. However it should be mentioned that resistance of the coating with inhibitors during first 24 hour of immersion is lower that for the reference coating. It can be explained by the micro-cracks formation around intercalated nanocontainers. The surfaces of all three samples remain relatively shiny after all these tests and did not show significant visible corrosion.

The significant difference between the samples occurs after creating the artificial defect with further placement into SST. After additional 24 hours the reference sample became completely corroded (24 hours from the formation of the defect or total 96 hours of SST). In contrast, samples with mixtures of inhibitors inside start to corrode but some shiny places of aluminum alloy still exist. These results can be much more comparable with the total 24 hours of corrosion during the normal routine SST than with 96 hours of the test and can be interpreted as the presence of inhibitors into the coating after long time of exposure and released only in the presence of large artificial defect.

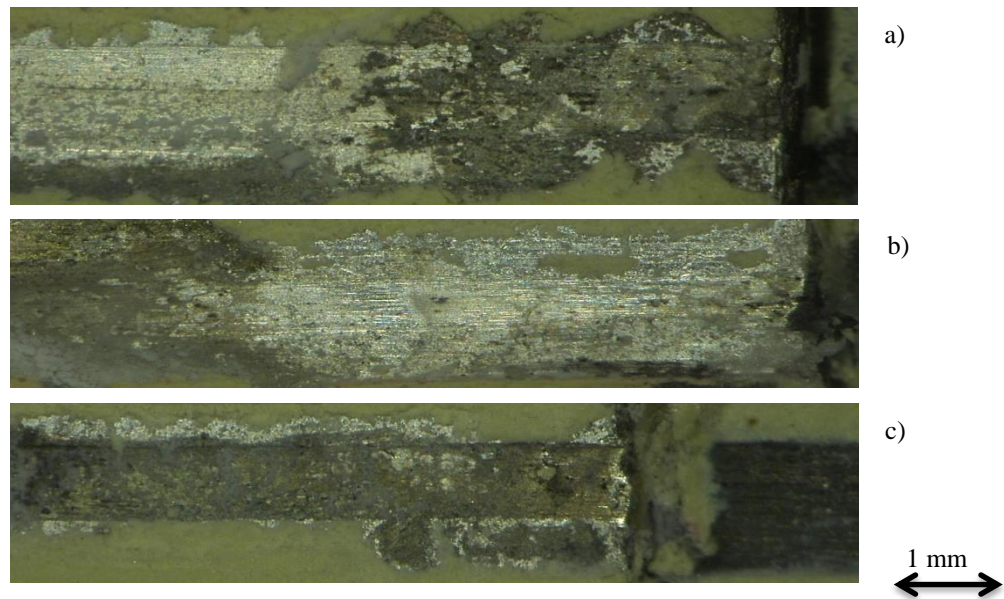


Figure 63 - Results from SST after 24 hours with new scratch applied, a) MBT loaded into Mg/Al LDH mixed with Ce^{3+} loaded into Bentonite, b) Tungstate loaded into Mg/Al LDH mixed with Ce^{3+} loaded into Bentonite and c) Reference paint without inhibitors into coating formulation.

4. Discussion

4.1. Sample holder

The sample holder used during the industrial parts of this work perfectly performs the role for which it was designed and created. However, some improvements can be proposed.

The main improvement can be proposed for the application of the holder with the samples of smaller dimensions. Currently for the samples with width smaller than actually used (40.5 mm), the sample holder is unable to hold and keep the samples on a completely flat surface.

However a way to avoid this problem can be proposed, by partially removing of the sample holder base and addition of a screw which would connect the two walls of the sample holder pressed together.

The other improvement, Lacomit “stopping-off” Lacquer F.65441 from Agar Company can be used in order to have a good isolation of the samples and avoid the solution to pass through the back side of the samples.

After these improvements the sample holder would be able to work more efficiently with smaller samples and without any infiltration.

4.2. Protection with inhibitors

In order to obtain better results with different types of protective coating formulations, the mechanisms of protection with “smart” coating must be understood. **Figure 64** represents (not in scale) the possible mechanism of substrate protection by the inhibitors (Inh^-) loaded into positively charged layers of the structure and applied during coating formation.

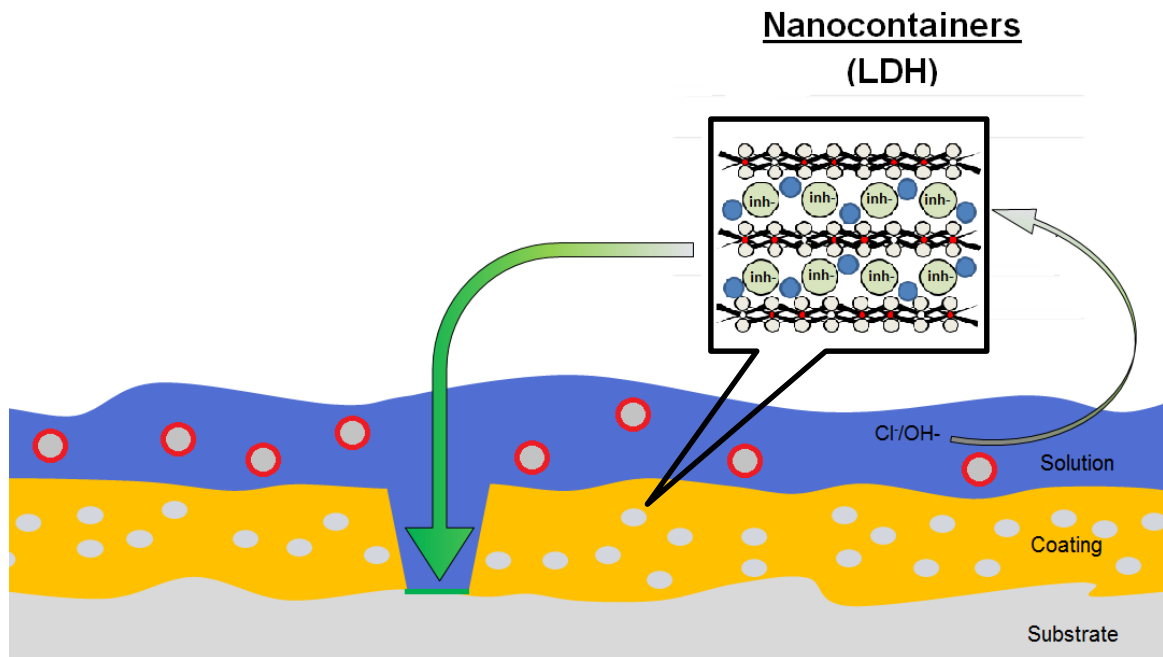
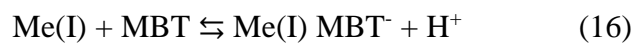


Figure 64 - Anion exchange reaction occurred with LDHs during corrosion protection

The significant difference of protection by the coating with and without inhibitors in the formulation can be explained by the formation of insoluble protective complexes between metals containing into the substrate and used inhibitors. The simplified **reactions 16 and 17** (for MBT and BTA respectively) can explain this formation:



Where Me(I) can be one of the next metals, copper, magnesium, iron and zinc [8].

The structure formed by reactions chemisorbed layer of the inhibitor was proposed as follows (**Figure 65**) [10]. This layer forms the barrier between AA2024 alloy and aggressive environment and prevents further corrosion reactions.

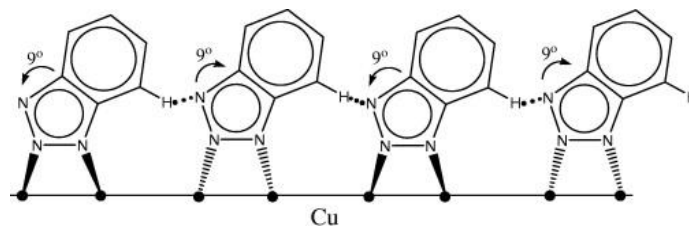
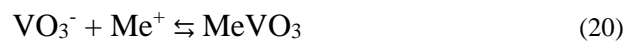
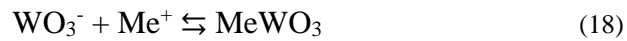


Figure 65 - The schematic presentation of the chemisorbed layer formed by BTA [8]

In the case of inorganic inhibitors (tungstate, molybdate and metavanadate during this work) the simplified reaction of insoluble compound formation can be presented as (reaction **18 - 20**):



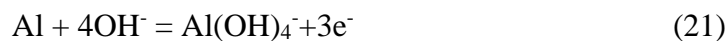
Where Me^{n+} corresponds to the metallic cation in the reaction. This metal can be copper, zinc, aluminum or magnesium [9].

These precipitates form the protective layer between the substrate and the aggressive environment and prevent further corrosion.

The release of the inhibitor from the LDH occurs in presence of hydroxides, which form during the cathodic reaction of water or oxygen reduction (**reactions 3 and 4**) or in the presence of chloride from the solution (corrosive agent).

These anion-exchange reactions are very important for two reasons:

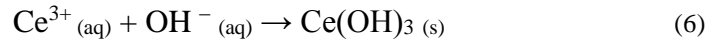
1. LDH incorporates hydroxides into the structure, impeding the progress of cathodic dissolution of aluminum according to the **reactions 8 and 21**:



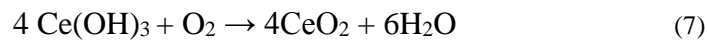
2. The anionic exchange reaction leads to the release of organic inhibitors, which form a protective layer on the surface of aluminum alloy and prevent further corrosion.

In contrast to the positively charged LDH layers, bentonite consists on negatively charged aluminosilicate sheets between which inhibiting cations can be intercalated. During this work Ce^{3+} was intercalated into the bentonite structure.

The presence of Ce^{3+} cations in the coating formulation also leads to the formation of the insoluble layer on the substrate during the corrosion processes. It happens in the presence of cathodically formed hydroxides and leads to the formation of $\text{Ce}(\text{OH})_3$ precipitations according to **reaction 6** [6].



Further oxidation of $\text{Ce}(\text{OH})_3$ leads to a formation of also insoluble CeO_2 (according to the **reaction 7**) which also precipitates on the surface and prevents the contact with the aggressive environment:



However, only the bentonite loaded with Ce^{3+} nanocontainers application did not show the effective inhibition of corrosion. In contrast, it even accelerates the corrosion reaction. This can be explained by the following reasons:

1. The intercalation of nanocontainers into the coating formulation increases its porosity (decreases its barrier properties) which is not sufficiently compensated by the protection with an inhibitor.
2. The formation of not homogeneous layer Ce hydroxide on the surface (the formation of “islands”) due to the intensive OH^- formation into the cathodic places of the system. This layer could not implement effective protection against aggressive environment.
3. The increase of the ionic strength of the solution near the surface leads to the acceleration of corrosion processes.

The anionic exchange ability of LDH present in the coating formulation helps Ce^{3+} to protect the aluminum alloy galvanically coupled with CFRP. In the presence of LDH two competitive reactions could occur with cathodically formed hydroxides:

1. Precipitate formation by the **reaction 6**, or
2. Anionic exchange with inhibitor loaded into Mg/Al LDH

In the presence of second reaction, the formation of “islands” of $\text{Ce}(\text{OH})_3$ becomes less intensive and the formation of more homogeneous protective layer occurs. It could lead to the formation of synergistic mixture of inhibitors and improve the protective properties of the coating.

4.3. Inhibition efficiency

The inhibition efficiency provided by the coating with different inhibitors into the formulations can be limited and explained by the efficiency of the inhibitor release near the defect formation zone. For the different inhibitors loaded into nanocontainers the process of release will be defined by the force which keeps inhibitor inside the nanocontainers (electrostatic force for the charged layer compensation, in the case of loaded LDH and bentonite), and the force which allow them to be released (diffusion anionic exchange). Whereas the second force (diffusion exchange) is defined by the external conditions (aggressive solution concentration, intensity of cathodic reaction) the electrostatic force for the charge layer compensation will be defined by the structure and charge of LDH layers and loaded inhibitors.

If the inhibitor could be simply replaced by the chloride from the solution or by the cathodically formed hydroxides, it will have easier access to the surface inside the defect and easier form the protective layer. In the case of difficulties to the exchange reaction, the problems with formation of new “self-healed” layer will also occur. This can explain the more effective inhibition of the corrosion by the coating containing tungstate loaded into Mg/Al LDH in comparison with other protective coatings even in the presence of smaller amount intercalated inhibitor.

Another possible reason for a poor efficiency of used systems in comparison with chromates can be explained by the small amount of inhibitors really concentrating near the surface. In the proposal case, nanocontainers are distributed into the coating and some amount of inhibitor can be lost in the bulk solution and not react with the surface. The increase of the amount will possibly destroy the coating and will lead to the further ineffective loss of the inhibitors. Possible alternative can be the creation of multi-layer protective construction, where the first layer will be saturated with inhibitors and the second layer will have the normal barrier formulation.

4.4. EIS improvement

The results achieved in EIS do not show any real difference between what can be observed for the reference sample and what is found in the samples coated by epoxy formulation loaded with inhibitors in the presence of artificial scratch. These results can be explained by the ineffective self-healing properties of the coating for such size (1mm * 5 mm * 0.1 mm) of the defect.

To improve these measurements for the future and obtain informative results, the scratch applied to samples has to be with of comparable depth and width with the thickness of the coating.

In order to obtain more informative results during EIS measurements, it was proposed to perform the experiment for the samples with needle artificial defect.

The obtained EIS results have proved that MBT loaded into Mg/Al LDH mixed with cerium loaded into bentonite and the standalone MBT loaded into Mg/Al LDH provide the most effective protection for the galvanically coupled AA2024 and CFRP in comparison with the other coatings formulation.

4.5. Synergistic effect

Table 11 represents the system efficiency for different coatings formulation containing standalone inhibitors and their mixtures estimated according to the equations **13**.

Table 11 - Synergistic effect for different coatings formulations in AA2024

Coatings formulation	System efficiency (%)
Cerium loaded into bentonite	- 613.84
MBT loaded into Mg/Al LDH	71.12 ✓
MBT loaded into Mg/Al LDH mixed with cerium loaded into bentonite	68.08 ✓
BTA loaded into Mg/Al LDH	-249.50
BTA loaded into Mg/Al LDH mixed with cerium loaded into bentonite	19.05 ✓
Metavanadate loaded into Mg/Al LDH	-122.08
Metavanadate loaded into Mg/Al LDH mixed with cerium loaded into bentonite	-134.466
Tungstate loaded into Mg/Al LDH	-1599.27
Tungstate loaded into Mg/Al LDH mixed with cerium loaded into bentonite	-59.83 ✓

The results of the synergistic effect proved efficiency of two combined inhibitors in the same coating formulation. Standalone tungstate loaded into Mg/Al LDH (-1599 %) show a poor efficiency, however in combination with cerium loaded into bentonite, the inhibition efficiency increases to (-59.83%).

In the case of MBT loaded into Mg/Al LDH, the inhibition efficiency decreases in combination with Ce^{3+} loaded into bentonite.

The obtained results are supported by the EIS results as well.

4.6.SVET

Figure 66 represents the SVET results for theoretical inhibition efficiency by standalone inhibitors and by the synergistic mixture of inhibitors for the scratched coated sample (not in scale). The theoretical results are compared with the expected corrosion current for the reference sample (also not in scale).

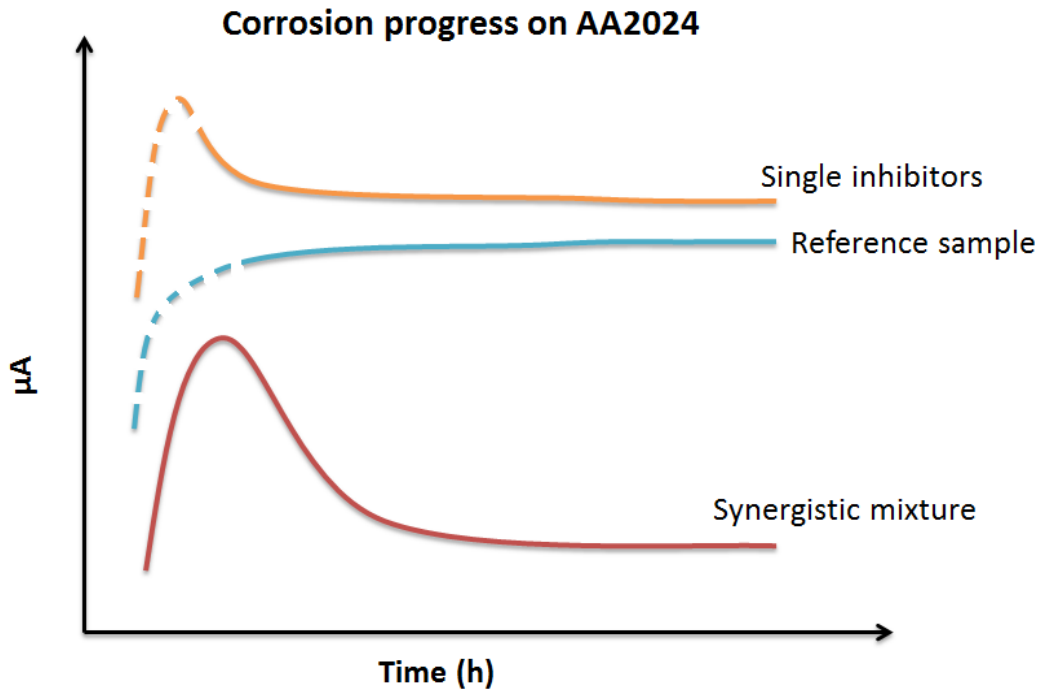


Figure 66 – Corrosion progress on AA2024 through time (not in scale)

Figure 66 shows the progress of corrosion currents through time, for the 3 different types of coatings formulations on AA2024 aluminum alloy. In the case of CFRP sample, the values of the current will be negative, but the tendency of current progress will be similar.

For the reference coatings without any inhibitors inside, the corrosion current firstly increases until stabilization after several hours of measurements. The average value of current for reference sample is higher than for a sample with synergistic mixture in the coating formulation. The results obtained during this work show a slowly increase of current during the 24 hours without any reduction of current during this time.

The corrosion progress for samples with coatings containing only one inhibitor can both be either more intensive (as in the case of coating formulation containing only Ce^{3+}) or less intensive (as in the case of coating formulation containing MBT loaded into Mg/Al LDH) in comparison with model. The more intensive corrosion processes can be explained

by the increase of the ionic strength on the solution. The decrease of corrosion activity in the presence of single inhibitor can be explained by effective absorption of this inhibitor and preventing of further corrosion by the formed protective layer even in the case of one inhibitor.

The coating formulations containing synergistic mixtures at the beginning show an immediately increase of corrosion current near the artificial scratch zone. However, after some time of immersion the inhibitors released from the nanocontainers in the presence of corrosion agents or products “arrive” to the surface of the aluminum alloy due to the diffusion processes and start to form the protective layer on the anodic and cathodic part of the system. When this happens the scratched area becomes isolated from the aggressive environment and corrosion processes blocks.

Comparing the results obtained with SVET for the samples containing MBT loaded into Mg/Al LDH mixed with cerium loaded into bentonite and tungstate loaded into Mg/Al LDH mixed with cerium loaded into bentonite with **Figure 66**, the MBT containing synergistic mixture represent the behavior similar to the theoretical during 24 hours (**Figure 29**). As during first 4 hours practically no corrosion activity was detected. It was assumed that the scratch was completely covered by this protective layer formed by the inhibitive mixture from the coating.

In the case of the coating containing tungstate loaded into Mg/Al LDH mixed with cerium loaded into bentonite, the progress was not so easy to see. However the values of current start to be lower after 10 hours of immersion. This can mean ineffective protection compared to the coating formulation containing MBT loaded into Mg/Al LDH mixed with cerium loaded into bentonite.

5. Conclusions

The analysis of all obtained results leads to several conclusions and ideas for future work:

1. “Smart” nanocontainers with anti-corrosion inhibitors were synthesized and characterized in both University of Aveiro and Airbus group.

Anionic anti-corrosion inhibitors were intercalated into layered double hydroxide (LDH) structure into the anionic form. In opposite way, for Ce^{3+} cations negatively charged bentonite sheets were used.

2. The synergistic mixture of inhibitors was used for corrosion protection of galvanically coupled AA2024 and CFRP. A mechanism of corrosion protection by inhibitors from the coating was proposed.

The sample covered with model reference epoxy coating without any inhibitors shows visible signs of corrosion much quicker in comparison with samples covered with model coating, loaded with mixture of inhibitors.

3. The most significant anti-corrosion effect for galvanically coupled AA 2024 and CFRP was obtained with the coating formulations containing MBT loaded into Mg/Al LDH mixed with Ce^{3+} loaded into bentonite and tungstate loaded into Mg/Al LDH mixed with Ce^{3+} loaded into bentonite.

For this particular system the MBT loaded into Mg/Al LDH alone show the best effect against corrosion.

4. The improvement of a methodology for carrying out electrochemical test was proposed (in particular for the EIS measurements).

In the frame of this work it was shown that the defects (1mm*5mm*0,1mm) applied in Airbus group is not sufficient for the analysis of self-healing ability performed by thin coatings (about 20µm). The size of the defect should be minimized to become comparable with the thickness of the coating.

5. A sample holder for the analysis of corrosion in industrial Airbus laboratory was successfully designed and created. Some further improvements of this design are also proposed.

To conclude, the coating containing synergistic mixture of inhibitor (MBT loaded into Mg/Al LDH mixed with Ce³⁺ loaded into bentonite) shows the best performance for the galvanic couple AA2024/CFRP.

Another important point is the fact that the proposed synergistic mixture can only be applied to AA2024/CFRP galvanic couple.

6. Bibliography

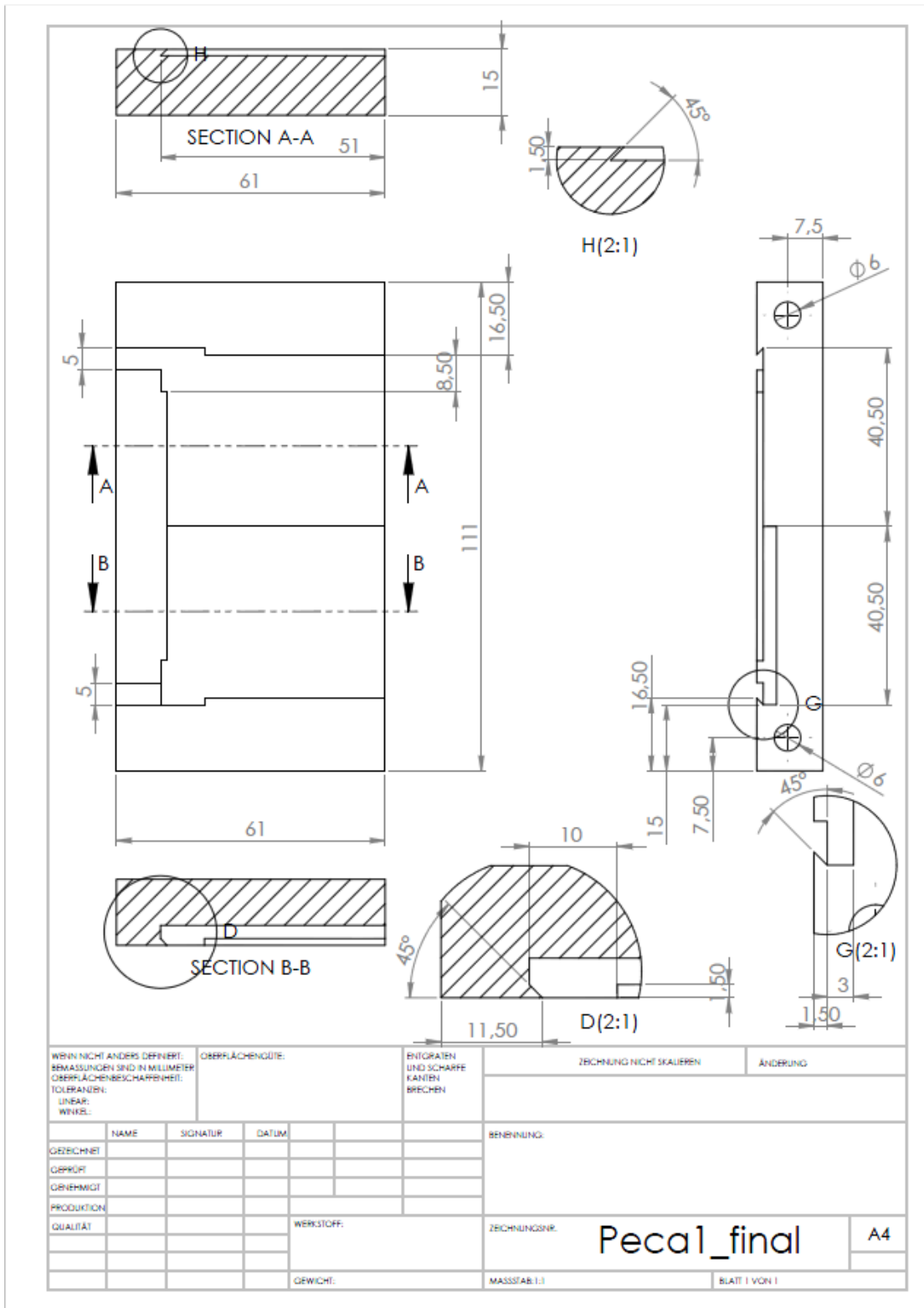
1. Serdechnova, M., “Le contrôle de réactivité d'aluminium en peinture anticorrosion résistant à la haute température”, PhD thesis, Paris (2012) pp. 215.
2. Zheludkevich, M. L., Tedim, J. & Ferreira, M. G. S. ‘Smart’ coatings for active corrosion protection based on multi-functional micro and nanocontainers. *Electrochimica Acta* 82, 314–323 (2012).
3. M.F. Montemor. Functional and smart coatings for corrosion protection: A review of recent advances. *Surface & coatings Technology* (2014).
4. Ferreira, Mário G. S., “Corrosão dos Materiais”, Aveiro (2001).
5. Guu, Y. H., Hocheng, H., Tai, N. H. & Liu, S. Y. Effect of electrical discharge machining on the characteristics of carbon fiber reinforced carbon composites. *Journal of Materials Science*. 36, 2037–2043 (2001).
6. Kallip, S., Bastos, A. C., Yasakau, K. A., Zheludkevich, M. L., Ferreira, M. G. S. Synergistic corrosion inhibition on galvanically coupled metallic materials. *Electrochemistry Communications*, 20, 101–104 (2012).
7. V. K. Gouda. Corrosion and Corrosion Inhibition of Reinforcing Steel: I. Immersed in Alkaline Solutions. *British Corrosion Journal*, 5, 198-203, 2013
8. Nanna, M., Bierwagen, G. Mg-rich coatings: A new paradigm for Cr-free corrosion protection of Al aerospace alloys. *Journal of Coating Technology and Research*, 1, 69–80 (2004).
9. Andreeva D. V., Skorb E.V., Multi-layer smart coatings for corrosion protection of aluminium alloys and steel. *Handbook of Smart Coatings for Materials Protection*, 307-327, (2014).

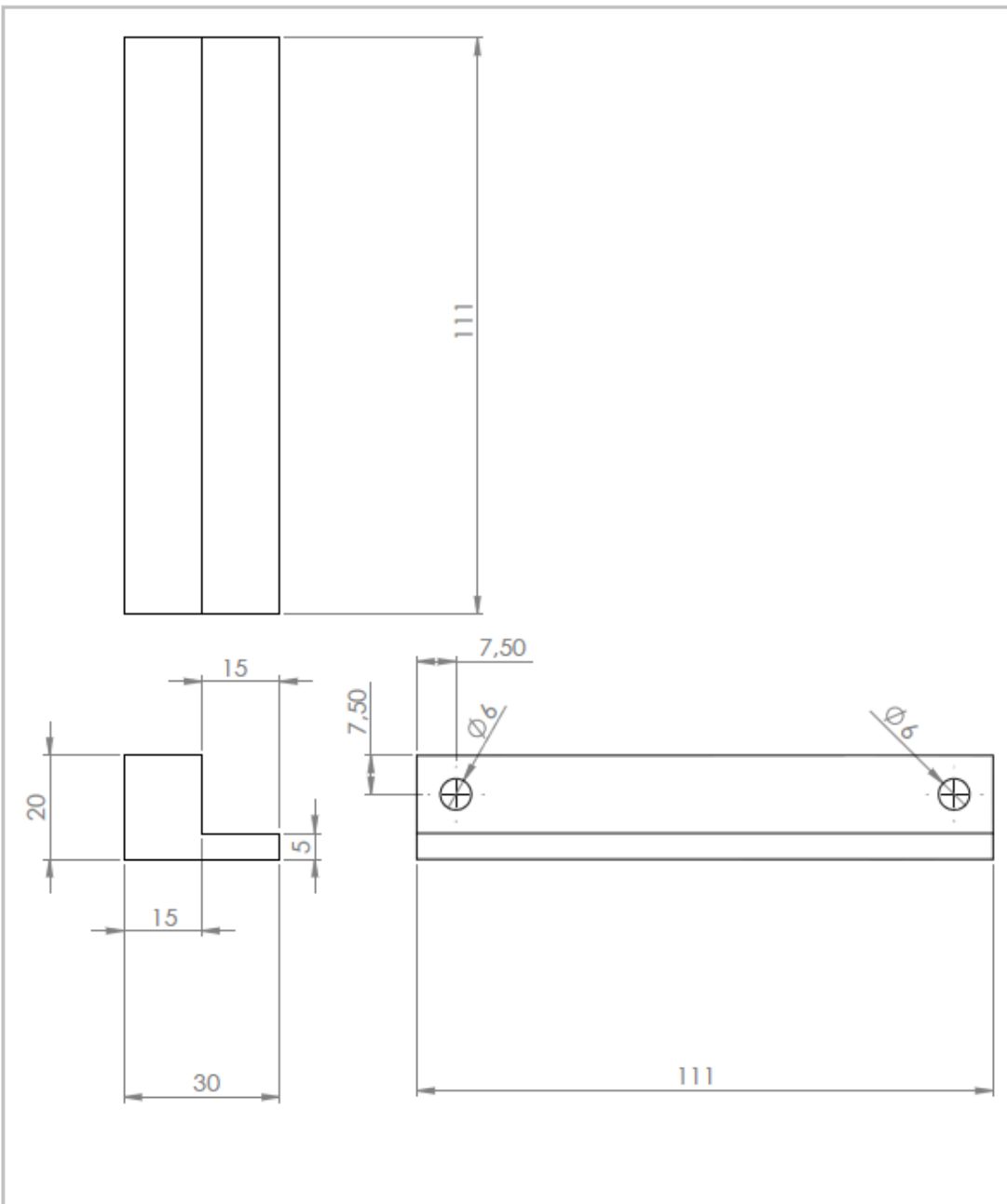
10. Kartsonakis, I. A., Koumoulos, E. P., Balaskas, A. C., Pappas, G. S., Charitidis, C. A., Kordas, G. C., Hybrid organic–inorganic multilayer coatings including nanocontainers for corrosion protection of metal alloys. *Corrosion Science* 57, 56–66 (2012).
11. Peng, Z., Nie, X. Galvanic corrosion property of contacts between carbon fiber cloth materials and typical metal alloys in an aggressive environment. *Surface Coatings Technology*, 215, 85–89 (2013).
12. Davis, J. R. Corrosion of Aluminum and Aluminum Alloys. (ASM International, 1999).
13. Palani, S., Hack, T., Deconinck, J., Lohner, H. Validation of predictive model for galvanic corrosion under thin electrolyte layers: An application to aluminium 2024-CFRP material combination. *Corrosion Science* 78, 89–100 (2014).
14. Finšgar, M., Milošev, I. Inhibition of copper corrosion by 1,2,3-benzotriazole: A review. *Corrosion Science*, 52, 2737–2749 (2010).
15. Campestrini, H. Terry, A. Hovestad, J.H.W de Wit Formation of a cerium-based conversion coating on AA2024: relationship with microstructure. *Surface and coatings technology* 176, 365-381 (2004).
16. Serdechnova, M., Kallip, S., Ferreira, M. G. S., Zheludkevich, M. L. Active self-healing coating for galvanically coupled multi-material assemblies. *Electrochemistry communications* 41, 51-54 (2014).
17. Yasakau, K.A., Tedim, J., Zheludkevich, M. L., Ferreira, M. G. S. Smart self-healing coatings for corrosion protection of aluminum alloys, *HandBook of smart coating for materials protection*, 10, 224-274 (2014).
18. Zaid, B., Saidi, D., Benzaid, A. & Hadji, S. Effects of pH and chloride concentration on pitting corrosion of AA6061 aluminum alloy. *Corrosion Science* 50, 1841–1847 (2008).

19. Lotsch, B., Millange, F., Walton, R. I., O'Hare, D.. Separation of nucleoside monophosphates using preferential anion exchange intercalation in layered double hydroxides. *Solid state sciences*, 3, 883-886 (2001).
20. Albarrana, N., Degueldreb, C., Missanaa, T., Alonsoa, U., García-Gutiérreza, M., López, T. Size distribution analysis of colloid generated from compacted bentonite in low ionic strength aqueous solutions. *Applied Clay Science*, 95, 284-293 (2014).
21. van Soestbergen, M., Baukhb, V., Erichb, S.J.F, Huinink, H.P., Adanb O.C.G, Release of cerium dibutylphosphate corrosion inhibitors from highly filled epoxy coating systems. *Progress in Organic coatings*, 77, 1562-1568 (2014).
22. Valdez, B., Kiyota, S., Stoytcheva, M., Zlatev, R., Bastidas, J. M. Cerium-based conversion coatings to improve the corrosion resistance of aluminium alloy 6061-T6, *Corrosion Science*, 87, 141-149 (2014).
23. Wanhill, R.J.H Aerospace Applications of Aluminum–Lithium Alloys, *Aluminum-lithium Alloys processing, properties and applications*, 15, 503-535, (2014)
24. Peng, Z., Nie, X. Galvanic corrosion property of contacts between carbon fiber cloth materials and typical metal alloys in an aggressive environment. *Surface Coatings Technology*. **215**, 85–89 (2013).
25. Karnik, S.R., Gaitonde, V.N., Rubio, J.C., Correia, A. E., Abrão, A. M. & Davim J.P. Delamination analysis in high speed drilling of carbon fiber reinforced plastics (CFRP) using artificial neural network model. *Materials & Design*, **29**, 1768–1776 (2008).
26. <http://www.eads.com/eads/int/en/our-company/What-we-do/Airbus/A350.html>, (27/11/2013).

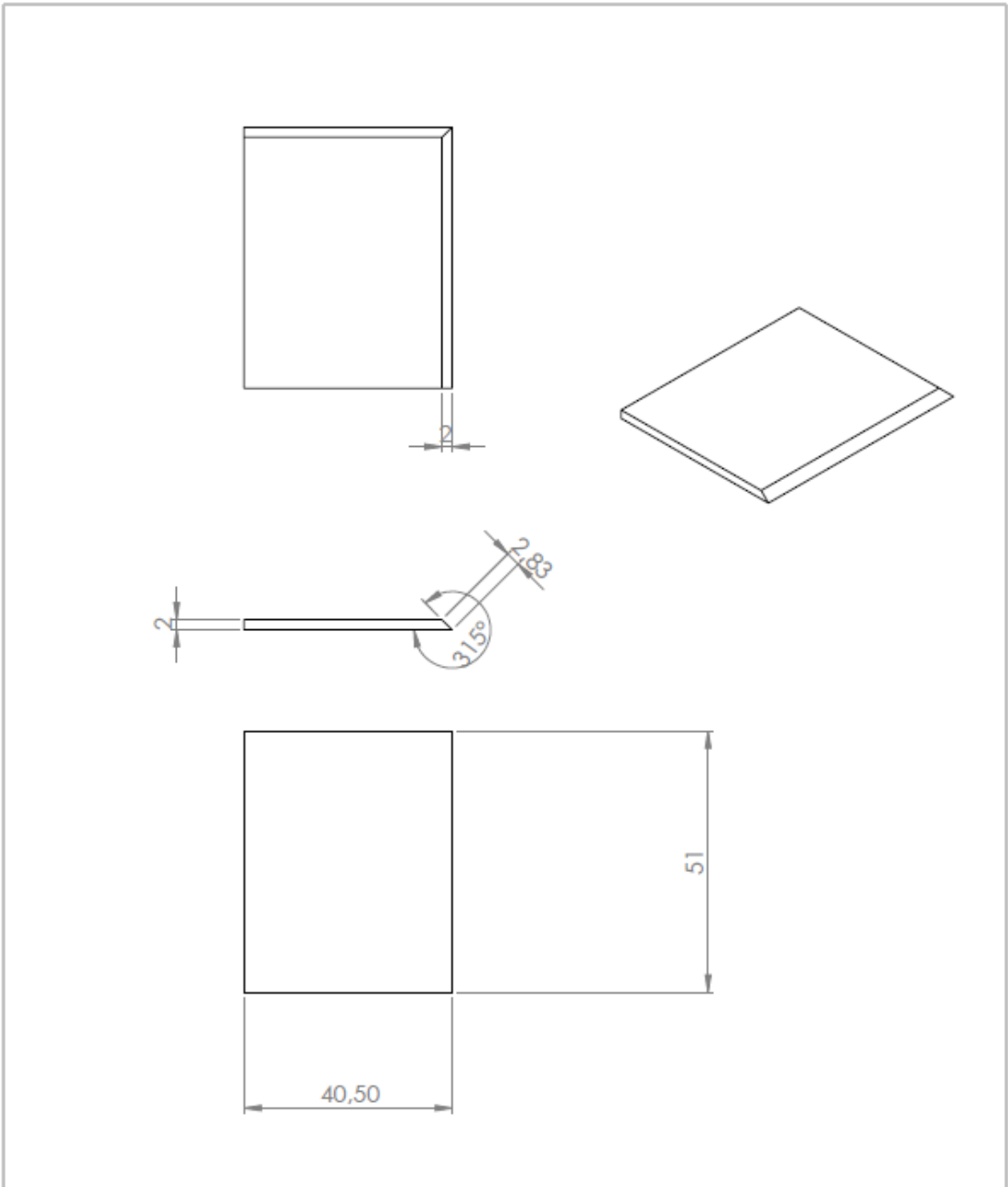
27. Wang, X., Liu C., Li, X., Li, F., Zhou, S. Photodegradation of 2-mercaptobenzothiazole in the γ -Fe₂O₃/oxalate suspension under UVA light irradiation. *Journal of Hazardous Materials* **153**, 426-433 (2008).
28. Evans, D. G., Slade, R. C.T. in“Layered Double Hydroxides“,*Springer Berlin Heidelberg* **119**, 1–87, (2006).

Annex:





WENN NICHT ANDERS DEFINIERT: ABMESSUNGEN SIND IN MILLIMETER OBERFLÄCHENBESCHAFFENHEIT: TOLERANZEN: LINEAR: WINKEL:		OBERFLÄCHENGÜTE:		ENTGRATEN UND SCHARFE KANTEN BRECHEN		ZEICHNUNG NICHT SKALIEREN		ÄNDERUNG	
NAME		SIGNATUR		DATUM		BEZEICHNUNG:			
GEZEICHNET		GEPÜFT		GEHEMIGT		ZEICHNUNGSNR.			
PRODUKTION		QUALITÄT		WERKSTOFF:		Peca2_final		A4	
GEWICHT:		MASSSTAB: 1:2		BLATT 1 VON 1					



WENN NICHT ANDERS DEFINIERT: ABMESSUNGEN SIND IN MILLIMETER OBERFLÄCHENBESCHAFFENHEIT: TOLERANZEN: LINEAR: WINKEL:				OBERFLÄCHENGÜTE:		ENTGRATEN UND SCHARFE KANTEN BRECHEN		ZEICHNUNG NICHT SKALIEREN		ÄNDERUNG	
								BENENNUNG:			
GEZEICHNET	NAME	SIGNATUR	DATUM			WERKSTOFF:		ZEICHNUNGSNR.		aluminium	
GEPRÜFT										A4	
GEBILDET											
PRODUKTION											
QUALITÄT						GEWICHT:		MASSSTAB: 1:1		BLATT 1 VON 1	

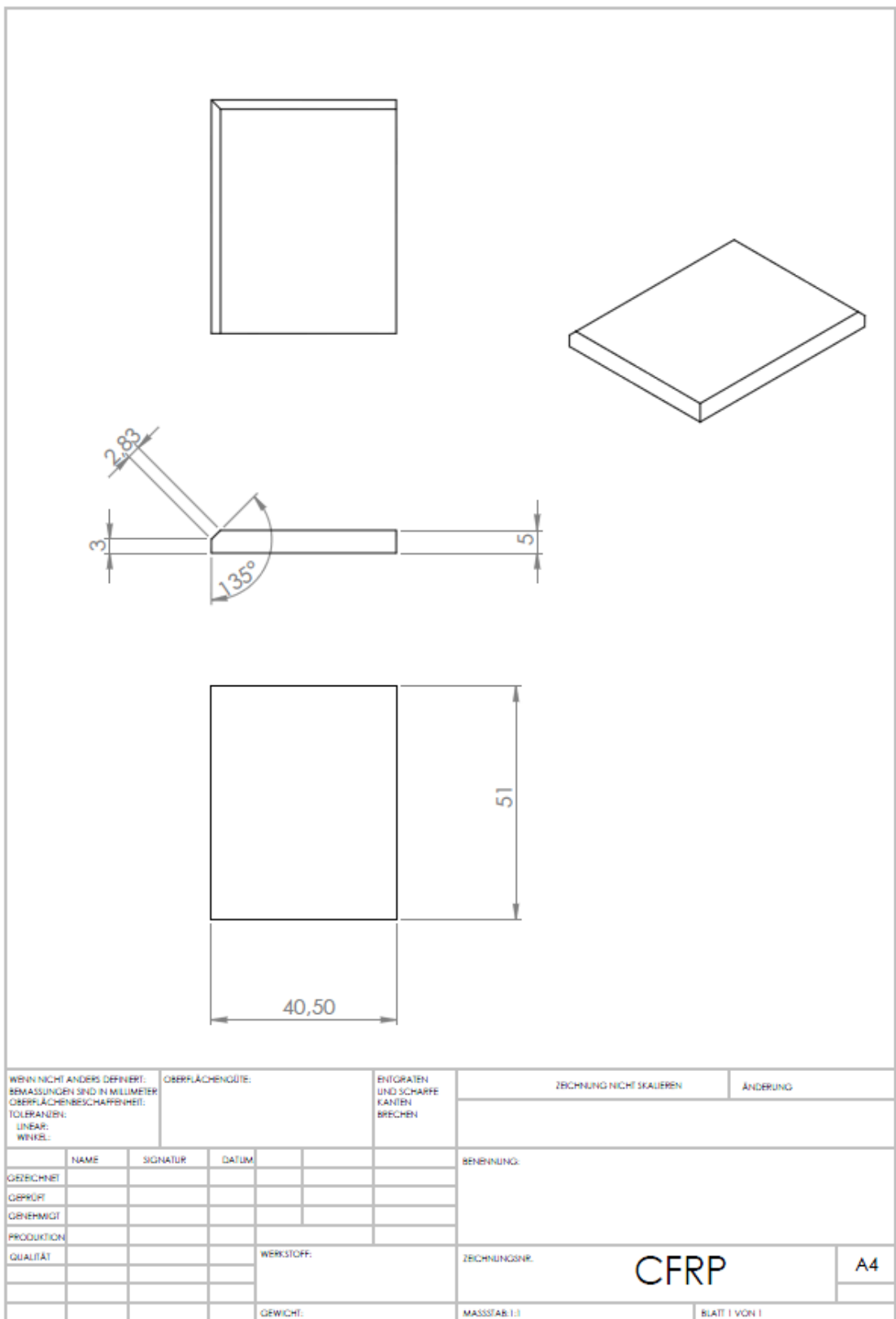


Figure A1 – Measurements off the sample holder, Al sample and CFRP sample

